

# A parameterization of anisotropic Gaussian fields with penalized complexity priors

L. Llamazares-Elias<sup>\*1</sup>, J. Latz<sup>2</sup>, and F. Lindgren<sup>1</sup>

<sup>1</sup>School of Mathematics, University of Edinburgh, United Kingdom

<sup>2</sup>Department of Mathematics, University of Manchester, United Kingdom

September 16, 2024

## Abstract

Gaussian random fields (GFs) are fundamental tools in spatial modeling and can be represented flexibly and efficiently as solutions to stochastic partial differential equations (SPDEs). The SPDEs depend on specific parameters, which enforce various field behaviors and can be estimated using Bayesian inference. However, the likelihood typically only provides limited insights into the covariance structure under in-fill asymptotics. In response, it is essential to leverage priors to achieve appropriate, meaningful covariance structures in the posterior. This study introduces a smooth, invertible parameterization of the correlation length and diffusion matrix of an anisotropic GF and constructs penalized complexity (PC) priors for the model when the parameters are constant in space. The formulated prior is weakly informative, effectively penalizing complexity by pushing the correlation range toward infinity and the anisotropy to zero.

*Keywords:* Anisotropy, Bayesian, Penalized Complexity, Prior, Stochastic Partial Differential Equation.

---

<sup>\*</sup>Corresponding author: L.S.Llamazares-Elias@sms.ed.ac.uk

# 1 Introduction

Gaussian random fields (GF) are widely used to model spatial phenomena [Banerjee et al. \(2003\)](#); [Bhatt et al. \(2015\)](#); [Wang and Zuo \(2021\)](#); [Rue and Held \(2005\)](#) while accounting for the uncertainty that may arise due to measurement error, model misspecification, or incomplete information. The prevalence of GFs is due to the fact that they are well understood theoretically, verify desirable properties, and are easily characterized – they are entirely specified by their mean and covariance [Jaynes \(2003\)](#); [Adler et al. \(2007\)](#); [Rasmussen \(2003\)](#).

A convenient way of representing certain GFs is as solutions to stochastic partial differential equations (SPDEs). This representation allows for physical interpretation to be assigned to the parameters of the equation. Furthermore, it allows for computationally efficient inference, prediction, and uncertainty quantification using a finite element (FEM) approximation of the field [Lindgren et al. \(2011\)](#); [Simpson et al. \(2012\)](#).

In the literature, a common choice is to model using isotropic fields. That is, the correlation of the field at two locations only depends on the Euclidean distance between said locations. While this may be an appropriate assumption in some cases, in others, it is inadvisable. This limitation can be overcome by introducing additional parameters to model the anisotropy present in the field as in [Fuglstad et al. \(2015\)](#). In the following, we consider the semi-parametric estimation of the random field and its anisotropy parameters. The existing work leaves us with two significant challenges:

1. The anisotropy parameterization from [Fuglstad et al. \(2015\)](#) is non-identifiable as it has two parameter combinations for each anisotropy matrix, leading to a multi-modal likelihood, making it unsuitable as a general parameterization.
2. Given that not all parameters can be recovered under in-fill asymptotic [Zhang \(2004\)](#),

the *choice of prior distribution* on the parameters of the model may significantly impact the posterior distribution. As a result, suitable priors need to be defined.

To address these issues, we make the following contributions:

1. **Alternative parameterization:** We present an alternative parameterization of the anisotropy that preserves parameter interpretability and which is smooth and invertible.
2. **Prior definition:** We construct penalized complexity (PC) priors [Simpson et al. \(2014\)](#); [Fuglstad et al. \(2019\)](#) for the parameters in the model. An additional benefit of this construction is that it avoids overfitting by favoring simpler base models.
3. **Validation and prediction:** We conduct a simulation study that shows that PC priors outperform “non-informative” priors. We then use the derived model to study precipitation in Norway and show that the anisotropic model outperforms the isotropic one in the presence of limited information.

The outline of the work is as follows. In Section 2, we introduce and motivate our anisotropic model. In Section 3, we address Contribution 1 and also construct a transformation that renders the parameters a Gaussian vector, providing the convenience of working with Gaussian random variables. In Section 4, we present Contribution 2. Next, in Section 5, we conduct a simulation study of the designed PC priors and compare the results to other possible priors on the parameters. In Section 6, we study the performance of the model and priors on a real data set. Finally, in Section 7, we synthesize the obtained results and discuss future avenues of research.

## 2 Anisotropic model

### 2.1 Formulation

In this section, we address the first main contribution. How can we introduce anisotropy in our model and parameterize it such that each parameter has an interpretable effect? We work in 2 dimensions and within the framework of the SPDE approach [Lindgren et al. \(2011, 2022\)](#). In this approach, the GF  $u$  is defined as the solution to a SPDE. Most commonly, the SPDE chosen is

$$(\kappa^2 - \Delta)^{\frac{\alpha}{2}} u = \dot{\mathcal{W}}. \quad (1)$$

Here,  $\dot{\mathcal{W}}$  is Gaussian white noise on  $L^2(\mathbb{R}^2)$ , and is defined such that given  $f, g \in L^2(\mathbb{R}^2)$  the random measure

$$\mathcal{W}(f) := \langle f, \dot{\mathcal{W}} \rangle$$

verifies

$$\mathbb{E}[\mathcal{W}(f)\mathcal{W}(g)] = \langle f, g \rangle_{L^2(\mathbb{R}^2)}.$$

The resulting field  $u$  has mean zero and is chosen to be isotropic to guarantee uniqueness. We recall that, by definition, the field  $u$  is isotropic if there exists some function  $r$  such that, for all  $\mathbf{x}, \mathbf{y} \in \mathbb{R}^2$ ,

$$K(\mathbf{x}, \mathbf{y}) := \text{Cov}[u(\mathbf{x}), u(\mathbf{y})] = r(\|\mathbf{y} - \mathbf{x}\|). \quad (2)$$

The isotropy of  $u$  may be an appropriate assumption in some cases. However, it is inadvisable if the correlation of the field is not equal in all spatial directions. To model this anisotropy, we will consider the model given by

$$(\kappa^2 - \nabla \cdot \mathbf{H} \nabla) \frac{u}{\sigma_u} = \sqrt{4\pi\kappa} \dot{\mathcal{W}}, \quad (3)$$

where the parameters are  $\kappa, \sigma_u \in (0, \infty)$  which are positive and bounded away from zero, and a symmetric positive definite matrix  $\mathbf{H} \in \mathbb{R}^{2 \times 2}$  with eigenvalues bounded away from zero. The parameters control the length scale, marginal variance, and anisotropy, respectively, as we will explain in the next subsections.

The formulation in (3) preserves the advantages of the SPDE approach. Namely, representing  $u$  as the solution of a SPDE gives it a physical interpretation. The term  $\kappa^2 u$  represents reaction whereas  $-\nabla \mathbf{H} \cdot \nabla u$  represents diffusion [Evans \(2010\)](#); [Roques et al. \(2022\)](#).

Furthermore, using a finite element method,  $u$  can be projected onto the finite-dimensional Hilbert space  $\mathcal{H}_n$  spanned by the basis functions  $\{\psi_1, \dots, \psi_n\}$  linked to a mesh  $M_n$  of the domain. This gives a sequence of Gaussian Markov random fields  $u_n$  with sparse precision matrices (the precision matrix is the inverse of the covariance matrix), which converges in distribution to  $u$  as the mesh becomes finer and finer. This sparsity allows for a significant speed-up in computations (Kriging, posterior simulation, likelihood evaluation, etc.) [Simpson et al. \(2012\)](#); [Lindgren et al. \(2011\)](#).

## 2.2 Derivation

We now motivate the choice of the SPDE (3). By definition, a field  $u$  on  $\mathbb{R}^d$  is *stationary* if its covariance  $K$  depends only on the relative position between two points. That is, for some function  $r$  called the *covariance function*

$$K(\mathbf{x}, \mathbf{y}) := \text{Cov}[u(\mathbf{x}), u(\mathbf{y})] = r(\mathbf{y} - \mathbf{x}), \quad \forall \mathbf{x}, \mathbf{y} \in \mathbb{R}^d. \quad (4)$$

Equation (4), which is an extension of (2), requires that the Euclidean translation  $\mathbf{y} - \mathbf{x}$  captures all relevant information related to the covariance of the field between any two spatial locations  $\mathbf{x}$  and  $\mathbf{y}$ . However, Euclidean geometry may not fit with the underlying properties of the field. For example, suppose that our field describes the geological prop-

erties of some homogeneous terrain. Even if the field was initially stationary, stationarity is lost if the terrain underwent a geological deformation  $\psi$ . Instead, the relationship

$$K(\mathbf{x}, \mathbf{y}) = r(\psi^{-1}(\mathbf{x}) - \psi^{-1}(\mathbf{y}))$$

would be more appropriate. This is the *deformation method* [Sampson and Guttorp \(1992\)](#) and is, for instance, sometimes used to connect different layers in deep Gaussian processes. In deep Gaussian processes, this transformation is then random and not diffeomorphic [Dunlop et al. \(2018\)](#).

The deformation method provides an easy way to construct non-stationary fields starting from stationary ones. Furthermore, it can be used in a layered approach, where a stationary field is first built through some appropriate method and then deformed into a non-stationary field.

As discussed previously, SPDEs provide a convenient framework for the construction of stationary fields, for example, through (1). Let us see what happens when we deform such a field. To this aim, consider an (unknown)  $d$ -dimensional manifold  $\tilde{\mathcal{D}}$  and our target manifold  $\mathcal{D}$  obtained through a diffeomorphic transformation

$$\psi : \tilde{\mathcal{D}} \rightarrow \mathcal{D}.$$

Further consider the solutions  $\tilde{u}$  to

$$(1 - \Delta)\tilde{u} = \sqrt{4\pi}\dot{\tilde{\mathcal{W}}}, \quad \text{on } \tilde{\mathcal{D}}. \quad (5)$$

Here, either  $\tilde{\mathcal{D}} = \mathbb{R}^d$ , in which case, to obtain uniqueness, we impose a stationarity condition. Otherwise,  $\tilde{\mathcal{D}}$  is some bounded subset of  $\mathbb{R}^d$ , in which case Neumann conditions or Dirichlet conditions are imposed on the boundary. Then, a change of variables yields that  $u := \sigma_u \cdot \tilde{u} \circ \psi^{-1}$  verifies the *non-stationary* SPDE

$$\frac{1}{\|\Psi\|} \left[ 1 - \|\Psi\| \nabla \cdot \frac{\Psi \Psi^T}{\|\Psi\|} \nabla \right] \frac{u}{\sigma_u} = \frac{\sqrt{4\pi}}{\|\Psi\|^{1/2}} \dot{\mathcal{W}} \quad \text{on } \mathcal{D}, \quad (6)$$

where  $\Psi$  is the Jacobian of  $\psi$ , and we denote its determinant by  $\|\Psi\|$  (Lindgren et al., 2011, Section 3.4).

Let us write  $\gamma$  for the geometric mean of the eigenvalues of  $\Psi$ . Then,  $\|\Psi\| = \gamma^d$  and we obtain from (6) that

$$\frac{1}{\gamma^d} [1 - \gamma^d \nabla \cdot \gamma^{2-d} \mathbf{H} \nabla] \frac{u(\mathbf{x})}{\sigma_u} = \frac{\sqrt{4\pi}}{\gamma^{d/2}} \mathcal{W} \quad \text{on } \mathcal{D}, \quad (7)$$

where we defined  $\mathbf{H} := \gamma^{-2} \Psi \Psi^T$ . Note that if we write  $\kappa := \gamma^{-1}$  and take the dimension  $d$  to be 2, we recover our model in (3). For general  $d$ , it follows from the definition of  $\mathbf{H}$  that

1.  $\mathbf{H}$  is symmetric.
2.  $\mathbf{H}$  has determinant 1.
3.  $\mathbf{H}$  is positive definite.

From now on, we will impose these three assumptions on  $\mathbf{H}$ . Furthermore, we will restrict ourselves to the stationary case by imposing that  $\mathbf{H}$  is constant in space, or equivalently, we impose that  $\psi$  is a linear deformation. That is,  $\psi(\mathbf{x}) = \Psi \mathbf{x}$ . By construction, the solution field  $u$  is thus *geometrically anisotropic* (Cressie and Wikle, 2015, Section 4.1). That is, if we replace the Euclidean metric with the *deformed metric*  $\|\mathbf{x}\|_{\Psi^{-1}} := \|\Psi^{-1} \mathbf{x}\|$ , we obtain analogously to (2) that, for some function  $r : \mathbb{R}^d \rightarrow \mathbb{R}$  called the *covariance function* of  $u$ ,

$$K(\mathbf{x}, \mathbf{y}) := \text{Cov}[u(\mathbf{x}), u(\mathbf{y})] = r(\|\mathbf{y} - \mathbf{x}\|_{\Psi^{-1}}), \quad \forall \mathbf{x}, \mathbf{y} \in \mathbb{R}^d,$$

In the case  $\tilde{\mathcal{D}} = \mathbb{R}^d$ , the marginal variance of  $\tilde{u}$  is  $\mathbb{E}[\tilde{u}(\tilde{\mathbf{x}})^2] = 1$  for all  $\tilde{\mathbf{x}} \in \tilde{\mathcal{D}}$  (Lindgren et al., 2011, Section 2.1) (we recall that the solution to SPDEs of the form (3) have mean 0). As a result, the marginal variance of  $u$  is  $\mathbb{E}[u(\mathbf{x})^2] = \sigma_u^2$  for all  $\mathbf{x} \in \mathcal{D}$ .

In the case where  $\mathcal{D}$  is a bounded domain, there is a boundary effect that affects the marginal variance of  $u$ . However, at a distance larger than twice the correlation length from the boundary, the bounded domain model is almost indistinguishable from the unbounded domain model. As a result, the boundary effect can be made negligible by embedding the region of interest in a sufficiently large domain.

### 3 Parameterization

In this section, we parameterize  $\mathbf{H}$  so that the parameters convey intrinsic geometric meaning about the field  $u$ . Recall conditions 1-3 and suppose for example that  $\kappa$  is fixed to 1 so that  $\Psi = \sqrt{\mathbf{H}}$ . Write

$$\{(\mathbf{v}, \lambda^2), (\mathbf{v}_\perp, \lambda^{-2})\}$$

for the eigensystem of  $\mathbf{H}$ , where  $\mathbf{v} := (v_1, v_2) \in \mathbb{R}^2$  and  $\mathbf{v}_\perp = (-v_2, v_1)$  and we can suppose  $\lambda \geq 1$  by reordering if  $\lambda < 1$ . Then, the previous discussion shows that  $u$  corresponds to deforming and rescaling the stationary field  $\tilde{u}$  through

$$u(\mathbf{x}) = \sigma_u \cdot \tilde{u}(\Psi\mathbf{x}), \quad \Psi\mathbf{x} = \lambda \langle \mathbf{x}, \mathbf{v} \rangle \mathbf{v} + \lambda^{-1} \langle \mathbf{x}, \mathbf{v}_\perp \rangle \mathbf{v}_\perp.$$

The rescaling by  $\sigma_u$  corresponds to changing the variance of the field. The deformation corresponds to stretching the initial domain by a factor of  $\lambda$  in the direction of  $\mathbf{v}$  and contracting, also by a factor of  $\lambda$ , in the orthogonal direction  $\mathbf{v}_\perp$ . The above shows that the eigensystem of  $\mathbf{H}$  carries fundamental geometric information and motivates a parameterization of  $\mathbf{H}$  in terms of its eigensystem.

Equation (3) was also considered in [Fuglstad et al. \(2015\)](#). Here, the authors defined  $\mathbf{v}(\alpha) := (\cos(\alpha), \sin(\alpha))$  and parameterized  $\mathbf{H}$  as

$$\mathbf{H}_{\mathbf{v}(\alpha)} = \gamma \mathbf{I} + \beta \mathbf{v}(\alpha) \mathbf{v}(\alpha)^T. \tag{8}$$



However, the map  $\alpha \mapsto \mathbf{H}_{v(\alpha)}$  is not injective as  $\mathbf{H}_{v(\alpha)} = \mathbf{H}_{-v(\alpha)}$ . Because of this, it is impossible to recover the sign of  $\mathbf{v}$  and, thus, this parameterization is not identifiable and leads to a bimodal likelihood.

The crucial step to obtain an identifiable parameterization is to consider the “half-angle” version  $\tilde{\mathbf{v}}$  of  $\mathbf{v}$  as an eigenvector of  $\mathbf{H}$ .

**Theorem 1** (parameterization). *Given  $\mathbf{v} = (v_1, v_2) \in \mathbb{R}^2$  define*

$$\tilde{\mathbf{v}} := \|\mathbf{v}\| \exp(i\alpha/2), \quad \text{where } \alpha := \arg(\mathbf{v}) \in [0, 2\pi). \quad (9)$$

Write  $\tilde{\mathbf{v}} = (\tilde{v}_1, \tilde{v}_2)$  and  $\tilde{\mathbf{v}}_\perp = (-\tilde{v}_2, \tilde{v}_1)$ . Then, the following defines a smooth, invertible parameterization on the space of symmetric positive definite matrices of determinant 1.

$$\mathbf{H}_v = \frac{\exp(\|\mathbf{v}\|)}{\|\mathbf{v}\|^2} \tilde{\mathbf{v}}\tilde{\mathbf{v}}^T + \frac{\exp(-\|\mathbf{v}\|)}{\|\mathbf{v}\|^2} \tilde{\mathbf{v}}_\perp\tilde{\mathbf{v}}_\perp^T = \cosh(\|\mathbf{v}\|) \mathbf{I} + \frac{\sinh(\|\mathbf{v}\|)}{\|\mathbf{v}\|} \begin{bmatrix} v_1 & v_2 \\ v_2 & -v_1 \end{bmatrix}. \quad (10)$$

The link with the parameterization in [Fuglstad et al. \(2015\)](#) is the following

**Proposition 1.** *Let  $\mathbf{H}_{v(\alpha)}$ ,  $\mathbf{H}_v$  be as in (8), (10), then if we set*

$$\mathbf{v}(\alpha) = \pm \tilde{\mathbf{v}}/\|\mathbf{v}\|, \quad \gamma = \exp(-\|\mathbf{v}\|), \quad \beta = (1 - \gamma^2)/\gamma.$$

*We obtain  $\mathbf{H}_{v(\alpha)} = \mathbf{H}_v$ .*

The idea behind the usage of the half angle version  $\tilde{\mathbf{v}}$  of  $\mathbf{v}$  is that it avoids any issues of identifiability in the sign as  $\tilde{\mathbf{v}}$  and  $-\tilde{\mathbf{v}}$  do not simultaneously belong to the parameter space. Parameterization using a Cholesky decomposition of  $\mathbf{H}$  is also possible and is more readily generalized to higher dimensions. However, it is not as easily interpretable in terms of intrinsic properties of  $u$ .

In [Figure 1](#), we show the half-angle vector field together with the parameterized diffusion matrices  $\mathbf{H}_v$ . Here, each  $\mathbf{H}_v$  is represented by the ellipse centred at  $\mathbf{v}$  whose main axis

is  $\exp(\|\mathbf{v}\|)\tilde{\mathbf{v}}/\|\mathbf{v}\|$  and whose secondary axis is  $\exp(-\|\mathbf{v}\|)\tilde{\mathbf{v}}_{\perp}/\|\mathbf{v}\|$ . That is, the axes of the ellipses correspond to the eigenvectors of  $\mathbf{H}_{\mathbf{v}}$  scaled by their respective eigenvalues. Figure 1 shows visually how the anisotropy increases with  $\|\mathbf{v}\|$  and is directed towards  $\tilde{\mathbf{v}}$ . It can also be seen how the parameterization is injective (no two ellipses are the same) and smooth (the ellipses vary smoothly with  $\mathbf{v}$ ).

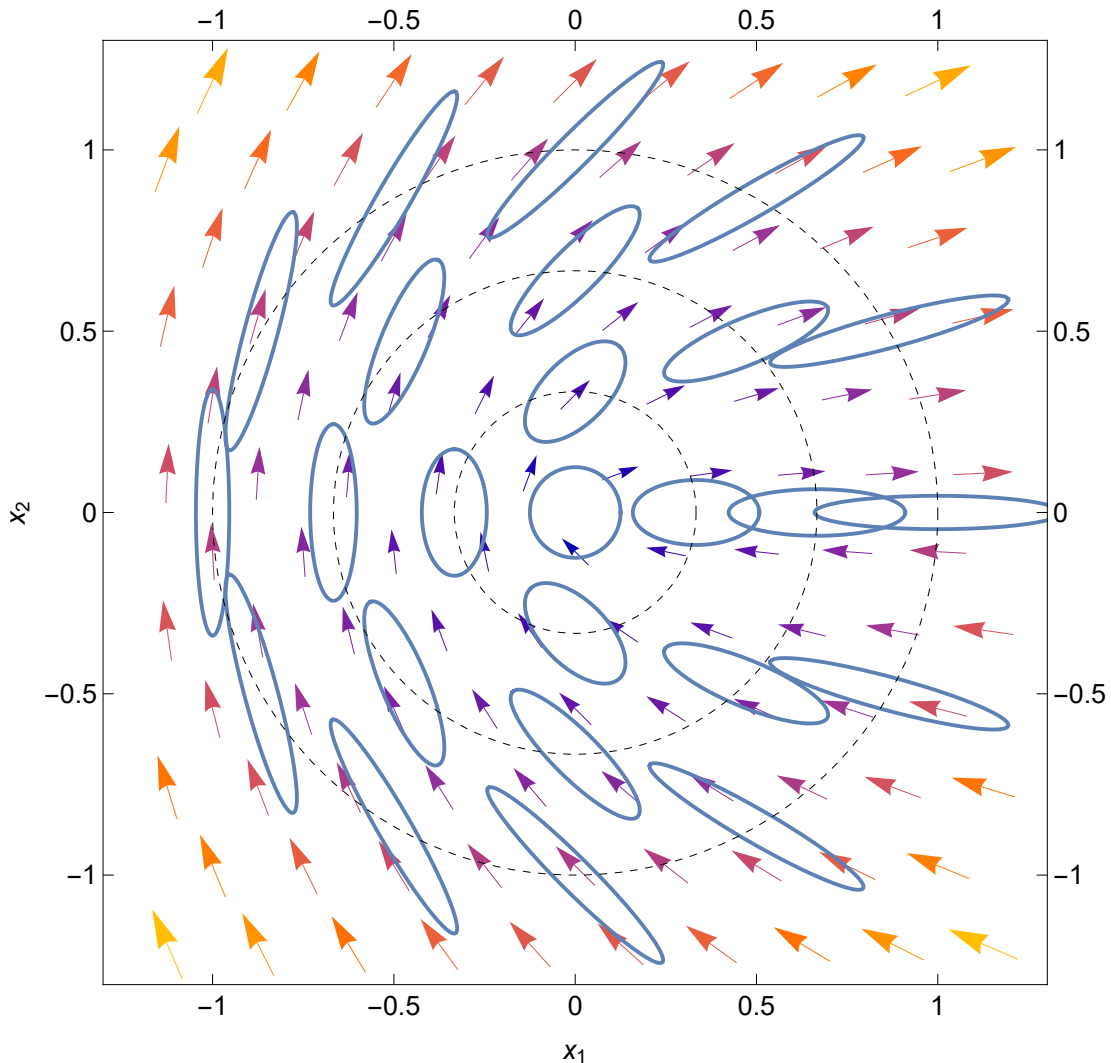
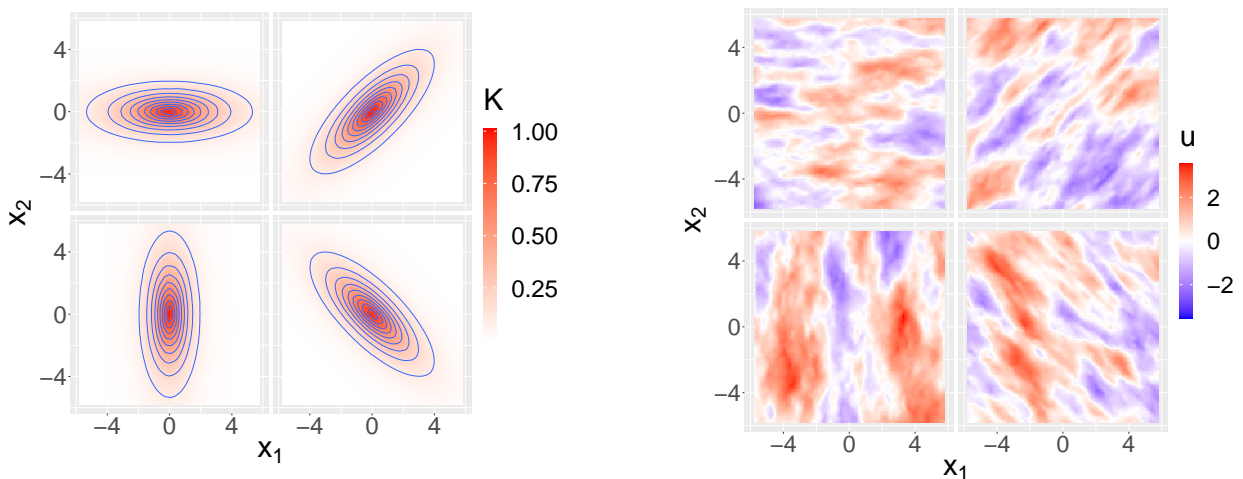


Figure 1: Figure of the half angle field  $\tilde{\mathbf{v}}$  and matrix  $\mathbf{H}_{\mathbf{v}}$  in (9),(10). Each  $\mathbf{H}_{\mathbf{v}}$  is represented by the ellipse centered at  $\mathbf{v}$  with axes the eigenvectors of  $\mathbf{H}_{\mathbf{v}}$  scaled by their respective eigenvalues.

In Figure 2 (a), we show the plot of the covariance  $K(\mathbf{x}, \mathbf{0}) = \mathbb{E}[u(\mathbf{x})u(\mathbf{0})]$  for  $\kappa = 1$

constant and as  $\mathbf{v}$  is rotated around the  $X$ -axis by  $90^\circ$  in each plot. As we can see, the vector field is most correlated in the direction of  $\tilde{\mathbf{v}}$ , which is rotated by  $45^\circ$  in each image, half the speed of rotation of  $\mathbf{v}$ , and is least correlated in the direction of  $\tilde{\mathbf{v}}_\perp$ . In Figure 2 (b), we show simulations of the field where again we leave  $\kappa = 1$  constant and rotate  $\mathbf{v}$  by  $90^\circ$  in each plot. The figure shows that the field diffuses the most in the direction of  $\tilde{\mathbf{v}}$  and the least in the direction of  $\tilde{\mathbf{v}}_\perp$ . The realizations of  $u$  are obtained using a FEM to solve the SPDE as detailed in Section 5.



(a) Covariance  $K(\mathbf{x}, \mathbf{0})$  as  $\mathbf{v}$  varies

(b) Realizations of  $u$  as  $\mathbf{v}$  varies

Figure 2: We fix  $\kappa = \sigma_u = 1$  and plot the covariance  $K(\cdot, \mathbf{0})$  and a realization of the solution  $u$  to (3) as  $\mathbf{v}$  varies from left to right and top to bottom through  $(1, 0)$ ,  $(0, 1)$ ,  $(-1, 0)$ ,  $(0, -1)$ .

Another method that could be used to simulate the field  $u$  and obtain the variance plots is the *spectral method*. The spectral method uses the *spectral density* of the field (the Fourier transform of the covariance function  $r$  if it exists)

$$S(\boldsymbol{\xi}) := \int_{\mathcal{D}} \exp(-2\pi i \boldsymbol{\xi} \cdot \mathbf{x}) r(\mathbf{x}) dx, \quad \boldsymbol{\xi} \in \widehat{\mathcal{D}}, \quad (11)$$

to sample from the field, where  $\widehat{\mathcal{D}}$  is Fourier domain (that is,  $\widehat{\mathcal{D}} = \mathbb{Z}^d$  if  $\mathcal{D} \subset \mathbb{R}^d$  is a box

and  $\widehat{\mathcal{D}} = \mathbb{R}^d$  if  $\mathcal{D} = \mathbb{R}^d$ ). The field  $u$  is then sampled using the stochastic integral. The spectrum for stationary fields  $u$  solving (3) is given by (see Section S2 and Lindgren (2012))

$$S(\boldsymbol{\xi}) = \frac{4\pi\kappa^2\sigma_u^2}{(\kappa^2 + 4\pi^2\boldsymbol{\xi}^T\mathbf{H}\boldsymbol{\xi})^2}. \quad (12)$$

Then, the covariance can be calculated as the Fourier transform of the spectrum, whereas the field  $u$  can be sampled using the stochastic integral

$$u(\mathbf{x}) = \int_{\mathcal{D}} u(\boldsymbol{\xi}) \exp(2\pi i\boldsymbol{\xi} \cdot \mathbf{x}) dZ(\boldsymbol{\xi}), \quad (13)$$

where  $Z(\boldsymbol{\xi})$  is called the *spectral process*. Using the fast Fourier transform, high-resolution samples of  $u$  can be obtained. See Lindgren et al. (2020) for the details.

Thus far, we have worked with constant  $\mathbf{v}$ . The same parameterization goes through when  $\mathbf{H}(\mathbf{x})$  is allowed to be spatially varying. In this case,  $\mathbf{v}(\mathbf{x})$  is a spatial vector field. In Figure 3, we take  $\kappa = \sigma_u = 1$  and show the covariance  $K(\mathbf{x}, (2, 2))$  and field  $u$  when  $\mathbf{v}(\mathbf{x})$  is chosen to be the “twice-angle” field of the rotational field  $\tilde{\mathbf{v}}(\mathbf{x}) = (-x_2, x_1)$  (left of each subfigure), and from when  $\mathbf{v}(\mathbf{x}) = (x_1, x_2)$  (right of each subfigure). The figures show how the information of the field diffuses infinitesimally in the direction of  $\tilde{\mathbf{v}}$ . The covariance and samples are once more obtained using the finite element method. In this non-stationary setting, the spectral method cannot be used as the spectrum is only defined for stationary fields.

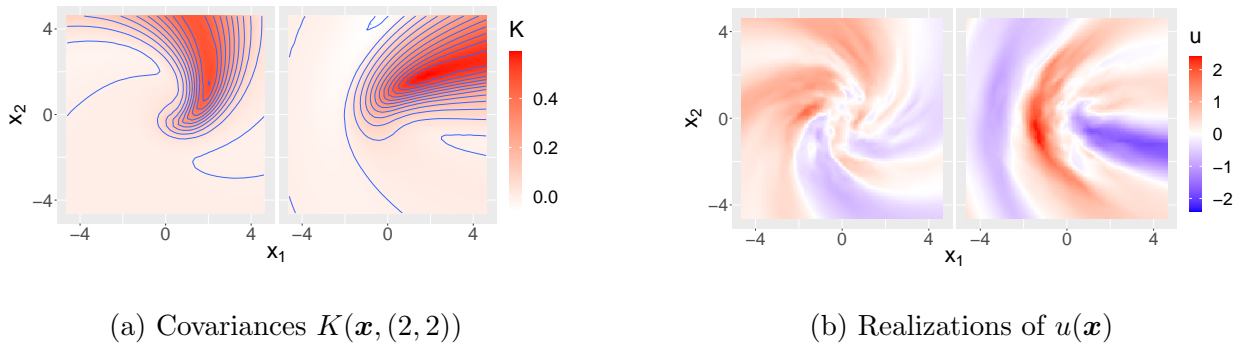


Figure 3: We fix  $\kappa = \sigma_u = 1$  and plot the covariance  $K(\cdot, (2, 2))$  and realizations of solution  $u$  to (3) for  $\tilde{\mathbf{v}}(\mathbf{x}) = (-x_2, x_1)$  on the left and  $\mathbf{v}(\mathbf{x}) = (x_1, x_2)$  on the right of each subfigure.

In summary, we have parameterized the anisotropic field  $u$  using parameters  $(\kappa, v_1, v_2, \sigma_u)$ , where  $u$  solves (3) and  $\mathbf{H} := \mathbf{H}_{\mathbf{v}}$  is given by (10). The parameterization is identifiable and smooth, and the parameters have an intrinsic geometric interpretation. This will be the parameterization used throughout the paper.

## 4 Penalized complexity priors

PC priors were originally developed in [Simpson et al. \(2014\)](#) to construct weakly informative priors while adhering to certain principles. The main idea is that one has a parametric family of models  $M_{\boldsymbol{\theta}}$  with parameter  $\boldsymbol{\theta}$  and a base model  $M_{\mathbf{0}}$  (by convention corresponding to  $\boldsymbol{\theta} = \mathbf{0}$ ).

One views  $M_{\mathbf{0}}$  as the most suitable in the absence of any information. The larger the distance  $\zeta(M_{\boldsymbol{\theta}}, M_{\mathbf{0}})$  between a model  $M_{\boldsymbol{\theta}}$  and  $M_{\mathbf{0}}$ , the smaller the prior density for  $\boldsymbol{\theta}$  should be, and the decrease is set to be exponential. That is, we choose the prior distribution for  $\boldsymbol{\theta}$ , such that:

$$d(\boldsymbol{\theta}) := \zeta(M_{\boldsymbol{\theta}}, M_{\mathbf{0}}) \sim \text{Exp}(\lambda_{\boldsymbol{\theta}}). \quad (14)$$

Here, the rate  $\lambda_{\boldsymbol{\theta}} > 0$  of the exponential distribution serves as a hyperparameter selected by

the user, which governs the model’s flexibility. A smaller value of  $\lambda_{\boldsymbol{\theta}}$  increases the model’s flexibility, allowing for greater deviations of  $M_{\boldsymbol{\theta}}$  from the base model  $M_{\mathbf{0}}$ . Conversely, a larger value of  $\lambda_{\boldsymbol{\theta}}$  imposes stricter penalties on these deviations, thereby reducing the model’s flexibility. In the previously cited [Simpson et al. \(2014\)](#), this notion of “distance” was taken to be

$$\eta(M_{\boldsymbol{\theta}}, M_{\mathbf{0}}) := \sqrt{2\text{KLD}(M_{\boldsymbol{\theta}}||M_{\mathbf{0}})},$$

where KLD is the Kullback-Leibler divergence

$$\text{KLD}(M_{\boldsymbol{\theta}}||M_{\mathbf{0}}) := \int_E \log \left( \frac{dM_{\boldsymbol{\theta}}}{dM_{\mathbf{0}}} \right) dM_{\boldsymbol{\theta}}.$$

One possible complication of using the KL divergence to define the distance is that the Radon–Nikodym derivative  $\frac{dM_{\boldsymbol{\theta}}}{dM_{\mathbf{0}}}$  does not exist. In fact, in the case of our model, if the variances of  $M_{\boldsymbol{\theta}}$  and  $M_{\mathbf{0}}$  are equal, for any possible base model  $u_{\mathbf{0}}$  and  $\boldsymbol{\theta} \neq \mathbf{0}$  the measures  $M_{\boldsymbol{\theta}}$  and  $M_{\mathbf{0}}$  are singular. That is, with the usual convention,

$$\text{KLD}(M_{\boldsymbol{\theta}}||M_{\mathbf{0}}) = \infty. \tag{15}$$

The proof of this fact is given in Section [S2.1](#). Equation [\(15\)](#) makes an exact adherence to the previous steps impossible. As a result, we will merely adopt the principles of the PC prior construction (exponential penalization of complexity) while altering how we measure complexity between models. The idea of modifying the metric used to measure complexity has also been carried out in different settings, such as in [Bolin et al. \(2023\)](#); [Uribe et al. \(2021\)](#), where a Wasserstein distance was used. The possibility of using the Wasserstein distance to measure the complexity of the model [\(3\)](#) was also considered. However, the Wasserstein distance is bounded in this setting (see Section [S2.3](#) in the supplementary material) and, as a result, was discarded. Thus, one of the main challenges is to find a computationally feasible distance that captures relevant information about our model. To this aim, we give the following definition.

**Definition 1.** Given two sufficiently regular models  $u_A \sim M_A, u_B \sim M_B$ , with respective spectral densities  $S_A, S_B$  and variances  $\sigma_A, \sigma_B$ , we define the pseudometric

$$D_2(M_A, M_B) := \left( \int_{\mathbb{R}^2} \|2\pi\xi\|^4 \left( \frac{S_A(\xi)}{\sigma_A^2} - \frac{S_B(\xi)}{\sigma_B^2} \right)^2 d\xi \right)^{\frac{1}{2}}. \quad (16)$$

The above definition uses the rescaled spectral densities of each field to define a Sobolev seminorm on the difference of the correlations of  $M_A, M_B$ . For more details on how this distance was chosen and other distances that were considered, see Section S2.

Write  $M_{\kappa, \mathbf{v}}$  for the model given by SPDE (3) with parameters  $(\kappa, \mathbf{v})$  and with variance fixed to  $\sigma_u = 1$ . Due to the rescaling of the spectral densities in Definition 1, the choice of  $\sigma_u$  does not affect the distance between models and can be set to any other positive value.

We define the base model as the limit in distribution of  $M_{\kappa, \mathbf{v}}$  as  $\kappa, \mathbf{v}$  go to zero

$$M_{\mathbf{0}} := \lim_{(\kappa_0, \mathbf{v}_0) \rightarrow \mathbf{0}} M_{\kappa_0, \mathbf{v}_0} = \mathcal{N}(0, \mathbf{1} \otimes \mathbf{1}),$$

where  $\mathbf{1} : \mathcal{D} \rightarrow \mathbb{R}$  is the constant function,  $z \in \mathcal{D} \mapsto 1$  and  $(f \otimes g)(\mathbf{x}, \mathbf{y}) := f(\mathbf{x})g(\mathbf{y})$ .

That is,  $u_{\mathbf{0}}$  is constant over space and follows a Gaussian distribution with variance 1. We choose this  $u_{\mathbf{0}}$  as our base model as it is simple, and  $(\kappa, \mathbf{v}) = \mathbf{0}$  is the only distinguished point in the parameter space.

To reflect the dependency of this distance on the parameters, we use the notation

$$d(\kappa, \mathbf{v}) := D_2(M_{\kappa, \mathbf{v}}, M_{\mathbf{0}}) := \lim_{(\kappa_0, \mathbf{v}_0) \rightarrow \mathbf{0}} D_2(M_{\kappa, \mathbf{v}}, M_{\kappa_0, \mathbf{v}_0}). \quad (17)$$

The exponential penalization in (14) imposes one condition on the prior of  $(\kappa, \mathbf{v})$  whereas, since  $(\kappa, \mathbf{v})$  is three dimensional, two more conditions are necessary to determine the prior distribution uniquely. In Fuglstad et al. (2019), this issue was circumvented by working iteratively, fixing one parameter while letting the other vary, building PC priors on each parameter, and then multiplying them together to get a joint prior. However, we prefer to

work jointly from the start. This approach is made possible by the structure of  $d$ , which is calculated to have the form

$$d(\kappa, \mathbf{v}) = f(\|\mathbf{v}\|)g(\kappa) \quad (18)$$

Since the angle  $\alpha := \arg(\mathbf{v})$  does not affect (18), we impose that  $\alpha$  is uniformly distributed in  $[0, 2\pi)$ . This choice guarantees that we do not favor the alignment of the covariance of  $u$  in any direction of the plane. Next, since the contribution of  $f$  and  $g$  to the distance is symmetric, we impose that  $f - f(0)$  and  $g$  knowing  $f$  are exponentially distributed. The translation is necessary as  $f$  takes a nonzero minimum  $f(0)$  at  $\|\mathbf{v}\| = 0$ , whereas  $g$  takes a minimum of 0 at  $\kappa = 0$ .

This construction leads to the distance  $d(\kappa, \mathbf{v})$  being exponentially distributed and gives us three conditions that uniquely determine  $(\kappa, \mathbf{v})$ .

**Theorem 2** (PC prior for  $(\kappa, \mathbf{v})$ ). *A PC prior for  $(\kappa, \mathbf{v})$  with base model  $(\kappa, \mathbf{v}) = \mathbf{0}$  is*

$$\pi(\kappa, \mathbf{v}) = \frac{\lambda_{\theta}\lambda_{\mathbf{v}}f'(\|\mathbf{v}\|)f(\|\mathbf{v}\|)}{2\pi\|\mathbf{v}\|} \exp(-\lambda_{\mathbf{v}}(f(\|\mathbf{v}\|) - f(0)) - \lambda_{\theta}f(\|\mathbf{v}\|)\kappa), \quad (19)$$

where  $\lambda_{\theta} > 0, \lambda_{\mathbf{v}} > 0$  are hyperparameters and

$$f(r) := \left(\frac{\pi}{3}(3 \cosh(2r) + 1)\right)^{\frac{1}{2}}, \quad f'(r) = \frac{\sqrt{\pi} \sinh(2r)}{\sqrt{\cosh(2r) + 1/3}}. \quad (20)$$

See Section S3 in the supplementary material for a proof of this and other results of this section. We plot the marginal density of the prior on  $\kappa$  and  $\mathbf{v}$  for  $\lambda_{\theta} = \lambda_{\mathbf{v}} = 16\pi^2$  in Figure 4. The marginal prior densities take a maximum at  $\kappa = 0$  and  $\mathbf{v} = 0$  respectively, and by construction, the prior on  $\mathbf{v}$  is radially symmetric.



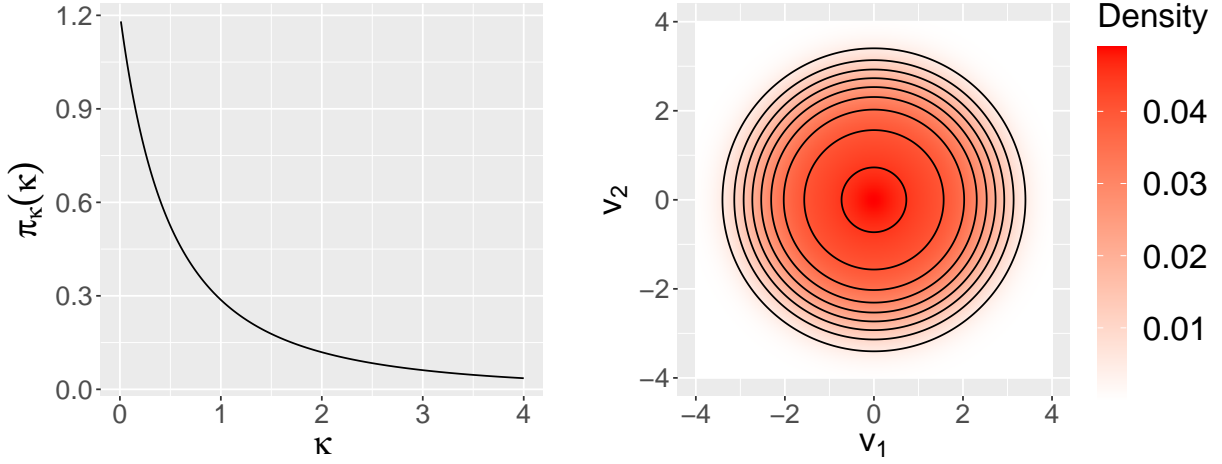


Figure 4: Marginal PC prior density of  $\kappa$  and  $\mathbf{v}$  obtained in Theorem 2 for  $\lambda_{\theta} = \lambda_{\mathbf{v}} = 0.1$ .

The hyperparameter  $\lambda_{\theta}$  determines the flexibility of the model (how much we penalize large values of  $d(\kappa, \mathbf{v})$ ), whereas  $\lambda_{\mathbf{v}}$  controls the degree of anisotropy (how much we penalize large values of  $\|\mathbf{v}\|$ ). Their values can be set to agree with desired quantiles using the following two results.

**Theorem 3.** *The prior for  $r := \|\mathbf{v}\|$  satisfies  $\mathbb{P}[r > r_0] = \beta$  if and only if*

$$\lambda_{\mathbf{v}} = -\frac{\log(\beta)}{f(r_0) - f(0)}.$$

**Theorem 4.** *The prior for  $\kappa$  satisfies  $\mathbb{P}[\kappa > \kappa_0] = \alpha$  if and only if*

$$\lambda_{\theta} = \frac{1}{\kappa_0} \left( \frac{1}{f(0)} W_0 \left( \frac{\exp(\lambda_{\mathbf{v}} f(0)) \lambda_{\mathbf{v}} f(0)}{\alpha} \right) - \lambda_{\mathbf{v}} \right),$$

where  $W_0$  is the principal branch of the Lambert function. That is,  $W_0(x)$  is the real-valued inverse of  $x \exp(x)$  for  $x \geq 0$ ,

$$x = W_0(x) \exp(W_0(x)), \quad \forall x \geq 0.$$

When specifying values of  $\lambda_{\theta}, \lambda_{\mathbf{v}}$ , it is useful to consider the ratio between the eigenvalues of  $\mathbf{H}_{\mathbf{v}}$  and the empirical correlation range. These measure respectively how much more

correlated the field is in one direction in space and the distance at which the field becomes essentially uncorrelated (see Section 3). We denote these by

$$a := \exp(\|\mathbf{v}\|), \quad \rho := \sqrt{8}\kappa^{-1}.$$

Theorem 3 and Theorem 4 can then be rewritten as follows.

**Theorem 5.** *The PC priors in satisfy that  $\mathbb{P}[a > a_0] = \beta$  and  $\mathbb{P}[\rho < \rho_0] = \alpha$  if and only if*

$$\lambda_{\mathbf{v}} = -\frac{\log(\beta)}{f(\log(a_0)) - f(0)}, \quad \lambda_{\theta} = \frac{\rho_0}{\sqrt{8}} \left( \frac{1}{f(0)} W_0 \left( \frac{\exp(\lambda_{\mathbf{v}} f(0)) \lambda_{\mathbf{v}} f(0)}{\alpha} \right) - \lambda_{\mathbf{v}} \right).$$

In a practical application,  $\alpha, \beta$  can be chosen to be small (for example 0.01),  $a_0$  can be chosen to be an unexpectedly large amount of anisotropy, and  $\rho_0$  can be chosen as a surprisingly small correlation range for the field.

The parameters  $(\kappa, \mathbf{v})$  can be written as a joint transformation of a three-dimensional vector with standard multivariate Gaussian distribution. Thus, it is possible to efficiently generate independent samples  $(\kappa, \mathbf{v})$  through sampling multivariate Gaussian random variables, which is straightforward.

**Theorem 6.** *Let  $\mathbf{Y} \sim \mathcal{N}(\mathbf{0}, \mathbf{I}_3)$  and write respectively  $\Phi, R$  for the CDFs of a univariate standard Gaussian and Rayleigh distribution with shape parameter 1. Define*

$$A := \sqrt{Y_1^2 + Y_2^2}, \quad B := f(0) - \log(1 - R(A))/\lambda_{\mathbf{v}}.$$

*Then, it holds that*

$$(v_1, v_2, \kappa) \stackrel{d}{=} \varphi(Y_1, Y_2, Y_3) := \left( f^{-1}(B) \frac{Y_1}{A}, f^{-1}(B) \frac{Y_2}{A}, -\frac{\log(1 - \Phi(Y_3))}{\lambda_{\theta} B} \right),$$

where  $f^{-1}(x) = \frac{1}{2} \cosh^{-1} \left( 4x^2 - \frac{1}{3} \right)$ .

The transformation  $\varphi$  only involves standard functions and can be evaluated efficiently.

For the proof, see Section S4.

## 5 Simulation study

### 5.1 Framework

This section aims to study the performance of the PC priors. To do so, we set different priors  $\pi_{\kappa, \mathbf{v}}$  on  $\kappa, \mathbf{v}$ , observe a noisy realization of the field, and compare the behavior of the posteriors, resulting from each prior. We consider the random field  $u$  that solves our model (3) on the square domain  $\mathcal{D} = [0, 10]^2$  and define the observation process

$$\mathbf{y} = \mathbf{A}\mathbf{u} + \boldsymbol{\varepsilon}, \quad (21)$$

where  $\mathbf{u} \in \mathbb{R}^n$  is a discrete approximation of the solution to (3) obtained through a FEM on a mesh with  $n$  nodes, and  $\mathbf{A} \in \mathbb{R}^{m \times n}$  linearly interpolates to observe  $\mathbf{u}$  at  $m = 15$  locations  $\{\mathbf{x}_j\}_{j=1}^m$  which are obtained by sampling uniformly from  $\mathcal{D}$ , and  $\boldsymbol{\varepsilon} \in \mathbb{R}^m$  is a noise vector with

$$\boldsymbol{\varepsilon} \sim \mathcal{N}(\mathbf{0}, \mathbf{Q}_{\boldsymbol{\varepsilon}}^{-1}), \quad \mathbf{Q}_{\boldsymbol{\varepsilon}} := \sigma_{\boldsymbol{\varepsilon}}^{-2} \mathbf{I}_n. \quad (22)$$

The details of how  $\mathbf{u}$  is sampled from and more detailed results can be found in Section S5.

We set independent priors

$$(\kappa, \mathbf{v}) \sim \pi_{\kappa, \mathbf{v}}, \quad \sigma_u \sim \text{Exp}(\lambda_{\sigma_u}), \quad \sigma_{\boldsymbol{\varepsilon}} \sim \text{Exp}(\lambda_{\sigma_{\boldsymbol{\varepsilon}}}). \quad (23)$$

The priors on  $\sigma_u, \sigma_{\boldsymbol{\varepsilon}}$  correspond to their respective PC priors (see respectively [Simpson et al. \(2014\)](#) Section 3.3, [Fuglstad et al. \(2019\)](#) Theorem 2.1) with hyperparameters  $\lambda_{\sigma_u}, \lambda_{\sigma_{\boldsymbol{\varepsilon}}}$  chosen so that

$$\mathbb{P}[\sigma_u > \sigma_0] = 0.01, \quad \mathbb{P}[\sigma_{\boldsymbol{\varepsilon}} > \sigma_1] = 0.01,$$

where we take  $\sigma_0 = 10, \sigma_1 = 1.5$ .

The prior  $\pi_{\kappa, \mathbf{v}}$  is one of the priors to be compared (among them the PC prior). We consider the following options for  $\pi_{\kappa, \mathbf{v}}$ :

1. The PC priors in (19) where the anisotropy hyperparameters  $\lambda_{\boldsymbol{\theta}}, \lambda_{\mathbf{v}}$  are chosen so that the anisotropy ratio  $a = \exp(|\mathbf{v}|)$  and the correlation range  $\rho = \sqrt{8}\kappa^{-1}$  satisfy

$$\mathbb{P}[a > a_0] = 0.01, \quad \mathbb{P}[\rho < \rho_0] = 0.01, \quad (24)$$

where we take  $a_0 = 10, \rho_0 = 1$ . This choice of hyperparameters corresponds to allowing with probability 0.01 that the field is 10 times more correlated in any given direction and, with the same probability, that the field has a correlation range smaller than 1. The values of  $\lambda_{\boldsymbol{\theta}}, \lambda_{\mathbf{v}}$  can then be calculated using Theorem 5.

2. Independent priors  $\kappa \sim \text{Exp}(\lambda_{\kappa})$  and  $\mathbf{v} \sim \mathcal{N}(\mathbf{0}, \sigma_{\mathbf{v}}^2 \mathbf{I}_2)$ . Under these priors,  $\kappa, \mathbf{v}$  have the same mode as the PC priors (0 in each case). Additionally,  $\lambda_{\kappa}, \sigma_{\mathbf{v}}^2$  are chosen such that, under these priors, (24) also holds. We denote this prior by  $\pi_{\text{EG}}$ .
3. Independent (improper) uniform priors for  $\log(\kappa), \mathbf{v}$  with infinite support. We denote this prior by  $\pi_{\text{U}}$ .
4. Independent linear transformations of beta priors on  $\log(\kappa), v_1, v_2$  with shape parameters 1.1 such that the correlation range is supported in  $[\rho_0/w, wL]$  and  $v_1, v_2$  are supported in  $[-wa_0, wa_0]$ . The shape parameter is chosen so that the distribution is approximately uniform while having smooth density, which is relevant for the optimization. The purpose of  $w > 1$  is to extend the support of the parameters past  $\rho_0, a_0$ . The same value of  $\rho_0 = 1$  is taken,  $L = 10$  is taken to be the length of  $\mathcal{D}$ , and  $w$  is set to 20. We denote this prior by  $\pi_{\beta}$ .

We simulate  $\boldsymbol{\theta}^{(j)\text{true}}$  from  $\pi_{\text{sim}} \in \{\pi_{\text{PC}}, \pi_{\text{EG}}, \pi_{\text{U}}, \pi_{\beta}\}$ , use the FEM to simulate  $\mathbf{u}^{(j)}$  from (3) and then simulate  $\mathbf{y}^{(j)}$  from (21). Then, for each of the four priors  $\pi_{\kappa, \mathbf{v}} \in \{\pi_{\text{PC}}, \pi_{\text{EG}}, \pi_{\text{U}}, \pi_{\beta}\}$  we approximate the posterior distribution of the parameters  $\boldsymbol{\theta} = (\kappa, \mathbf{v}, \sigma_u, \sigma_{\epsilon})$  given the data  $\mathbf{y}^{(j)}$  and evaluate the performance of each of the four priors. This process is repeated

$J = 600$  times and repeated for each of the four possible values of  $\pi_{\text{sim}}$ . Since the posterior is not available in closed form, it is necessary to approximate it. We considered three choices: approximating the posterior by the Gaussian  $Z$  with the same median and whose precision is minus the Hessian of the posterior at its median, using importance sampling with  $Z$  as the proposal distribution, and using smoothed importance sampling with  $Z$  as the proposal distribution. Of these three approximations, the best performing method was *smoothed importance sampling*. As a result, this is the method we use in the following section to approximate integrals against the posterior. The details of the different approximations can be found in Section S5.3 in the supplementary material.

## 5.2 Results

The focus of our study is the anisotropy parameters  $(\kappa, v_1, v_2)$ . As a result, in this section, we will focus on the performance of the different priors on these parameters and relegate the results for the remaining parameters to Section S5.

We first show in Figure 5 the empirical cumulative distribution function (eCDF) of the vector of distances of the true anisotropy parameters  $(\log(\kappa^{\text{true}}), v_1^{\text{true}}, v_2^{\text{true}})$  to the MAP estimates  $(\log(\hat{\kappa}), \hat{v}_1, \hat{v}_2)$  for each of the four different distributions on  $\boldsymbol{\theta}^{\text{true}}$ .

We observe that  $\pi_{\text{PC}}$  and  $\pi_{\text{EG}}$  perform the best and give almost identical results, to the point where it is difficult to distinguish them from the plots. This behavior is to be expected as both these priors are similar and lead to almost identical posteriors, as is discussed further in Section S5.

The difference in performance between  $\pi_{\text{PC}}, \pi_{\text{EG}}$  and  $\pi_{\text{U}}, \pi_{\beta}$  is clearest for  $v_1, v_2$  whereas for  $\log(\kappa)$ , when  $\boldsymbol{\theta}^{\text{true}} \sim \pi_{\text{U}}$  or  $\boldsymbol{\theta}^{\text{true}} \sim \pi_{\beta}$  all four models give comparable results. The figures relative to the parameters  $v_1$  and  $v_2$  are almost identical. This is expected by the

symmetry in the priors and the likelihood, as there is no preferred direction of anisotropy.

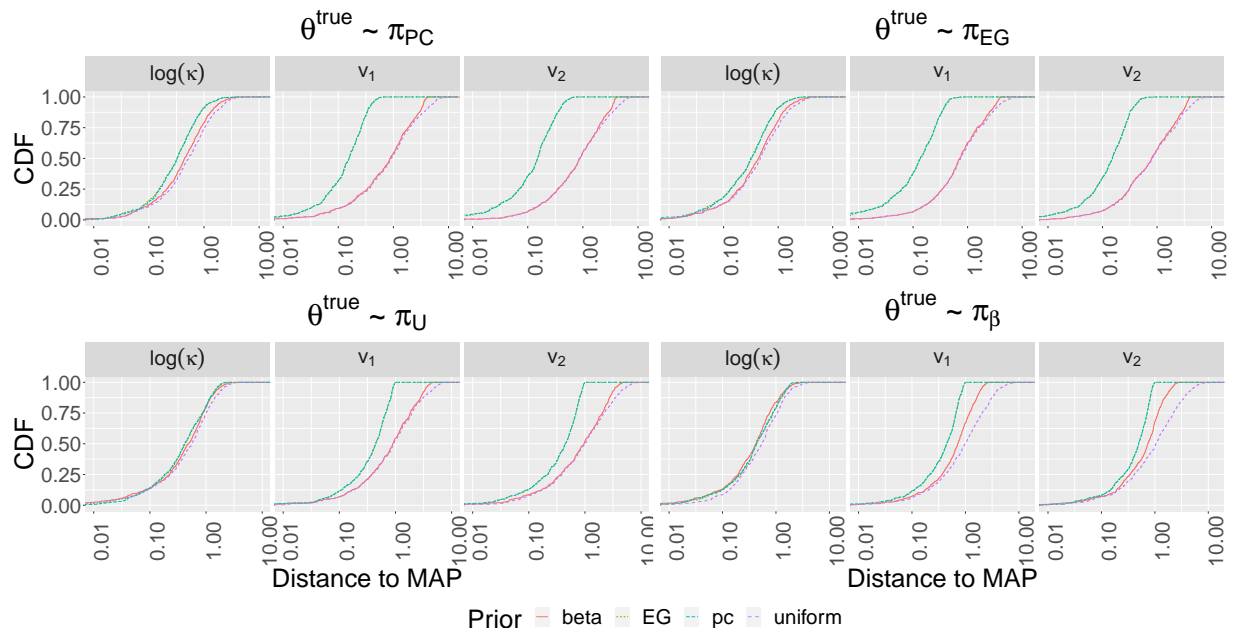


Figure 5: Empirical cumulative distribution function (eCDF) of the absolute distances between true parameter value ( $\theta_i^{\text{true}}$ ) and their estimated values ( $\hat{\theta}_i$ ) for each of  $\log(\kappa)$ ,  $v_1$ ,  $v_2$ . In the plots, arranged from left to right and top to bottom,  $\theta^{\text{true}}$  is simulated from the four distributions— $\pi_{\text{PC}}$ ,  $\pi_{\text{EG}}$ ,  $\pi_{\text{U}}$ , and  $\pi_{\beta}$ . Then,  $\mathbf{y} = \mathbf{A}\mathbf{u} + \boldsymbol{\varepsilon}$  is observed with true parameter value  $\theta^{\text{true}}$ . Finally, for each prior (red, green, teal, purple), the MAP estimate  $\hat{\boldsymbol{\theta}}$  is computed, and the eCDF over 600 simulations of the distances between  $\theta^{\text{true}}$  and  $\hat{\boldsymbol{\theta}}$  is plotted.

Next, in Figure 6, we show the length of the symmetric equal-tailed 0.95 credible interval for each parameter. As can be seen from the plots, both  $\pi_{\text{PC}}$  and  $\pi_{\text{EG}}$  limit the length of the credible intervals to a similar extent while  $\pi_{\text{U}}, \pi_{\beta}$  give much wider credible intervals. This connects with the motivating factor for the construction of the PC priors which is to penalize the complexity of the model.

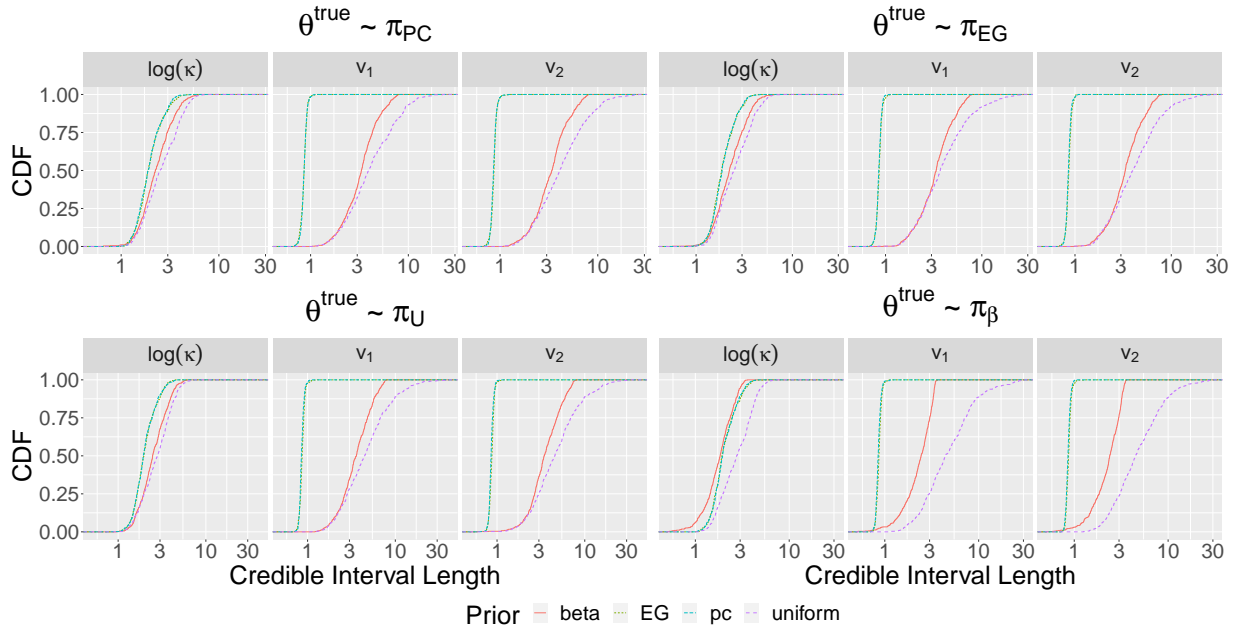


Figure 6: Empirical cumulative distribution function (eCDF) of the length of symmetric equal-tailed 0.95 credible intervals (CIs) for the posterior of  $\log(\kappa)$ ,  $v_1$ ,  $v_2$ . In the plots, arranged from left to right and top to bottom,  $\theta^{\text{true}}$  is simulated from the four distributions— $\pi_{\text{PC}}$ ,  $\pi_{\text{EG}}$ ,  $\pi_{\text{U}}$ , and  $\pi_{\beta}$ . Then,  $\mathbf{y} = \mathbf{A}\mathbf{u} + \varepsilon$  is observed with true parameter value  $\theta^{\text{true}}$ . Finally, for each prior (red, green, teal, purple), the length of the CIs is estimated using smoothed importance sampling as explained in Section S5.3 in the supplementary material.

In Figure 7, we show the eCDF of the posterior mean complexity  $\mathbb{E}_{\pi_{\theta|\mathbf{y}}} [d(\kappa, \mathbf{v})]$ , where the complexity  $d$  is defined in (1) for each of the four different true distributions on  $\theta$ . As can be seen, in all four cases, the PC and exponential-Gaussian priors reduce model complexity as compared to the uniform and beta priors.

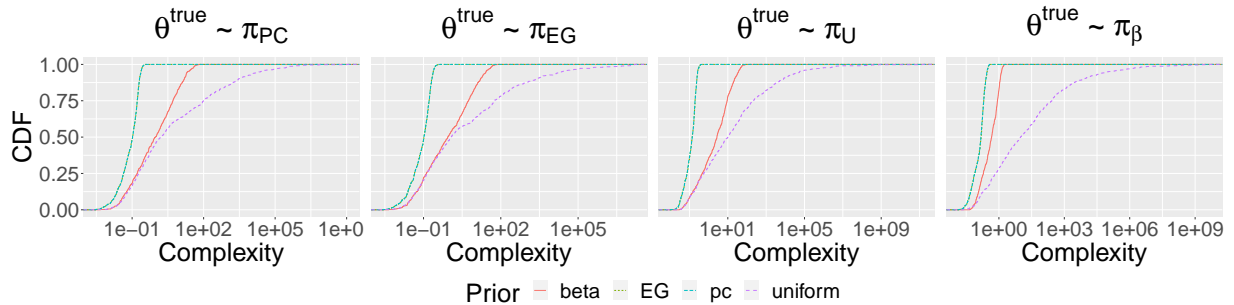


Figure 7: Empirical CDF of the complexity  $d(\hat{\kappa}, \hat{\mathbf{v}})$  defined in (17). In the plots, arranged from left to right,  $\boldsymbol{\theta}^{\text{true}}$  is simulated from the four distributions— $\pi_{\text{PC}}$ ,  $\pi_{\text{EG}}$ ,  $\pi_{\text{U}}$ , and  $\pi_{\beta}$ . Then,  $\mathbf{y} = \mathbf{A}\mathbf{u} + \boldsymbol{\varepsilon}$  is observed with true parameter value  $\boldsymbol{\theta}^{\text{true}}$ . Finally, for each prior (red, green, teal, purple),  $\mathbb{E}_{\pi_{\boldsymbol{\theta}|\mathbf{y}}}[d(\kappa, \mathbf{v})]$  is computed using smoothed importance sampling.

## 6 An application to rainfall data

### 6.1 Framework

In this section, we analyze the performance of the anisotropic model and the PC priors on a data set for total annual precipitation in southern Norway between September 1, 2008, and August 31, 2009. This data set was studied in [Simpson et al. \(2014\)](#), [Ingebrigtsen et al. \(2015\)](#) using a linear model.

$$y_i = \beta_0 + \beta_1 h_i + u(\mathbf{x}_i) + \varepsilon_i, \quad i = 1, \dots, m = 233, \quad (25)$$

where  $y_i$  is the total annual precipitation at location  $\mathbf{x}_i$ ,  $h_i$  is the altitude at location  $\mathbf{x}_i$ ,  $u(\mathbf{x}_i)$  is a spatially correlated random effect, and  $\boldsymbol{\varepsilon} \sim \mathcal{N}(\mathbf{0}, \sigma_{\varepsilon}^2 \mathbf{I})$  is a noise term. In the articles above,  $u$  was modeled using a non-stationary Matérn process

$$(\kappa^2(\mathbf{x}) - \Delta) \left( \frac{u(\mathbf{x})}{\sigma_u(\mathbf{x})} \right) = \sqrt{4\pi\kappa(\mathbf{x})} \dot{\mathcal{W}}.$$



The non-stationarity  $\kappa^2(\mathbf{x}), \sigma_u(\mathbf{x})$  was parameterized by a log-linear model with covariates elevation and gradient of elevation and, in [Simpson et al. \(2014\)](#), priors motivated through the PC prior approach were constructed for these extra parameters.

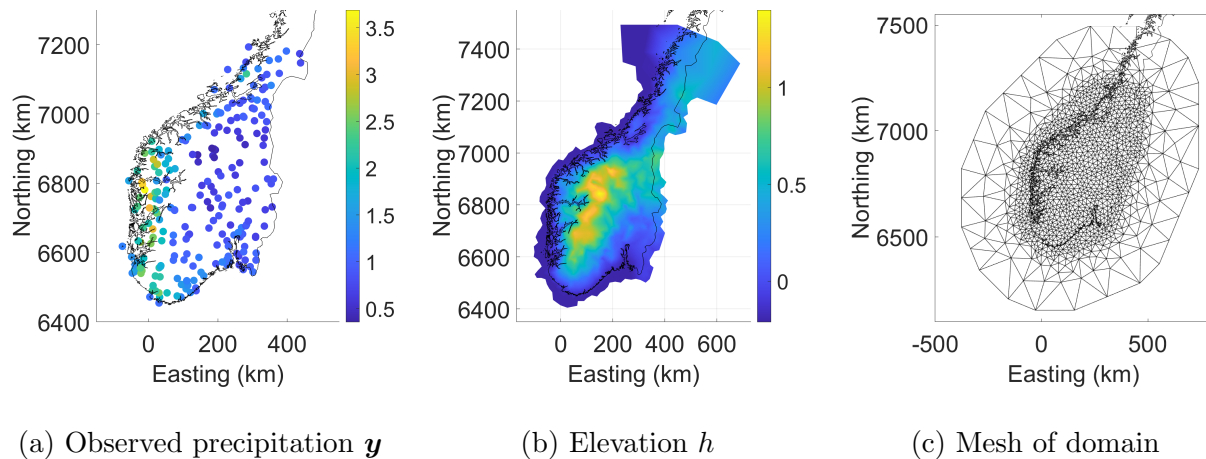


Figure 8: The observed precipitation  $\mathbf{y}$ , the elevation  $h$ , and the mesh of the domain for the precipitation data set.

We will only study the stationary anisotropic setting where  $u|\boldsymbol{\theta}$  is a solution to (3) with spatially constant parameters. By incorporating  $\boldsymbol{\beta} := (\beta_0, \beta_1)$  into  $\mathbf{u}$ , our linear model (25) fits into the framework of Section 5, where now

$$\mathbf{A}_\beta := (\mathbf{1}_m, \mathbf{h}, \mathbf{A}), \quad \mathbf{u}_\beta := (\boldsymbol{\beta}, \mathbf{u})$$

take the place of  $\mathbf{A}, \mathbf{u}$  in (21). We will consider

$$\boldsymbol{\beta} \sim \mathcal{N}(\mathbf{0}, \mathbf{Q}_\beta^{-1}), \quad \mathbf{Q}_\beta = \tau_\beta \mathbf{I}_2$$

independent from  $\mathbf{u}, \boldsymbol{\theta}$  and where we set the precision parameter to be  $\tau_\beta = 10^{-4}$ .

## 6.2 Maximum a posteriori estimates

We compare the model in (25) under anisotropic PC and EG priors (see Item 1 and Item 2) on  $(\kappa, \mathbf{v})$  and isotropic PC priors where  $\mathbf{v}$  is set to  $\mathbf{0}$ . To do so, we must first derive an

isotropic PC prior on  $\kappa$  using the distance metric (16) restricted to the case where  $\mathbf{v} = \mathbf{0}$ .

Using equation (37) we obtain the following result.

$$D_2(M_{\kappa, \mathbf{0}}, M_0) = \frac{1}{\sqrt{12\pi}}\kappa.$$

So, by the principle of exponential penalization,  $\kappa \sim \text{Exp}(\lambda_{\text{iso}})$ . As in [Simpson et al. \(2014\)](#),

we choose the hyperparameters in the three priors so that

$$\mathbb{P}(\rho < 10) = 0.05, \quad \mathbb{P}(\sigma_u > 3) = 0.05, \quad \mathbb{P}(\sigma_\varepsilon > 3) = 0.05.$$

For the anisotropy parameter  $\mathbf{v}$  we choose the hyperparameter  $\lambda_{\mathbf{v}}$  so that  $\mathbb{P}[a > 10] = 0.05$ . This choice of hyperparameters imposes that with probability 0.05, the field has a correlation range that is 10 times larger in any given direction.

In Figure 9, we plot the density of the priors on  $\rho$ . Since the marginal density of  $\rho$  is the same for the isotropic PC and EG priors, we do not plot it. We also plot the density of the PC and (anisotropic) EG priors on  $r := \|\mathbf{v}\|$ .

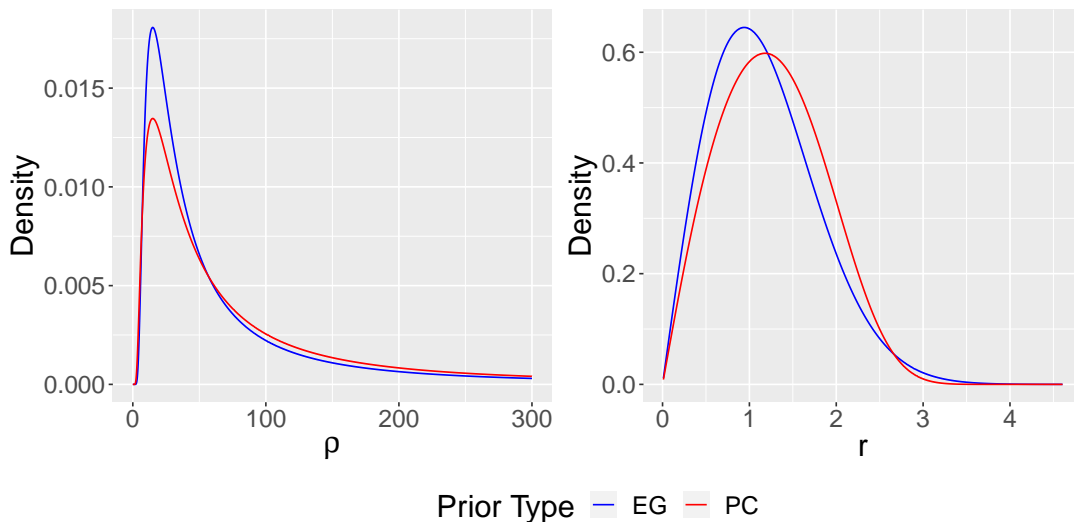


Figure 9: Marginal densities on  $\rho$  and  $r = \|\mathbf{v}\|$  of PC and EG priors

The decay of the marginal PC prior on  $\kappa$  and of the EG prior are both exponential. The

decay rate of the marginal PC prior on  $v$  is  $\exp(-c_1 \exp(\|\mathbf{v}\|))$ , whereas for the EG prior it decays slower, as  $\exp(-c_2 \|\mathbf{v}\|^2)$  for some constants  $c_1, c_2$ .

The MAP estimates and symmetric 95% credible intervals for the anisotropic PC, anisotropic EG, and isotropic PC models are shown in Table 1.

Parameter	MAP Estimates			95% Credible Intervals		
	ANISO PC	ANISO EG	ISO PC	ANISO PC	ANISO EG	ISO PC
$\hat{\rho}$	201	201	193	(132, 310)	(132, 311)	(128, 290)
$\hat{v}_1$	-0.45	-0.43	-	(-0.81, -0.11)	(-0.78, -0.10)	-
$\hat{v}_2$	0.04	0.03	-	(-0.28, 0.35)	(-0.28, 0.34)	-
$\hat{\sigma}_u$	0.63	0.64	0.65	(0.46, 0.88)	(0.46, 0.89)	(0.47, 0.90)
$\hat{\sigma}_\varepsilon$	0.14	0.14	0.13	(0.11, 0.18)	(0.11, 0.18)	(0.10, 0.16)

Table 1: MAP estimates and 95% credible intervals for the parameters of the three different precipitation models: the anisotropic model with PC priors (ANISO PC), the anisotropic model with EG priors (ANISO EG), and the isotropic model with PC priors (ISO PC).

The credible intervals for  $v_1$  in the anisotropic models do not contain 0, indicating that with high confidence, anisotropy is present in the precipitation field.

The half angle vector of the MAP for the anisotropic model with PC priors  $\hat{\mathbf{v}}$  is  $\tilde{\mathbf{v}} = (0.02, 0.48)$ , and indicates that the precipitation is  $a = 1.64$  times more correlated in the North-South direction than in the East-West direction. In Figure 10, we plot the posterior prediction, latent field, and the covariance function of the anisotropic field  $\mathbf{u}$  with parameters  $\hat{\kappa}, \hat{\mathbf{v}}$ .

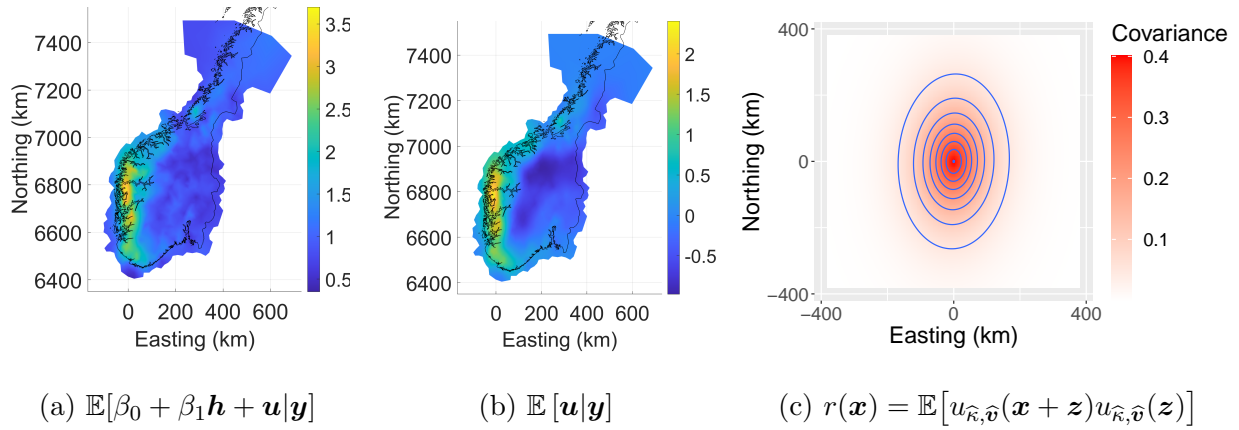


Figure 10: Predictive mean, latent field and covariance function of the anisotropic field  $\mathbf{u}$  for the precipitation data set.

### 6.3 Model performance

To assess the performance of the models, we calculate a variety of scores for each model. We recall that, given a (predictive) distribution  $P$  and an (observed) point  $y$ , a score is a function  $S(P, y)$  that measures how closely the prediction  $P$  matches the observation  $y$ . If  $y$  follows the distribution  $Q$ , then the expected score is

$$S(P, Q) := \mathbb{E}_Q[S(P, y)].$$

The score should be minimized when the true distribution  $Q$  matches the predictive distribution  $P$ . In this case, the score is said to be *proper*. It is *strictly proper* if it is minimized if and only if  $P = Q$ . We will consider the following scores

- Given a distribution  $dF$  and an observation  $x \in \mathbb{R}$  the *squared error* (SE) is defined as

$$\text{SE}(F, x) := \left( x - \int_{-\infty}^{\infty} t dF(t) \right)^2.$$

The expression above defines a proper scoring rule (its value is minimized when  $x$

follows the predictive distribution). However, it is not strictly proper (the minimum in  $F$  is not unique).

- Given a CDF  $F$  and an observation  $x \in \mathbb{R}$ , the *continuous ranked probability score* (CRPS) is defined as [Gneiting and Raftery \(2007\)](#)

$$\text{CRPS}(F, x) := \int_{\mathbb{R}} (F(t) - \mathbf{1}\{x \leq t\})^2 dt.$$

The CRPS is a strictly proper scoring rule on distributions with finite expectations.

- Given a random variable  $\mathbf{X}$  with mean  $\boldsymbol{\mu}$  and precision  $\mathbf{Q}$ , the *Dawid-Sebastiani score* (DSS) is defined as [Dawid and Sebastiani \(1999\)](#)

$$\text{DSS}(\mathbf{X}; \mathbf{x}) := -\log(\|\mathbf{Q}\|) + (\mathbf{x} - \boldsymbol{\mu})^T \mathbf{Q} (\mathbf{x} - \boldsymbol{\mu}).$$

The DSS is similar to a log Gaussian density score and is a strictly proper scoring rule for Gaussian random variables. Still, it also defines a proper score for non-Gaussian random variables.

Given a sample  $\mathbf{y} = (y_1, \dots, y_n)$ , a vector of predictive distributions  $\mathbf{F} = (F_1, \dots, F_n)$  and a score  $S$ , the *mean score* is defined as

$$\overline{S}(\mathbf{F}, \mathbf{y}) := \frac{1}{n} \sum_{i=1}^n S(F_i, y_i).$$

By the linearity of the expectations, if  $S$  is a (strictly) proper scoring rule, then so is  $\overline{S}$ .

## 6.4 Score results

In this section, we calculate the mean scores

$$\text{RMSE} := (\overline{SE}(\mathbf{F}, \mathbf{y}))^{\frac{1}{2}}, \quad \overline{\text{CRPS}}(\mathbf{F}, \mathbf{y}), \quad \overline{\text{DSS}}(\mathbf{F}, \mathbf{y}),$$

where  $F_i := \pi(y_i|\mathbf{y}_{-i})$  is the LOO predictive distribution under each of the three models in Subsection 6.2, and  $\mathbf{y}$  is the observation.

An initial calculation showed that the scores of the previous sections are very similar under all three priors. From this, we conclude that the model is very informative, and the influence of the priors is limited. As a result, to better compare the priors, we uniformly sub-sample  $\mathbf{y}$  and observe only  $\mathbf{y}' \in \mathbb{R}^{n'_y}$  with  $n'_y < n_y = 233$ . We then calculate the scores from the previous sections. Due to the extra variability introduced by sub-sampling the observations, we repeat this process 10 times. The resulting mean scores are shown in Figure 11. The anisotropic models perform better with lesser data, with the PC prior performing slightly better than the EG prior. Whereas with more data the results are almost equivalent.

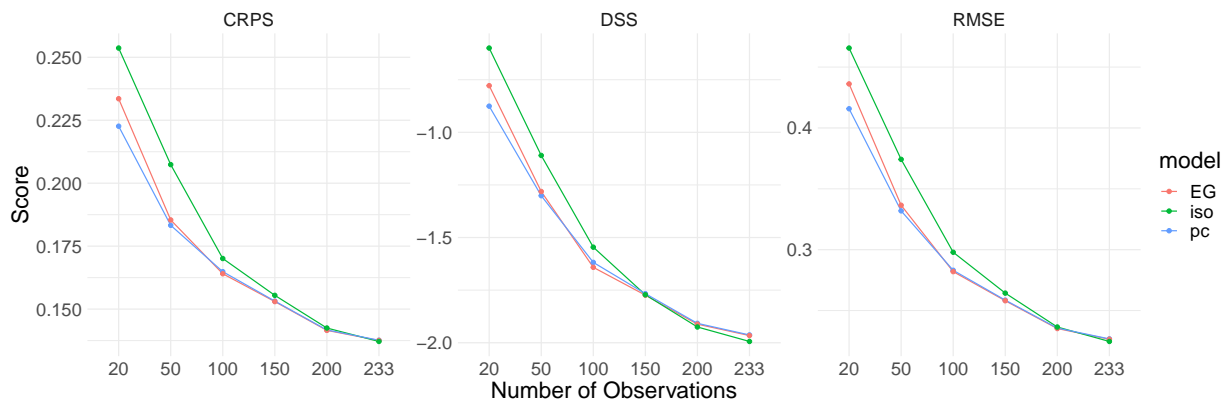


Figure 11: Scores for variable number of observations  $n'_y$

From the trend of the above results it is reasonable to check whether the isotropic model outperforms the other two models with a larger amount of observations. To check this hypothesis we conducted a simulation study where a larger amount of observations are generated, up to  $n_y = 1000$ . The results are included in Section S6.3 in the supplementary material and show that this is not the case. The isotropic model does not outperform the anisotropic models with a larger amount of observations.

## 7 Discussion

In this study, we constructed a smooth, identifiable, and geometrically interpretable parameterization for a 2D anisotropic spatial Gaussian model. We developed penalized complexity (PC) priors for these parameters, defining model complexity as a Sobolev seminorm of the correlation function. This distance was calculated in a closed form using the spectral density.

Our performance comparison of the PC prior against other priors demonstrated its effectiveness in penalizing model complexity. We found that priors designed to match the quantiles of the PC prior yielded similar results. Both these priors significantly outperformed the other non-informative priors considered, highlighting the necessity of incorporating penalization in prior information to prevent overfitting.

Applying the anisotropic model to a real dataset of precipitation in Southern Norway, we observed that the anisotropic model outperformed the isotropic model when the number of observations was small, with the PC prior slightly outperforming the other choices. However, with a larger number of observations, the isotropic model performed similarly to the anisotropic models. These results indicate that the anisotropic model is more informative when the data is scarce, but as the number of observations increases, the isotropic model becomes more competitive. The results also suggest that a nonstationary model could be better suited to capture spatially varying patterns in the data.

In conclusion, we advocate for the use of informative priors for the anisotropy parameters in spatial Gaussian models. The PC prior is highly effective, but other priors designed to match desired quantiles can also be effective and are simpler to construct.

Looking forward, we aim to extend this study to the non-stationary setting where the model parameters vary spatially. This presents a challenge as there is no agreed-upon

definition of correlation function or spectral density, necessitating a different definition of complexity. We are also interested in extending the parameterization to higher dimensions. The current construction relies on a “half-angle” parameterization of the anisotropy vector, which is not easily extendable to higher dimensions. Finally, we are interested in extending the construction to different orders of regularity.



# Supplementary Material

## S1 Proof of Theorem 1

*Proof.* By definition,  $\mathbf{H}_v$  is symmetric with determinant 1. Furthermore, it is positive definite as its eigenvalues are positive. Given a positive definite symmetric matrix  $\mathbf{A}$  with determinant 1,  $\mathbf{A}$  has an eigensystem of the form

$$\{(\mathbf{w}, \lambda), (\mathbf{w}^\perp, \lambda^{-1})\},$$

where  $\lambda \geq 1$ . By normalizing and taking  $-\mathbf{w}$  if necessary we may suppose that  $\mathbf{w} = \exp(\alpha i)$  with  $\alpha \in [0, \pi)$ . Then, we obtain  $\mathbf{A} = \mathbf{H}_v$  for

$$\mathbf{v} = \log(\lambda) \exp(2\alpha i).$$

This proves that the parameterization is surjective. Suppose now that  $\mathbf{H}_v = \mathbf{H}_{v'}$  then their eigenvalues and eigenvectors must be equal so

$$\exp(\|\mathbf{v}\|) = \exp(\|\mathbf{v}'\|), \quad \tilde{v} = a\tilde{v}'.$$

For some  $a \in \mathbb{R}$ . From the first condition, we deduce that  $\|\mathbf{v}\| = \|\mathbf{v}'\|$ . Taking absolute values in the second condition thus gives  $|a| = 1$ . By construction  $\tilde{v} \neq -\tilde{v}'$  for all  $v, v'$  so necessarily  $\mathbf{v} = \mathbf{v}'$ . This proves that the parameterization is invertible.

Next, to derive the second equality in (10), we use the half-angle formula

$$\cos\left(\frac{\alpha}{2}\right) = \sqrt{\frac{1 + \cos(\alpha)}{2}} \text{sign}(\sin(\alpha)), \quad \sin\left(\frac{\alpha}{2}\right) = \sqrt{\frac{1 - \cos(\alpha)}{2}}.$$

This gives that

$$\tilde{\mathbf{v}}\tilde{\mathbf{v}}^T = \frac{\|\mathbf{v}\|^2}{2}\mathbf{I} + \frac{\|\mathbf{v}\|}{2} \begin{bmatrix} v_1 & v_2 \\ v_2 & -v_1 \end{bmatrix}, \quad \tilde{\mathbf{v}}_\perp\tilde{\mathbf{v}}_\perp^T = \frac{\|\mathbf{v}\|^2}{2}\mathbf{I} - \frac{\|\mathbf{v}\|}{2} \begin{bmatrix} v_1 & v_2 \\ v_2 & -v_1 \end{bmatrix}.$$

The proof follows immediately by using the definition of  $\mathbf{H}_v$  (first line of (10)). □

## S2 Selection of a distance

In this section, we discuss the choice of the Sobolev distance in Equation (17). We first examine other possible choices, such as the Kullback-Leibler divergence, the  $L^2$  distance, the Wasserstein distance, and the Hellinger distance, and show that they are unsuitable for our purposes. We then derive the exact form of the Sobolev distance in 37 and show a possible alternative definition in 35.

Without pretending full generality we will use the following notation. Firstly, given a domain  $\mathcal{D} = [\mathbf{a}, \mathbf{b}] \subset \mathbb{R}^d$  we denote the *orthonormal Fourier basis* on  $\mathcal{D}$  by

$$e_{\mathbf{k}}(\mathbf{x}) := \text{vol}(\mathcal{D})^{-1/2} \exp\left(\boldsymbol{\omega}_{\mathbf{k}} \cdot \frac{\mathbf{x}}{\mathbf{b} - \mathbf{a}}\right), \quad \boldsymbol{\omega}_{\mathbf{k}} := 2\pi i \mathbf{k} \quad \mathbf{k} \in \mathbb{Z}^d, \quad (26)$$

where we used the elementwise division  $[\mathbf{x}/(\mathbf{b} - \mathbf{a})]_i := x_i/(b_i - a_i)$ . Given a stationary field  $u$  on  $\mathcal{D}$ , we denote its *covariance function*  $r$  and *spectral density*, if they exist, by

$$r(\mathbf{x}) := \text{Cov}[u(\mathbf{x}), u(\mathbf{0})], \quad S(\mathbf{k}) := \int_{\mathcal{D}} r(\mathbf{x}) \overline{e_{\mathbf{k}}(\mathbf{x})} d\mathbf{x}.$$

Additionally, we will denote the *covariance operator* of  $u$  by  $K$ . For stationary  $u \in L^2([\mathbf{a}, \mathbf{b}])$  this is given by

$$\langle Kf, g \rangle_{L^2(\mathcal{D})} := \int_{\mathcal{D}} \int_{\mathcal{D}} r(\mathbf{y} - \mathbf{x}) f(\mathbf{x}) g(\mathbf{y}) d\mathbf{x} d\mathbf{y}, \quad f, g \in L^2(\mathcal{D}).$$

For the calculations, the following lemma will be very useful.

**Lemma 1.** *Let  $u$  be a stationary field in  $L^2(\mathcal{D})$  with spectral density  $S$ . Then, the covariance operator of  $u$  diagonalizes in the orthonormal Fourier basis  $\{e_{\mathbf{k}}\}_{\mathbf{k} \in \mathbb{Z}^d}$  with eigenvalues  $S(\mathbf{k})$ .*

*Proof.* By the Bochner theorem, the covariance function  $r$  of  $u$  is the Fourier transform of

its spectral density  $S$ . As a result, for all  $f, g \in L^2(\mathcal{D})$  we have

$$\langle Kf, g \rangle_{L^2(\mathcal{D})} = \int_{\mathcal{D}} \int_{\mathcal{D}} r(\mathbf{y} - \mathbf{x}) f(\mathbf{x}) g(\mathbf{y}) \, d\mathbf{x} \, d\mathbf{y} = \int_{\mathcal{D}} \int_{\mathcal{D}} \sum_{\mathbf{k} \in \mathbb{Z}^d} S(\mathbf{k}) \overline{e_{\mathbf{k}}(\mathbf{y} - \mathbf{x})} f(\mathbf{x}) g(\mathbf{y}) \, d\mathbf{x} \, d\mathbf{y} \quad (27)$$

$$= \sum_{\mathbf{k} \in \mathbb{Z}^d} S(\mathbf{k}) \int_{\mathcal{D}} f(\mathbf{x}) \overline{e_{\mathbf{k}}(\mathbf{x})} \, d\mathbf{x} \int_{\mathcal{D}} g(\mathbf{y}) e_{\mathbf{k}}(\mathbf{y}) \, d\mathbf{y} = \sum_{\mathbf{k} \in \mathbb{Z}^d} S(\mathbf{k}) \widehat{f}(\mathbf{k}) \overline{\widehat{g}(\mathbf{k})}, \quad (28)$$

Applying this to  $f = e_j$  and  $g = e_{\mathbf{k}}$  shows that

$$\langle Ke_j, e_{\mathbf{k}} \rangle_{L^2(\mathcal{D})} = S(\mathbf{k}) \delta_{j\mathbf{k}}.$$

This concludes the proof.  $\square$

We will also repeatedly use the expression of the spectral density of the solution  $u$  to (3).

To calculate this, note that the covariance operator of  $u$  is given by  $K = \mathcal{L}^{-2}$  where

$$\mathcal{L} := \frac{\kappa^2 - \nabla \cdot \mathbf{H} \nabla}{\sqrt{4\pi\kappa\sigma_u}}.$$

Let us consider first the case where  $\mathcal{D} = \mathbf{a}, \mathbf{b} \subset \mathbb{R}^d$ . Using that  $\nabla e_{\mathbf{k}} = i\boldsymbol{\omega}_{\mathbf{k}} e_{\mathbf{k}}$  we obtain that  $\mathcal{L}$  diagonalizes in the Fourier basis

$$[\mathcal{L}]_{j\mathbf{k}} := \langle \mathcal{L}e_j, e_{\mathbf{k}} \rangle_{L^2(\mathcal{D})} = \frac{\kappa^2 - \boldsymbol{\omega}_{\mathbf{k}} \cdot \mathbf{H} \boldsymbol{\omega}_{\mathbf{k}}}{\sqrt{4\pi\kappa\sigma_u}} \delta_{j\mathbf{k}}, \quad [\mathcal{L}^{-1}]_{j\mathbf{k}} = \frac{\sqrt{4\pi\kappa\sigma_u}}{\kappa^2 - \boldsymbol{\omega}_{\mathbf{k}} \cdot \mathbf{H} \boldsymbol{\omega}_{\mathbf{k}}} \delta_{j\mathbf{k}}.$$

As a result, by Lemma 1, the spectral density of  $u$  is given by

$$S(\mathbf{k}) = \frac{4\pi\kappa^2\sigma_u^2}{(\kappa^2 - \boldsymbol{\omega}_{\mathbf{k}}^T \mathbf{H} \boldsymbol{\omega}_{\mathbf{k}})^2}, \quad \mathbf{k} \in \mathbb{Z}^d. \quad (29)$$

If now  $\mathcal{D} = \mathbb{R}^d$ , the defining property of the spectral density is that, analogously to (27), it holds that (Gel'fand and Vilenkin, 2014, Volume IV page 264)

$$\langle Kf, g \rangle_{L^2(\mathbb{R}^d)} = \int_{\mathbb{R}^d} S(\boldsymbol{\xi}) \widehat{f}(\boldsymbol{\xi}) \overline{\widehat{g}(\boldsymbol{\xi})} \, d\boldsymbol{\xi}, \quad \forall f, g \in L^2(\mathbb{R}^d).$$

Using that the Fourier transform is an isometry on  $L^2(\mathbb{R}^d)$ ,

$$\begin{aligned} \langle Kf, g \rangle_{L^2(\mathbb{R}^d)} &= \langle \mathcal{L}^{-1}f, \mathcal{L}^{-1}g \rangle_{L^2(\mathbb{R}^d)} = \langle \widehat{\mathcal{L}^{-1}f}, \widehat{\mathcal{L}^{-1}g} \rangle_{L^2(\mathbb{R}^d)} \\ &= \int_{\mathbb{R}^d} \frac{4\pi\kappa^2\sigma_u^2}{(\kappa^2 - 4\pi^2\xi^T \mathbf{H} \xi)^2} \widehat{f}(\xi) \overline{\widehat{g}(\xi)} \, d\xi. \end{aligned}$$

So the stationary solution to (3) on  $\mathbb{R}^d$  has spectral density

$$S(\xi) = \frac{4\pi\kappa^2\sigma_u^2}{(\kappa^2 - 4\pi^2\xi^T \mathbf{H} \xi)^2}. \quad (30)$$

## S2.1 Kullback-Leibler divergence

As previously discussed, the KLD is unsuitable as a notion of distance between models as it is infinite for every possible parameter value. As a result, a different way to measure distance between models is necessary. This section discusses some of the options considered and how Definition 1 was eventually chosen. We begin by showing that the KLD is infinite for every possible parameter value with the same variance. To do so, we first give a sufficient condition for two stationary measures to be mutually singular. This is essentially the converse direction of (Stein, 2004, Theorem A.1). See also (Dunlop et al., 2017, Proposition 3).

**Lemma 2.** *Write  $\mathcal{D} = [\mathbf{a}, \mathbf{b}] \subset \mathbb{R}^d$  and let  $u_A, u_B$  be two stationary Gaussian fields in  $L^2(\mathcal{D})$  with spectral densities  $S_A, S_B$ . Suppose that*

$$\sum_{\mathbf{k} \in \mathbb{Z}^d} \left( \frac{S_A(\mathbf{k})}{S_B(\mathbf{k})} - 1 \right)^2 < \infty.$$

*Then, the Gaussian measures defined by  $u_A, u_B$  are mutually singular.*

*Proof.* Denote the covariance operators of  $u_A, u_B$  by  $K_A, K_B$  respectively and let  $I$  be the identity on  $L^2(\mathcal{D})$ . By the Feldman–Hájek theorem, a necessary condition for  $u_A, u_B$  to

not be mutually singular is that the following operator is Hilbert Schmidt,

$$T := \left( K_B^{-1/2} K_A^{1/2} \right) \left( K_B^{-1/2} K_A^{1/2} \right)^* - I.$$

is a Hilbert-Schmidt operator where  $K_A, K_B$  are the covariance operators of  $u_A, u_B$  and  $I$  is the identity operator on  $L^2(\mathcal{D})$ . By Lemma 1,  $K_A, K_B$  both diagonalize in the orthonormal Fourier basis with eigenvalues given respectively by  $S_A(\mathbf{k})$  and  $S_B(\mathbf{k})$ . As a result, the Hilbert-Schmidt norm of  $T$  is given by

$$\|T\|_{\text{HS}}^2 = \sum_{\mathbf{k} \in \mathbb{Z}^d} \left( \frac{S_A(\mathbf{k})}{S_B(\mathbf{k})} - 1 \right)^2.$$

The result follows by the necessary condition for mutual singularity.  $\square$

Using the just proved Lemma 2, we show that the KLD between two different solutions to (3) is infinite if they have the same variance parameter. In particular, if we were to renormalize the spectral densities of the two solutions to have the same variance, the KLD would be infinite for all different parameter values.

**Proposition 2.** *Let  $u_A, u_B$  be the solutions to (3) with Neumann or Dirichlet boundary conditions and parameters  $(\kappa_A, \mathbf{v}_A, \sigma_A), (\kappa_B, \mathbf{v}_B, \sigma_B)$  respectively. Then, the measures defined by  $u_A, u_B$  are mutually singular unless  $\kappa_A/\kappa_B = \sigma_A/\sigma_B$  and  $\mathbf{v}_A = \mathbf{v}_B$ . In particular, if  $u_A \neq u_B$  both share the same variance then*

$$KLD(\mu_A || \mu_B) = \infty.$$

*Proof.* We have by (29) that

$$\sum_{\mathbf{k} \in \mathbb{Z}^2} \left( \frac{S_A(\mathbf{k})}{S_B(\mathbf{k})} - 1 \right)^2 = \sum_{\mathbf{k} \in \mathbb{Z}^2} \left( \frac{\kappa_A^2 \sigma_A^2 (\kappa_B^2 + 4\pi^2 \mathbf{k} \cdot \mathbf{H}_{\mathbf{v}_B} \mathbf{k})^2}{\kappa_B^2 \sigma_B^2 (\kappa_A^2 + 4\pi^2 \mathbf{k} \cdot \mathbf{H}_{\mathbf{v}_A} \mathbf{k})^2} - 1 \right)^2. \quad (31)$$

Since  $H_{\mathbf{v}_A}, H_{\mathbf{v}_B}$  are positive definite, if their eigenvectors and eigenvalues are different, the term  $\mathbf{k} \cdot \mathbf{H}_{\mathbf{v}_B} \mathbf{k} / \mathbf{k} \cdot \mathbf{H}_{\mathbf{v}_A} \mathbf{k}$  can be made arbitrarily large by choosing  $\mathbf{k}$  large enough. As a

result, the sum diverges unless  $\mathbf{v}_A = \mathbf{v}_B$  and

$$\sum_{\mathbf{k} \in \mathbb{Z}^2} \left( \frac{\kappa_A^2 \sigma_A^2 (\kappa_B^2 + 4\pi^2 \mathbf{k} \cdot \mathbf{H}_{\mathbf{v}_A} \mathbf{k})^2}{\kappa_B^2 \sigma_B^2 (\kappa_A^2 + 4\pi^2 \mathbf{k} \cdot \mathbf{H}_{\mathbf{v}_A} \mathbf{k})^2} - 1 \right)^2 < \infty. \quad (32)$$

The limit of the terms in the sum above as  $\mathbf{k} \rightarrow \infty$  is

$$\lim_{\|\mathbf{k}\| \rightarrow \infty} \frac{\kappa_A^2 \sigma_A^2 (\kappa_B^2 + 4\pi^2 \mathbf{k} \cdot \mathbf{H}_{\mathbf{v}_A} \mathbf{k})^2}{\kappa_B^2 \sigma_B^2 (\kappa_A^2 + 4\pi^2 \mathbf{k} \cdot \mathbf{H}_{\mathbf{v}_A} \mathbf{k})^2} - 1 = \frac{\kappa_A^2 \sigma_A^2}{\kappa_B^2 \sigma_B^2} - 1.$$

This limit is zero if and only if  $\kappa_A/\kappa_B = \sigma_A/\sigma_B$ . We deduce that the sum in (31), and so also the sum in (31), diverges unless  $\kappa_A/\kappa_B = \sigma_A/\sigma_B$  and  $\mathbf{v}_A = \mathbf{v}_B$ . The result follows by Lemma 2.  $\square$

## S2.2 The $L^2$ distance

One possible option is to consider the  $L^2$  distance between  $u, u_0$ . An application of Fubini shows that given two Gaussian fields  $u_A \sim \mathcal{N}(0, K_A), u_B \sim \mathcal{N}(0, K_B)$

$$\mathbb{E} \left[ \|u_A - u_B\|_{L^2(\mathcal{D})}^2 \right] = \text{Tr}(K_A + K_B - 2K_{AB}),$$

where  $K_{AB}$  is the covariance between  $u_A, u_B$  and  $\text{Tr}$  is the trace. It is unclear what choice of  $K_{AB}$  would be the most appropriate. For example, choosing  $K_{AB} = 0$  would be too coarse a measure as it would not consider any of the non-stationarity that occurs off the diagonal of  $K_A, K_B$  (see Lemma 1). One can also choose  $K_{AB}$  as to minimize the  $L^2$  norm while keeping  $(u_A, u_B)$  jointly Gaussian by taking

$$K_{AB} = \left( \sqrt{K_B} K_A \sqrt{K_B} \right)^{\frac{1}{2}}.$$

This leads to the Wasserstein distance, which we discuss in the following subsection.

## S2.3 Wasserstein distance between Gaussian measures

Consider a bounded domain  $\mathcal{D} = [0, T]^d$ . Each solution to SPDE (3) induces a measure on  $L^2(\mathcal{D})$ . As a result, one possible way to measure the distance between  $u$  and  $u_0$  is to

take the Wasserstein distance between the induced Gaussian measures. It is known that given two Gaussian measures  $M_A \sim \mathcal{N}(m_A, K_A)$ ,  $\mu_B \sim \mathcal{N}(m_B, K_B)$  on a separable Hilbert space, the Wasserstein distance between them is given by (Gelbrich, 1990, Theorem 3.5)

$$W_2(\mu_A, \mu_B) = \|m_A - m_B\|_{L^2(\mathcal{D})} + \text{Tr} \left( K_A + K_B - 2 \left( \sqrt{K_B} K_A \sqrt{K_B} \right)^{\frac{1}{2}} \right), \quad (33)$$

where  $\text{Tr}$  is the trace. However, this approach poses some difficulties. Let us write  $K_A, K_B$  for the covariance operators of two stationary solutions  $u_A \sim M_A, u_B \sim M_B$  to (3) with parameters  $(\kappa_A, \mathbf{v}_A, \sigma_A), (\kappa_B, \mathbf{v}_B, \sigma_B)$  respectively. By Lemma 1,  $K_A, K_B$  diagonalize on the same basis, and using the expression of the spectral density in (29), we obtain that

$$\begin{aligned} W_2(M_A, M_B) &= \left( \sqrt{K} - \sqrt{K_0} \right)^2 = \sum_{j, k \in \mathbb{Z}^d} \left| \left[ \sqrt{K} - \sqrt{K_0} \right]_{jk} \right|^2 \\ &= \sum_{j \in \mathbb{Z}^d} \left( \frac{\sqrt{4\pi} \kappa_A \sigma_A}{\kappa_A^2 + 4\pi^2 \boldsymbol{\xi}_j^T \mathbf{H}_{\mathbf{v}_A} \boldsymbol{\xi}_j} - \frac{\sqrt{4\pi} \kappa_B \sigma_B}{\kappa_B^2 + 4\pi^2 \boldsymbol{\xi}_j^T \mathbf{H}_{\mathbf{v}_B} \boldsymbol{\xi}_j} \right)^2. \end{aligned}$$

Making the domain  $\mathcal{D}$  go to infinity shows that, by definition of  $\boldsymbol{\xi}_j$  our discrete sum becomes an integral with

$$W_2(M_A, M_B) = \frac{\text{vol}(\mathcal{D})}{\pi} \int_{\mathbb{R}^2} \left( \frac{\kappa_A}{\kappa_A^2 + \boldsymbol{\xi}^T \mathbf{H}_{\mathbf{v}_A} \boldsymbol{\xi}} - \frac{\kappa_B}{\kappa_B^2 + \boldsymbol{\xi}^T \mathbf{H}_{\mathbf{v}_B} \boldsymbol{\xi}} \right)^2 d\boldsymbol{\xi} + O(1).$$

The Wasserstein distance between  $\mu_0, \mu_1$  scales as  $\text{vol}(\mathcal{D})$  times the Hellinger distance of the spectral densities of  $u_A, u_B$ . Thus, a reasonable option could be to define the scaling as the distance

$$D_{W_2}(M_A, M_B) := \lim_{T \rightarrow \infty} \frac{W_2(M_A, M_B)}{\text{vol}(\mathcal{D})} = \text{Hell}(S_A, S_B).$$

However, a calculation in this simplified case shows that this will be bounded. For example, in the case where, as in the base model,  $\mathbf{v}_A = \mathbf{v}_B = \mathbf{0}$ , and  $\sigma_A = \sigma_B = 1$ , we have the following.

$$D_{W_2}(u_A, u_B) = 2 \left( 1 - \frac{\kappa_A \kappa_B (\log(\kappa_A^2) - \log(\kappa_B^2))}{\kappa_A^2 - \kappa_B^2} \right).$$

The above expression takes a maximum of 2. This makes putting an exponential distribution on the Wasserstein distance impossible, and as a result, the Wasserstein distance cannot be used to define PC priors for our model (3).

## S2.4 Sobolev distance between fields

Given a stationary field  $u$  on  $\mathcal{D}$  with  $s$ -times differentiable covariance function  $r(x) := \text{Cov}[u(\mathbf{x}, u(\mathbf{0}))]$ , we define the seminorm  $|\cdot|_s$  as the Sobolev seminorm of order  $s$  of  $r$ . That is,

$$|u|_s := \|\nabla^s r\|_{L^2(\mathcal{D})} = \left\| \|2\pi\boldsymbol{\xi}\|^s S(\boldsymbol{\xi})\right\|_{L^2(\widehat{\mathcal{D}})} := \left( \int_{\widehat{\mathcal{D}}} \|2\pi\boldsymbol{\xi}\|^{2s} S(\boldsymbol{\xi})^2 d\boldsymbol{\xi} \right)^{\frac{1}{2}}, \quad (34)$$

where  $\widehat{\mathcal{D}}$  is the Fourier domain of  $\mathcal{D}$ . That is,  $\widehat{\mathcal{D}} = \mathbb{Z}^d$  if  $\mathcal{D}$  is a box and  $\widehat{\mathcal{D}} = \mathbb{R}^d$  if  $\mathcal{D} = \mathbb{R}^d$ . If we think of the  $L^2(\mathcal{D})$  norm of  $r$  as a measure of the total “random energy” present in  $u$ . Then,  $|\cdot|_s$  measures the oscillation size in this energy to order  $s$ .

We now discuss which value of  $s$  is appropriate. In our case, as we saw in (30), the solution  $u$  to (3) with parameters  $\kappa, \mathbf{v}, \sigma_u$  has spectral density

$$S_{\kappa, \mathbf{v}, \sigma_u}(\boldsymbol{\xi}) = \frac{4\pi\kappa^2\sigma_u^2}{(\kappa^2 + 4\pi^2\boldsymbol{\xi} \cdot \mathbf{H}_{\mathbf{v}}\boldsymbol{\xi})^2}.$$

A change of variables  $\xi \rightarrow \kappa\xi$  shows that, for dimension  $d = 2$ , the behavior in  $\kappa$  is

$$|u|_s \sim \kappa^{s-1}.$$

If we take  $s = 0$ , then  $|u|_0$  becomes infinite, whereas if we choose  $s = 1$ , we obtain that  $|u|_1$  is bounded in  $\kappa$  and thus cannot be exponentially distributed. This leads to the choice  $s = 2$  used in Definition 1.

**Observation 1.** *The seminorm  $|u|_s$  is different to the Sobolev seminorm of  $u$  as we have that, given a multi-index  $\alpha \in \mathbb{Z}^d$ , the derivative  $D^\alpha u$  of a stationary field  $u$  exists as long*



as

$$\int_{\widehat{\mathcal{D}}} |(2\pi\boldsymbol{\xi})^{2\alpha}| S(\boldsymbol{\xi}) \, d\boldsymbol{\xi} < \infty.$$

Thus, one possible choice of metric, corresponding to  $s = 1/2$ , could also be to set

$$|u|_* := \int_{\widehat{\mathcal{D}}} \|2\pi\boldsymbol{\xi}\| S(\boldsymbol{\xi}) \, d\boldsymbol{\xi}.$$

This distance is unbounded in  $\kappa$  and finite at the base model. A calculation gives a distance of a similar form to the one derived for the distance used in this paper in Lemma 3.

$$d_*(\kappa, \mathbf{v})^2 := \lim_{\kappa_0, \mathbf{v} \rightarrow 0} \int_{\widehat{\mathcal{D}}} \|2\pi\boldsymbol{\xi}\| \left( \frac{S_{\kappa, \mathbf{v}, \sigma_u}}{\sigma_u^2} - \frac{S_{\kappa, \mathbf{v}, \sigma_0}}{\sigma_0^2} \right) d\boldsymbol{\xi} = 2\pi E (1 - \exp(-2\|\mathbf{v}\|)) \exp\left(-\frac{\|\mathbf{v}\|}{2}\right) \kappa, \quad (35)$$

where  $E$  is the complete elliptic integral

$$E(m) := \int_0^{\pi/2} (1 - m \sin^2(\alpha))^{\frac{1}{2}} \, d\alpha.$$

This distance is unbounded in  $\kappa$  and  $\mathbf{v}$  and 0 at the base model. As a result, using  $d_*$  instead of  $d$  could also provide a valid alternative.

### S3 Derivation of PC priors

**Lemma 3.** *Let  $M_{\kappa, \mathbf{v}, \sigma_u}, M_{\kappa_0, \mathbf{0}, \sigma_0}$  be the stationary models given by (3) with parameters  $(\kappa, \mathbf{v}, \sigma_u)$  and  $(\kappa_0, \mathbf{0}, \sigma_0)$  respectively. Then,*

$$d(\kappa, \mathbf{v}) := \lim_{\kappa_0 \rightarrow 0} D_2(M_{\kappa, \mathbf{v}, \sigma_u}, M_{\kappa_0, \mathbf{0}, \sigma_0})^2 = \frac{\pi}{3} \kappa^2 (3 \cosh(2\|\mathbf{v}\|) + 1).$$

*Proof.* For any  $(\kappa, \mathbf{v}, \sigma_u)$  the spectral density of  $u_{\kappa, \mathbf{v}, \sigma_u}$  is

$$S_{\kappa, \mathbf{v}, \sigma_u}(\boldsymbol{\xi}) = \frac{4\pi\kappa^2\sigma_u^2}{(\kappa^2 + 4\pi^2\boldsymbol{\xi}^T \mathbf{H} \boldsymbol{\xi})^2}.$$

As a result, in a distributional sense

$$\lim_{\kappa_0 \rightarrow 0} \frac{S_{\kappa_0, \mathbf{0}, \sigma_0}}{\sigma_0^2}(\boldsymbol{\xi}) = \lim_{\kappa_0 \rightarrow 0} \frac{4\pi\kappa_0^2}{(\kappa_0^2 + 4\pi^2\|\boldsymbol{\xi}\|^2)^2} = \delta\mathbf{0}(\boldsymbol{\xi}),$$

where  $\delta\mathbf{0}$  is the Dirac delta at 0. In consequence, expanding the square in (16) and using the change of variable  $\boldsymbol{\xi} \rightarrow \kappa\boldsymbol{\xi}/(2\pi)$ , we obtain that

$$\lim_{\kappa_0 \rightarrow 0} D_2(M_{\kappa, \mathbf{v}, \sigma_u}, M_{\kappa_0, \mathbf{0}, \sigma_0})^2 = \int_{\mathbb{R}^2} \|2\pi\boldsymbol{\xi}\|^4 \frac{S_{\kappa, \mathbf{v}, \sigma_u}(\boldsymbol{\xi})^2}{\sigma_u^4} d\boldsymbol{\xi} = 4\kappa^2 \int_{\mathbb{R}^2} \frac{\|\boldsymbol{\xi}\|^4}{(1 + \boldsymbol{\xi}^T \mathbf{H}_v \boldsymbol{\xi})^4} d\boldsymbol{\xi}.$$

Let  $\alpha := \arg(\mathbf{v})$  and  $B_{\alpha/2}$  be a rotation by  $\alpha/2$  radians. Then

$$B_{\alpha/2} \mathbf{H}_v B_{\alpha/2}^{-1} = \begin{bmatrix} \exp(-\|\mathbf{v}\|) & 0 \\ 0 & \exp(\|\mathbf{v}\|) \end{bmatrix}.$$

Thus, by rotating and then changing to polar coordinates, we obtain

$$\begin{aligned} \lim_{\kappa_0 \rightarrow 0} D_2(M_{\kappa, \mathbf{v}, \sigma_u}, M_{\kappa_0, \mathbf{0}, \sigma_0})^2 &= 4\kappa^2 \int_0^{2\pi} \int_0^\infty \frac{r^5}{(1 + r^2 (\exp(\|\mathbf{v}\|) \sin^2(\phi) + \exp(-\|\mathbf{v}\|) \cos^2(\phi)))^4} dr d\phi \\ &= \int_0^{2\pi} \frac{4\kappa^2}{6 (\exp(\|\mathbf{v}\|) \sin^2(\phi) + \exp(-\|\mathbf{v}\|) \cos^2(\phi))^3} d\phi = \frac{\pi}{3} (3 \cosh(2\|\mathbf{v}\|) + 1) \kappa^2. \end{aligned}$$

This concludes the proof.  $\square$

As we see from Lemma 3,  $d(\kappa, \mathbf{v})$  is independent of the argument  $\alpha$  of  $\mathbf{v}$  and depends only on  $\kappa$  and  $r := \|\mathbf{v}\|$ . For this reason, we consider  $\alpha$  to be independent of  $\kappa, \mathbf{v}$  and, since a priori, there is no preferred direction for the anisotropy, we set a uniform prior on  $\alpha$

$$\pi_\alpha(\alpha) = \frac{1}{2\pi} 1_{[0, 2\pi]}(\alpha) \quad (36)$$

We will now define priors on  $\kappa, r$  following a sequential construction. To do so, we will use the fact that the distance to the base model  $\rho(\kappa, \mathbf{v})$  decomposes as a product

$$d(\mathbf{v}, \kappa) = f(r)g(\kappa), \quad f(r) := \left( \frac{\pi}{3} (3 \cosh(2\|\mathbf{v}\|) + 1) \right)^{\frac{1}{2}}, \quad g(\kappa) := \kappa. \quad (37)$$

Together with the following lemma,

**Lemma 4** (Distribution of product). *Let  $X, Y$  be two positive random variables such that  $Y|X$  has density*

$$f_{Y|X}(y, x) = \lambda x \exp(-\lambda xy) 1_{[0, +\infty)}(y).$$

*Then, the product  $Z := XY$  follows an exponential distribution with parameter  $\lambda$ .*

*Proof.* By the law of total expectation, the cumulative density function of  $Z$  verifies

$$\begin{aligned} F_Z(z) &= \mathbb{P}[XY \leq z] = \mathbb{E}[\mathbb{E}[1_{XY \leq z} | X]] = \mathbb{E} \left[ \int_0^{z/X} f_{Y|X}(y|X) dy \right] \\ &= \int_0^\infty \int_0^{z/x} f_{Y|X}(y|x) d\mathbb{P}_X(x), \end{aligned}$$

where  $\mathbb{P}_X$  is the push-forward of  $\mathbb{P}$  by  $X$ . Applying the fundamental theorem of calculus shows that the density of  $Z$  is

$$F'_Z(z) = \int_0^\infty \frac{1}{x} f_{Y|X}(z/x|x) d\mathbb{P}_X(x) = \lambda \exp(-\lambda z) \int_0^\infty d\mathbb{P}_X(x) = \lambda \exp(-\lambda z).$$

This concludes the proof. □

The above lemma states that if we want the distance  $d = fg$  to be exponentially distributed, it suffices to let  $f$  follow *any* distribution and have  $g$  conditional on  $f$  be exponentially distributed with parameter proportional to  $f$ . Since  $f$  takes a minimum of

$$f(0) = \sqrt{4\pi/3},$$

the conditional distribution of  $f$  given  $g$  cannot follow an exponential distribution. Therefore, we will instead select the conditional distribution of  $g$  given  $f$  to be exponential.

While Lemma 4 allows complete freedom in choosing a distribution for  $f$ , the symmetry in the distance  $fg$  implies there is no intrinsic reason to prefer penalizing an increase in  $f$  either more or less than an increase in  $g$ . Consequently, we will also impose an exponential penalty on  $f$  by setting its marginal density to be equal to the following,

$$\pi_f(f) = \lambda_v \exp(-\lambda_v(f - f(0))) 1_{[f(0), \infty)}.$$

We can set priors in the stationary setting in the same way as in the previous section.

### S3.1 Proof of Theorem 2

*Proof.* Let us write

$$r = \|\mathbf{v}\|, \quad \alpha = \arg(\mathbf{v}).$$

We have already determined the prior distributions

$$\pi_f(f) = \lambda_{\mathbf{v}} \exp(-\lambda_{\mathbf{v}}(f - f(0)))1_{[f(0), \infty)}(f), \quad \pi_{\kappa|f}(\kappa|f) = \lambda_{\boldsymbol{\theta}} f \exp(-\lambda_{\boldsymbol{\theta}} f \kappa)1_{[0, \infty)}(\kappa) \quad (38)$$

Since  $f : [0, \infty) \rightarrow [f(0), \infty)$  is bijective, we may apply a change variables to obtain that the marginal prior for  $r$  is

$$\pi_r(r) = \pi_f(f(r))|f'(r)| = \lambda_{\mathbf{v}} \exp(-\lambda_{\mathbf{v}}(f(r) - f(0)))|f'(r)|. \quad (39)$$

Again, by the bijectivity of  $f$ , we obtain that

$$\pi_{\kappa|r} = \pi_{\kappa|f=f(r)} = \lambda_{\boldsymbol{\theta}} f(r) \exp(-\lambda_{\boldsymbol{\theta}} f(r) \kappa)1_{[0, \infty)}(\kappa). \quad (40)$$

Since  $\alpha$  is uniformly distributed on  $[0, 2\pi]$  independently of  $r, \kappa$  the joint prior for  $(\kappa, \alpha, r)$  is

$$\pi_{\kappa, \alpha, r}(\kappa, \alpha, r) = \frac{1_{[0, 2\pi]}(\alpha)}{2\pi} \pi_r(r) \pi_{\kappa|r}(\kappa|r).$$

Changing variables from polar to Cartesian coordinates gives

$$\pi_{\kappa, \mathbf{v}}(\kappa, \mathbf{v}) = \frac{1}{2\pi\|\mathbf{v}\|} \pi_r(\|\mathbf{v}\|) \pi_{\kappa|r}(\kappa | \|\mathbf{v}\|). \quad (41)$$

Using equations (39) and (40) in (41) and using the expression for  $f$  derived in (37) concludes the proof.  $\square$

### S3.2 Proof of Theorem 3

*Proof.* The prior for  $f$  is defined in (38). Since  $f$  is increasing, we obtain that the cumulative distribution function of  $r$  is for all  $r_0 \geq 0$

$$F_r(r_0) = \mathbb{P}(r \leq r_0) = \mathbb{P}(f(r) \leq f(r_0)) = 1 - \exp(-\lambda_{\boldsymbol{\theta}}(f(r_0) - f(0))). \quad (42)$$

The theorem follows by a straightforward algebraic manipulation.  $\square$

### S3.3 Proof of Theorem 4

*Proof.* We begin by calculating the prior  $\pi_{\kappa}$  for  $\kappa$ . A calculation shows that for all  $\kappa > 0$

$$\begin{aligned} \pi_{\kappa}(\kappa) &= \int_{\mathbb{R}} \pi_f(f) \pi_{\kappa|f}(\kappa|f) df = \int_{f(0)}^{\infty} \lambda_{\mathbf{v}} \lambda_{\boldsymbol{\theta}} f \exp(-\lambda_{\mathbf{v}}(f - f(0)) - \lambda_{\boldsymbol{\theta}} f \kappa) df \\ &= \frac{\lambda_{\boldsymbol{\theta}} \lambda_{\mathbf{v}} \exp(-f(0)\kappa\lambda_{\boldsymbol{\theta}}) (f(0)\kappa\lambda_{\boldsymbol{\theta}} + f(0)\lambda_{\mathbf{v}} + 1)}{(\kappa\lambda_{\boldsymbol{\theta}} + \lambda_{\mathbf{v}})^2}, \end{aligned}$$

whereas for  $\kappa < 0$  we have  $\pi_{\kappa}(\kappa) = 0$ . A further calculation shows that the CDF of  $\kappa$  is

$$F_{\kappa}(\kappa_0) = \int_{-\infty}^{\kappa_0} \pi_{\kappa}(\kappa) d\kappa = \left(1 - \frac{\lambda_{\mathbf{v}} \exp(-f(0)\lambda_{\boldsymbol{\theta}}\kappa_0)}{\lambda_{\boldsymbol{\theta}}\kappa_0 + \lambda_{\mathbf{v}}}\right) \mathbf{1}_{[0, \infty]}(\kappa_0). \quad (43)$$

Now solving for  $\lambda_{\boldsymbol{\theta}}$  gives that for any  $\kappa_0 > 0$

$$\mathbb{P}[\kappa > \kappa_0] = \alpha \iff \lambda_{\boldsymbol{\theta}} = \frac{1}{f(0)\kappa_0} W_0\left(\frac{\exp(\lambda_{\mathbf{v}} f(0)) \lambda_{\mathbf{v}} f(0)}{\alpha}\right) - \frac{\lambda_{\mathbf{v}}}{\kappa_0} \quad (44)$$

This concludes the proof.  $\square$

## S4 Joint transformation

In this section, we show how to write  $(\kappa, \mathbf{v})$  jointly as a function of a three-dimensional standard Gaussian  $\mathbf{Y} \stackrel{d}{=} \mathcal{N}(\mathbf{0}, \mathbf{I}_3)$ . Our idea will be to generalize the method of inverse sampling. This is done by building an invertible generalization of the cumulative distribution function.

**Definition 2.** Given a random variable  $\mathbf{X} = (X_1, X_2) \in \mathbb{R}^2$  we define the generalized CDF of  $\mathbf{X}$  as

$$\varphi(\mathbf{X}, \mathbf{x}) := \varphi_{\mathbf{X}}(\mathbf{x}) := (\mathbb{P}[X_1 \leq x_1], \mathbb{P}[X_2 \leq x_2 | X_1 = x_1]).$$

**Observation 2.** In the case where  $X_1, X_2$  are independent we obtain that

$$\varphi_{\mathbf{X}}(\mathbf{x}) = (F_{X_1}(x_1), F_{X_2}(x_2)).$$

By construction  $\varphi_{\mathbf{X}} : \mathbb{R}^2 \rightarrow [0, 1]^2$ . The definition can be extended without difficulty to dimensions larger than 2. However, the notation becomes more cumbersome. The motivation for the above definition is given by the following properties, which mimic that of the 1-dimensional CDF.

**Lemma 5.** Let  $\mathbf{X}$  be a two-dimensional random variable, then the following hold

1. The distribution of  $\mathbf{X}$  is determined by  $\varphi$ . That is if  $\mathbf{Y}$  is a two dimensional random variable such that  $\varphi_{\mathbf{X}} = \varphi_{\mathbf{Y}}$ , then  $\mathbf{X} \stackrel{d}{=} \mathbf{Y}$ .
2. Consider a function  $\phi : A \rightarrow \mathbb{R}^2$  defined on some subset  $A \subset \mathbb{R}^2$  of the form

$$\phi(x_1, x_2) = (\phi_1(x_1), \phi_2(x_1, x_2)), \tag{45}$$

where  $\phi_1$  is invertible and  $\phi_1, \phi_2(x_1, \cdot)$  are monotone functions. Then,

$$\varphi(\phi(\mathbf{X}), \phi(\mathbf{x})) = \varphi(\mathbf{X}, \mathbf{x}), \quad \forall \mathbf{x} \in A.$$

3. Let  $\mathbf{X}$  be a  $\mathbb{R}^2$  valued random variable. Then  $\varphi_{\mathbf{X}}$  has a generalized inverse and  $\varphi_{\mathbf{X}}, \varphi_{\mathbf{X}}^{-1}$  are both of the form (45).

*Proof.* We prove the above points in order.

1. Suppose  $\varphi_{\mathbf{X}} = \varphi_{\mathbf{Y}}$ , then by definition of  $\varphi$  we have that for all  $\mathbf{x} = (x_1, x_2) \in \mathbb{R}^2$

$$\mathbb{P}[X_1 \leq x_1] = \mathbb{P}[Y_1 \leq x_1], \quad \mathbb{P}[X_2 \leq x_2 | X_1 = x_1] = \mathbb{P}[Y_2 \leq x_2 | Y_1 = x_1].$$

From the basic theory of random variables, the left-hand side of the above implies that  $X_1 \stackrel{d}{=} Y_1$ . As a result, we obtain that

$$\begin{aligned} \mathbb{P}[X_2 \leq x_2] &= \int_{\mathbb{R}} \mathbb{P}[X_2 \leq x_2 | X_1 = x_1] d\mathbb{P}_{X_1}(x_1) \\ &= \int_{\mathbb{R}} \mathbb{P}[Y_2 \leq x_2 | Y_1 = x_1] d\mathbb{P}_{Y_1}(x_1) = \mathbb{P}[Y_2 \leq x_2]. \end{aligned}$$

Since this holds for all  $x_2 \in \mathbb{R}$  we deduce as previously that  $X_2 \stackrel{d}{=} Y_2$ . Thus we obtain that  $\mathbf{X} \stackrel{d}{=} \mathbf{Y}$ , as desired.

2. To prove item 2 we work with  $\varphi$  componentwise. By the monotonicity of  $\phi_1$ , it is clear that for the first component,

$$\varphi_1(\phi(\mathbf{X}), \phi(\mathbf{x})) := \mathbb{P}[\phi_1(X_1) \leq \phi_1(x_1)] = \mathbb{P}[X_1 \leq x_1] = \varphi_1(\mathbf{X}, \mathbf{x}).$$

The second part is proved similarly. We have that

$$\begin{aligned} \varphi_2(\phi(\mathbf{X}), \phi(\mathbf{x})) &:= \mathbb{P}[\phi_2(X_1, X_2) \leq \phi_2(x_1, x_2) | \phi_1(X_1) = \phi_1(x_1)] \\ &= \mathbb{P}[\phi_2(X_1, X_2) \leq \phi_2(x_1, x_2) | X_1 = x_1] = \mathbb{P}[\phi_2(x_1, X_2) \leq \phi_2(x_1, x_2) | X_1 = x_1] \\ &= \mathbb{P}[X_2 \leq x_2 | X_1 = x_1] = \varphi_2(\mathbf{X}, \mathbf{x}), \end{aligned}$$

where in the second equality, we used that  $\phi_1$  is invertible, so the  $\sigma$ -algebra generated by  $X_1$  is the same as that generated by  $\phi(X_1)$  and  $\phi(X_1) = \phi(x_1)$  if and only if  $X_1 = x_1$ . And in the fourth equality, we used that  $\phi_2(x_1, \cdot)$  is monotone.

3. We first prove  $\varphi_{\mathbf{X}}$  is invertible. Let us take  $\mathbf{p} = (p_1, p_2) \in [0, 1]^2$ . Then, the first component of  $\varphi_{\mathbf{X}}$  is the univariate CDF  $F_{X_1}$ , and we can define

$$x_1 := F_{X_1}^{-1}(p_1).$$

Now, since  $\varphi_2(\mathbf{X}, (x_1, \cdot))$  is increasing (as a function of the dot) for each  $x_1$ , it has a generalized inverse

$$x_2 := \varphi_2(\mathbf{X}, (x_1, \cdot))^{-1}(p_2).$$

An algebraic verification now shows that  $\varphi_{\mathbf{X}}$  has generalized inverse

$$\varphi_{\mathbf{X}}^{-1}(\mathbf{p}) = (x_1, x_2). \quad (46)$$

Furthermore, since  $\varphi_{\mathbf{X}}$  is monotone in each component, so is  $\varphi_{\mathbf{X}}^{-1}$ .

This completes the proof. □

**Lemma 6.** *Given random variables  $\mathbf{X}, \mathbf{Y}$  valued in  $\mathbb{R}^2$  it holds that*

$$\varphi_{\mathbf{X}}^{-1} \circ \varphi_{\mathbf{Y}}(\mathbf{Y}) \stackrel{d}{=} \mathbf{X}$$

*Proof.* By item 1 of Lemma 5, it suffices to prove that the generalized CDFs of  $\mathbf{X}$  and  $\mathbf{Y}$  coincide. To this aim, we have that, by item 2 of the previous lemma

$$\varphi(\varphi_{\mathbf{X}}^{-1} \circ \varphi_{\mathbf{Y}}(\mathbf{Y}), \mathbf{x}) = \varphi(\mathbf{Y}, \varphi_{\mathbf{Y}}^{-1} \circ \varphi_{\mathbf{X}}(\mathbf{x})) = \varphi_{\mathbf{Y}}(\varphi_{\mathbf{Y}}^{-1}(\varphi_{\mathbf{X}}(\mathbf{x}))) = \varphi_{\mathbf{X}}(\mathbf{x}).$$

This concludes the proof. □

We now calculate the transformation which makes  $(\kappa, r)$  Gaussian.

**Lemma 7.** *Let  $(\mathbf{v}, \kappa)$  be distributed according to the PC priors  $\pi(\mathbf{v}, \kappa)$  and define  $r := \|\mathbf{v}\|$ .*

*Then, given  $\mathbf{U} \sim \mathcal{N}(\mathbf{0}, \mathbf{I}_2)$  it holds that*

$$(r, \kappa) \stackrel{d}{=} \left( f^{-1} \left( f(0) - \frac{\log(1 - \Phi(U_1))}{\lambda_{\mathbf{v}}} \right), \left( \frac{\log(1 - \Phi(U_1))}{\lambda_{\mathbf{v}}} - f(0) \right)^{-1} \frac{\log(1 - \Phi(U_2))}{\lambda_{\theta}} \right),$$

*where  $\Phi$  is the CDF of a univariate standard Gaussian and  $r := \|\mathbf{v}\|$ .*



*Proof.* The CDF  $F_r$  of  $r$  was calculated in (42). An inversion gives

$$x_1 := F_r^{-1}(p_1) = f^{-1}\left(f(0) - \frac{\log(1 - p_1)}{\lambda_{\mathbf{v}}}\right)$$

To calculate the CDF of  $\kappa|r$ , we work with the density in (38). This gives

$$\varphi_2((r, \kappa), (x_1, x_2)) = 1 - \exp(-\lambda_{\boldsymbol{\theta}} f(x_1)x_2).$$

For each fixed  $x_1$ , the above has the inverse

$$x_2 := \varphi_2((r, \kappa), (x_1, \cdot))^{-1}(p_2) = -\frac{\log(1 - p_2)}{\lambda_{\boldsymbol{\theta}} f(x_1)}$$

This, combined with (46), the preceding Lemma 6 (with  $\mathbf{Y} = \mathbf{U}$ ), and Observation 2 (applied to  $\mathbf{U}$ ), completes the proof.  $\square$

#### S4.1 Proof of Theorem 6

*Proof.* Let  $\alpha \sim \mathcal{U}_{[0, 2\pi]}$  be independent from  $r$ . Then, by the definition  $r = \|\mathbf{v}\|$ ,

$$\mathbf{v} \stackrel{d}{=} (r \cos(\alpha), r \sin(\alpha)),$$

The proof then follows from Lemma 7 and by observing that  $R(\sqrt{Y_1^2 + Y_2^2})$ ,  $\Phi(Y_3)$  are i.i.d. uniformly distributed on  $[0, 1]$ , and that

$$\frac{Y_1}{\sqrt{Y_1^2 + Y_2^2}} \stackrel{d}{=} \cos(\alpha), \quad \frac{Y_2}{\sqrt{Y_1^2 + Y_2^2}} \stackrel{d}{=} \sin(\alpha).$$

$\square$

#### S4.2 Proof of Proposition 1

*Proof.* The determinant of  $\mathbf{H}_{\mathbf{v}(\alpha)}$  is  $(\beta + \gamma)\gamma$ . Setting this equal to 1 gives  $\beta = (1 - \gamma^2)/\gamma$ .

Next, we note that given any vector  $\mathbf{e}$ , it holds that

$$\mathbf{I} = \mathbf{e}\mathbf{e}^T + \mathbf{e}_{\perp}\mathbf{e}_{\perp}^T.$$

Substituting this into (8) with  $e = v(\alpha)$

$$\mathbf{H}_{v(\alpha)} = (\gamma + \beta)\mathbf{v}(\alpha)\mathbf{v}(\alpha)^T + \gamma\mathbf{v}(\alpha)_\perp\mathbf{v}(\alpha)_\perp^T = \frac{1}{\gamma}\mathbf{v}(\alpha)\mathbf{v}(\alpha)^T + \gamma\mathbf{v}(\alpha)_\perp\mathbf{v}(\alpha)_\perp^T.$$

Setting  $\mathbf{H}_v = \mathbf{H}_{v(\alpha)}$ , we obtain the condition

$$\frac{1}{\gamma}\mathbf{v}(\alpha)\mathbf{v}(\alpha)^T + \gamma\mathbf{v}(\alpha)_\perp\mathbf{v}(\alpha)_\perp^T = \frac{\exp(\|\mathbf{v}\|)}{\|\mathbf{v}\|^2}\tilde{\mathbf{v}}\tilde{\mathbf{v}}^T + \frac{\exp(-\|\mathbf{v}\|)}{\|\mathbf{v}\|^2}\tilde{\mathbf{v}}_\perp\tilde{\mathbf{v}}_\perp^T.$$

Thus, equality holds in the conditions of the theorem.  $\square$

## S5 Simulation study details

In this section, we expand on the simulation study of Section 5. We will discuss the details of the simulation of the SPDE, compare the priors, and show some additional results.

### S5.1 Sampling from the SPDE

To simulate the Gaussian field resulting from (3), we use the `fmesh` package. This package uses a FEM method to calculate to approximate the precision matrix of  $u$ . That is, we approximate  $u$  to be in the Hilbert space  $H$  spanned by our finite element basis  $\{\phi_i\}_{i=1}^n$  and impose

$$[\langle \phi_i, \mathcal{L}u \rangle, i \in \{1, \dots, n\}] = \left[ \left\langle \phi_i, \kappa \dot{W} \right\rangle, i \in \{1, \dots, n\} \right] \quad (47)$$

The condition that  $u \in H$  leaves us with

$$u(x) = \sum_{i=1}^n \phi_i(x)u_i, \quad (48)$$

where one can show that the vector of weights  $\mathbf{u} = (u_1, \dots, u_n)$  is Gaussian. Let us write  $\mathbf{Q}_u$  for its precision matrix,  $\mathbf{u} \sim \mathcal{N}(\mathbf{0}, \mathbf{Q}_u^{-1})$ . Then, from (48), knowing  $\mathbf{Q}_u$  determines

$\mathbf{u}$ . The value of  $\mathbf{Q}_u$  is determined in turn by (47), as substituting in (48) and applying integration by parts gives

$$\mathbf{L}\mathbf{u} \sim \mathcal{N}(\mathbf{0}, \mathbf{C}_\kappa), \quad (49)$$

where

$$\mathbf{L} = \mathbf{C}_\kappa + \mathbf{G}_\mathbf{H}, \quad [\mathbf{C}_\kappa]_{ij} = \langle \phi_i, \kappa^2 \phi_j \rangle_{L^2(\mathcal{D})}, \quad [\mathbf{G}_\mathbf{H}]_{ij} = \langle \nabla \phi_i, \mathbf{H} \nabla \phi_j \rangle_{L^2(\mathcal{D})}. \quad (50)$$

From (49) we deduce that the precision  $\mathbf{Q}$  of the weight vector  $w$  is

$$\mathbf{Q}_u = (\mathbf{C}_\kappa + \mathbf{G}_\mathbf{H})^\dagger \mathbf{C}_\kappa^{-1} (\mathbf{C}_\kappa + \mathbf{G}_\mathbf{H}) = \mathbf{C}_\kappa + 2\mathbf{G}_\mathbf{H} + \mathbf{G}_\mathbf{H} \mathbf{C}_\kappa^{-1} \mathbf{G}_\mathbf{H}, \quad (51)$$

where we used that since  $\mathbf{H}$  is symmetric, and we are considering real-valued functions,  $\mathbf{C}_\kappa, \mathbf{G}_\mathbf{H}$  are symmetric.

The finite element basis is chosen so that  $\mathbf{C}_\kappa, \mathbf{G}_\mathbf{H}$  are sparse. Since  $\mathbf{C}_\kappa$  is not sparse, it is approximated by the mass lumped version

$$[\tilde{\mathbf{C}}_\kappa]_{ij} := \delta_{ij} \sum_{k=1}^n [\mathbf{C}_\kappa]_{ik}.$$

After this approximation we obtain a sparse precision  $\tilde{\mathbf{Q}}_u$  which allows us to sample efficiently from  $\mathbf{u}$  (or rather, its approximation  $\tilde{u} \sim \mathcal{N}(\mathbf{0}, \tilde{\mathbf{Q}}_u)$ ) by using a Cholesky decomposition  $\tilde{\mathbf{Q}}_u = \mathbf{L}\mathbf{L}^T$  and solving  $\mathbf{L}^T z = u$  where  $z \sim \mathcal{N}(\mathbf{0}, \mathbf{I})$ .

It remains to discuss how the integrals defining  $\mathbf{C}_\kappa, \mathbf{G}_\mathbf{H}$  are calculated. Let  $\mathcal{T}$  be the mesh of the domain. For each triangle  $T \in \mathcal{T}$  we denote the average value of  $\kappa, \mathbf{H}$  on the nodes of  $T$  as  $\kappa^2(T), \mathbf{H}(T)$  and approximate the integrals in (50) by

$$[\mathbf{C}_\kappa]_{ij} \approx \sum_{T \in \rightarrow} \kappa^2(T) \int_T \phi_i \phi_j \, d\mathbf{x}, \quad [\mathbf{G}_\mathbf{H}]_{ij} \approx \sum_{\substack{T \in \rightarrow \\ k,l=1,2}} [\mathbf{H}(T)]_{kl} \int_T \partial_k \phi_i \partial_l \phi_j \, d\mathbf{x}. \quad (52)$$

Finally, we take  $\phi_i$  to be piecewise linear equal to 1 on node  $i$  and equal to 0 on every other node. An explicit formula for the integrals in (52) can be found in (Lindgren et al., 2011, Appendix A2).

## S5.2 Comparison of priors for the simulation study

To better understand the four priors  $\pi_{\text{PC}}, \pi_{\text{EG}}, \pi_{\text{U}}, \pi_{\beta}$  and their corresponding posteriors, in Figure 12 and Figure 13, we fix  $\sigma_u, \sigma_\varepsilon$  and plot each of the marginal prior and posterior densities mentioned above (up to a multiplicative constant) in  $\log(\kappa)$  and  $v$  respectively, for a given observation  $\mathbf{y}$ . As we can see,  $\pi_{\text{PC}}$  and  $\pi_{\text{EG}}$  give similar prior and (as a result) posterior densities, to the point where it is impossible to distinguish them in the plots. The uniform and beta priors and posteriors are similar to each other and differ mainly in the size of support. The beta priors and posteriors resemble a cutoff version of their uniform analogs. This indicates that choosing  $\pi_{\text{PC}}$  and  $\pi_{\text{EG}}$  as priors will give similar results. Likewise,  $\pi_{\text{U}}, \pi_{\beta}$  will also give similar results to each other. This is borne out in the results.

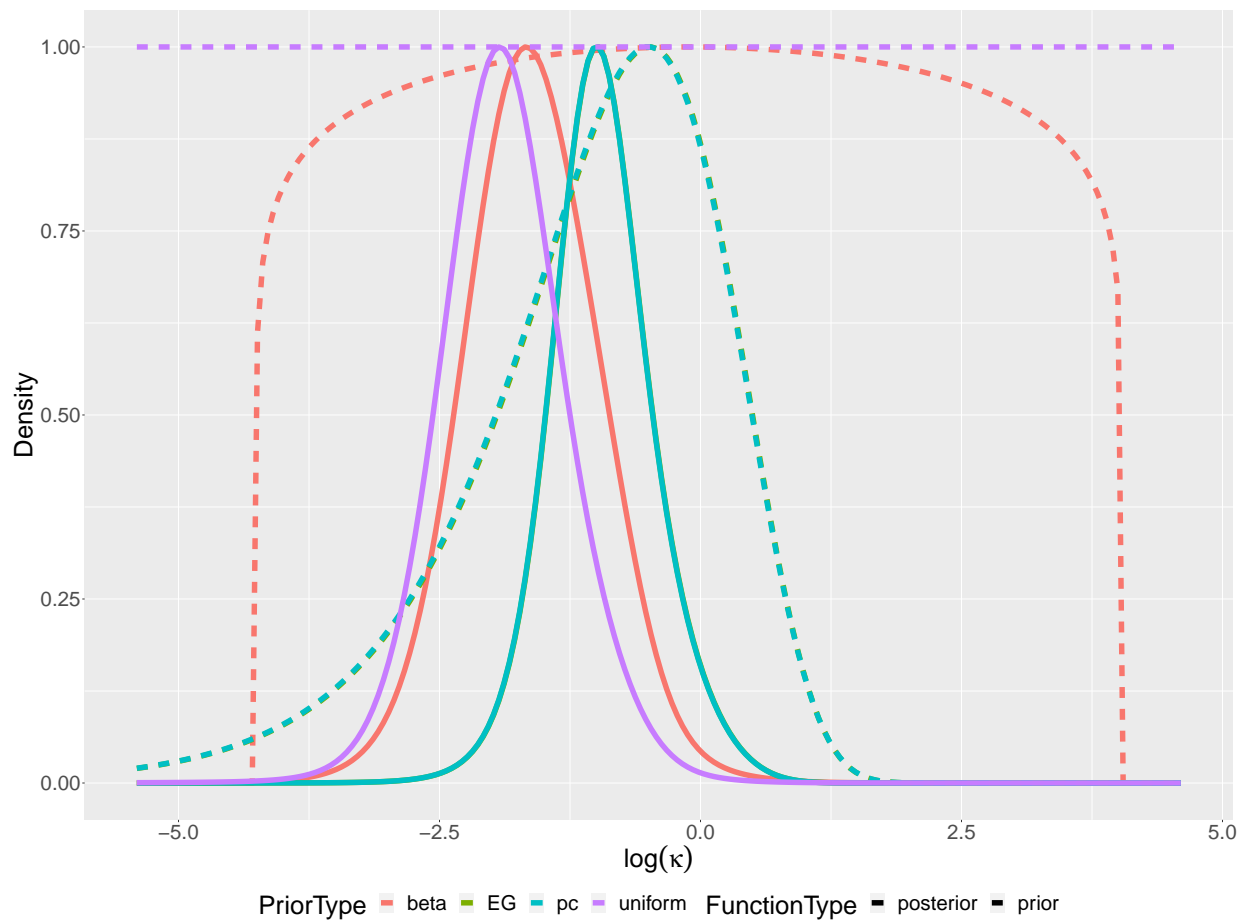


Figure 12: Renormalized marginal prior and posterior densities of  $\log(\kappa)$  for each of the four priors  $\pi_{\text{PC}}, \pi_{\text{EG}}, \pi_{\text{U}}, \pi_{\beta}$  and for a given observation  $\mathbf{y}$ .

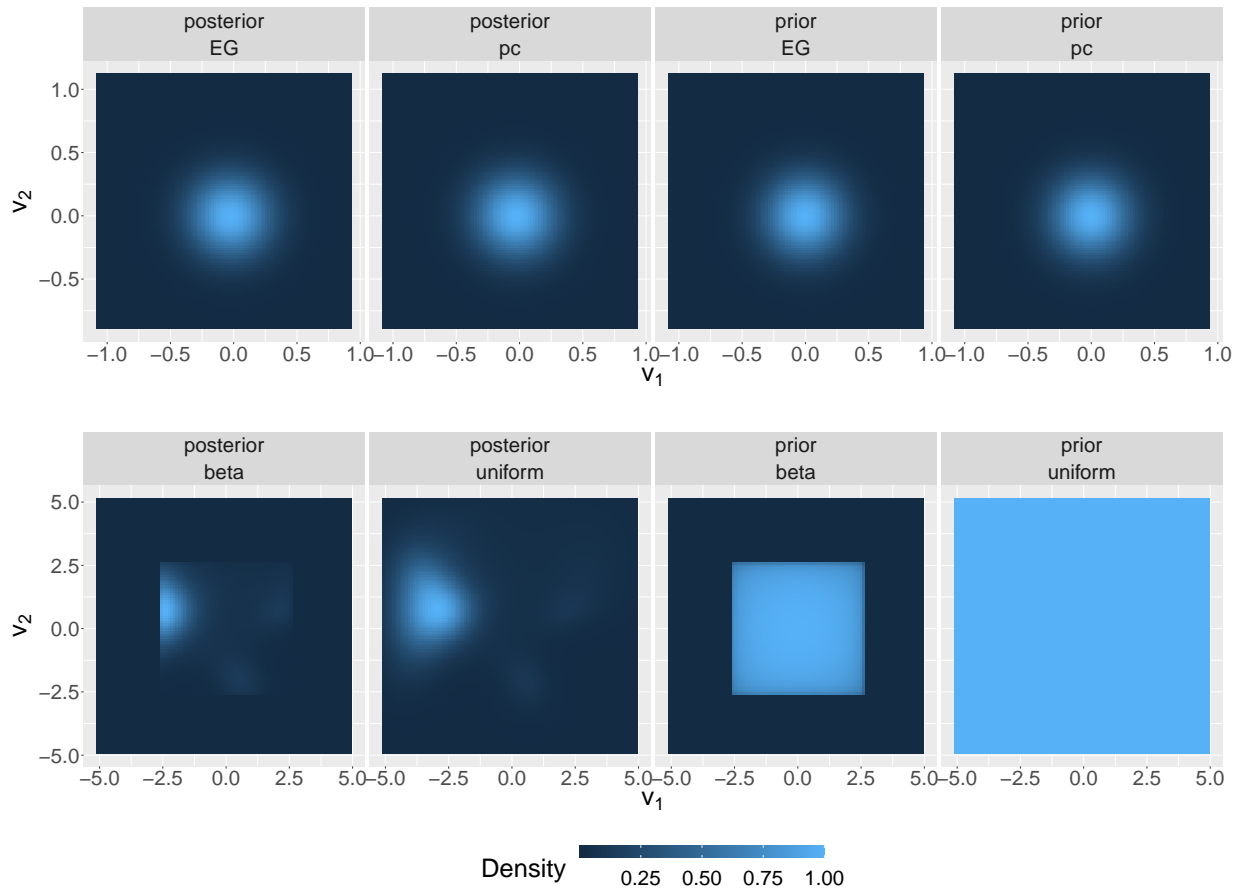


Figure 13: Marginal prior and posterior densities of  $v$  for each of the four priors  $\pi_{PC}, \pi_{EG}, \pi_U, \pi_\beta$  and for a given observation  $\mathbf{y}$

### S5.3 Posterior sampling

Returning to the simulation, our parameters are  $\boldsymbol{\theta} = (\log \kappa, \mathbf{v}, \log(\sigma_u), \log(\sigma_\varepsilon)) \in \mathbb{R}^5$ . Bayes formula gives for any prior  $\pi(\boldsymbol{\theta})$  on  $\boldsymbol{\theta}$  that

$$\pi(\boldsymbol{\theta}|\mathbf{y}) = \frac{\pi(\boldsymbol{\theta}, \mathbf{y}) \pi(\mathbf{u}|\boldsymbol{\theta}, \mathbf{y})}{\pi(\mathbf{y}) \pi(\mathbf{u}|\boldsymbol{\theta}, \mathbf{y})} = \frac{\pi(\boldsymbol{\theta})\pi(\mathbf{u}|\boldsymbol{\theta})\pi(\mathbf{y}|\mathbf{u}, \boldsymbol{\theta})}{\pi(\mathbf{y})\pi(\mathbf{u}|\boldsymbol{\theta}, \mathbf{y})}. \quad (53)$$

We note that the right-hand side of (54) involves  $\mathbf{u}$ . However, the resulting expression is independent of the value of  $\mathbf{u}$  chosen. As a result, the log posterior  $\ell(\boldsymbol{\theta}|\mathbf{y})$  is up to an

additive constant given by

$$\tilde{\ell}(\boldsymbol{\theta}|\mathbf{y}) = \ell(\boldsymbol{\theta}) + \ell(\mathbf{u}|\boldsymbol{\theta}) + \ell(\mathbf{y}|\mathbf{u}, \boldsymbol{\theta}) - \ell(\mathbf{u}|\boldsymbol{\theta}, \mathbf{y}) \quad (54)$$

**Observation 3.** *The maximum of the right-hand side of (54) is independent of  $\mathbf{u}$ . However, in the case where  $\ell(\mathbf{u}|\boldsymbol{\theta}, \mathbf{y})$  were not known, the value of  $\mathbf{u}$  would affect the result. If  $\mathbf{u}|\boldsymbol{\theta}, \mathbf{y}$  were approximated to be Gaussian, it would make the most sense to take  $\mathbf{u}$  as the mode  $\mathbf{m}_{\mathbf{u}}$  of this Gaussian approximation.*

In our case, all terms in (54) are known exactly. The log prior  $\ell(\boldsymbol{\theta})$  is determined by (23) and the remaining terms are given by

$$\begin{aligned} \ell(\mathbf{u}|\boldsymbol{\theta}) &= \frac{1}{2} \left( \log \|\mathbf{Q}_u\| - \|\mathbf{u} - \mathbf{m}_u\|_{\mathbf{Q}_u}^2 - n \log(2\pi) \right) \\ \ell(\mathbf{y}|\mathbf{u}, \boldsymbol{\theta}) &= \frac{1}{2} \left( \log \|\mathbf{Q}_\varepsilon\| - \|\mathbf{y} - \mathbf{A}\mathbf{u}\|_{\mathbf{Q}_\varepsilon}^2 - m \log(2\pi) \right) \\ \ell(\mathbf{u}|\boldsymbol{\theta}, \mathbf{y}) &= \frac{1}{2} \left( \log \|\mathbf{Q}_{\mathbf{u}|\mathbf{y}, \boldsymbol{\theta}}\| - \|\mathbf{u} - \mathbf{m}_{\mathbf{u}|\mathbf{y}, \boldsymbol{\theta}}\|_{\mathbf{Q}_{\mathbf{u}|\mathbf{y}, \boldsymbol{\theta}}}^2 - n \log(2\pi) \right), \end{aligned} \quad (55)$$

where we defined  $\|\mathbf{x}\|_{\mathbf{Q}}^2 := \mathbf{x}^T \mathbf{Q} \mathbf{x}$  and  $m$  is the dimension of  $\mathbf{y}$ . The precision  $\mathbf{Q}_u$  of  $\mathbf{u}$  is calculated by FEM and is given by (51) divided by  $4\pi\sigma_u^2$ . The remaining precision matrices are

$$\mathbf{Q}_{\mathbf{u}|\mathbf{y}, \boldsymbol{\theta}} := \mathbf{Q}_u + \mathbf{A}^T \mathbf{Q}_\varepsilon \mathbf{A}, \quad \mathbf{m}_{\mathbf{u}|\mathbf{y}, \boldsymbol{\theta}} := \mathbf{Q}_{\mathbf{u}|\mathbf{y}, \boldsymbol{\theta}}^{-1} (\mathbf{Q}_u \mathbf{m}_u + \mathbf{A}^T \mathbf{Q}_\varepsilon \mathbf{y}). \quad (56)$$

Maximizing the expression in (54) is made possible by the fact that the precision matrices are sparse. We obtain the MAP estimate

$$\hat{\boldsymbol{\theta}} := \arg \max_{\boldsymbol{\theta} \in \mathbb{R}^3} \ell(\boldsymbol{\theta}|\mathbf{y}) = \arg \max_{\boldsymbol{\theta} \in \mathbb{R}^3} \tilde{\ell}(\boldsymbol{\theta}|\mathbf{y}). \quad (57)$$

Using this, we do the following simulations. We fix as our domain the square  $[-1, 1]^2$  from which we sample uniformly and independently  $m = 15$  locations  $\{\mathbf{x}_j\}_{j=1}^m$  and use a mesh with  $n = 2062$  degrees of freedom. Then, we do the following.

For  $\pi_{\text{sim}} \in \{\pi_{\text{PC}}, \pi_{\text{EG}}, \pi_{\text{U}}, \pi_{\beta}\}$ :

1. For  $j = 1, \dots, N = 200$ :

(a) We simulate  $\boldsymbol{\theta}^{(j)\text{true}}$  from  $\pi_{\text{sim}}$ , use the FEM to simulate  $\mathbf{u}^{(j)}$  from (3) and then simulate  $\mathbf{y}^{(j)}$  from (21).

(b) For prior  $\pi_{\text{est}} \in \{\pi_{\text{PC}}, \pi_{\text{EG}}, \pi_{\text{U}}, \pi_{\beta}\}$  on  $\boldsymbol{\theta}$ :

i. We calculate a maximum a posteriori estimate  $\widehat{\boldsymbol{\theta}}^{(j)}$  using (57).

ii. We calculate  $\left| \theta_i^{(j)\text{true}} - \widehat{\theta}_i \right|$ .

iii. We calculate a Gaussian approximation to the posterior distribution. To do so, we write

$$\mathbf{Z} \sim \mathcal{N}\left(\widehat{\boldsymbol{\theta}}^{(j)}, \boldsymbol{\Sigma}_{\widehat{\boldsymbol{\theta}}|\mathbf{y}^{(j)}}\right), \quad (58)$$

where the precision, covariance, and marginal standard deviations of  $\mathbf{Z}$  are, respectively

$$\left[ \mathbf{M}_{\widehat{\boldsymbol{\theta}}^{(j)}|\mathbf{y}^{(j)}} \right]_{ij} = - \left( \frac{\partial^2 \ell\left(\widehat{\boldsymbol{\theta}}|\mathbf{y}^{(j)}\right)}{\partial \theta_i \partial \theta_j} \right), \quad \boldsymbol{\Sigma}_{\widehat{\boldsymbol{\theta}}^{(j)}|\mathbf{y}^{(j)}} = \mathbf{M}_{\widehat{\boldsymbol{\theta}}^{(j)}|\mathbf{y}^{(j)}}^{-1}.$$

We write  $\pi_{\mathbf{Z}}(\boldsymbol{\theta})$  for the density of  $\mathbf{Z}$ . If the posterior distribution is Gaussian, then  $\pi_{\mathbf{Z}} = \pi(\boldsymbol{\theta}|\mathbf{y}^{(j)})$ .

iv. We approximate the posterior measure using self-normalized importance sampling. This step is necessary as we only have access to the unnormalized  $\tilde{\ell}$  (see (54)).

We do this step both with and without Pareto smoothing [Vehtari et al. \(2015\)](#). In both cases, using  $\mathbf{Z}$  as our proposal distribution. Let  $\{\boldsymbol{\theta}^{(s)} \sim \mathbf{Z}, s = 1, \dots, S\}$  be i.i.d. We denote the normalized, unnormalized and self-normalized importance ratios by

$$r(\boldsymbol{\theta}) = \frac{\pi(\boldsymbol{\theta}|\mathbf{y}^{(j)})}{\pi_{\mathbf{Z}}(\boldsymbol{\theta})}, \quad \tilde{r}(\boldsymbol{\theta}) = \frac{\exp\left(\tilde{\ell}(\boldsymbol{\theta})\right)}{\pi_{\mathbf{Z}}(\boldsymbol{\theta})}, \quad \bar{r}(\boldsymbol{\theta}^{(s)}) := \frac{\tilde{r}(\boldsymbol{\theta}^{(s)})}{\sum_{s=1}^S \tilde{r}(\boldsymbol{\theta}^{(s)})}.$$



Since we do not have access to the normalizing constant of  $\pi(\boldsymbol{\theta}|\mathbf{y}^{(j)})$ , it is the last two ratios that we use. Using  $\bar{r}(\boldsymbol{\theta}^{(s)})$  calculate the normalized smoothed weights  $w(\boldsymbol{\theta}^{(s)})$  and approximate

$$\pi(\boldsymbol{\theta}|\mathbf{y}^{(j)}) \approx \pi_{\text{IS}}(\boldsymbol{\theta}|\mathbf{y}^{(j)}) := \sum_{s=1}^S w(\boldsymbol{\theta}^{(s)}) \delta_{\boldsymbol{\theta}^{(s)}}(\boldsymbol{\theta}).$$

In the case where Pareto smoothing is not used, we directly take  $w(\boldsymbol{\theta}^{(s)}) = \bar{r}(\boldsymbol{\theta}^{(s)})$ . The reason for using smoothing and no smoothing is to see if Pareto smoothing improves the approximation (for example, by comparing the frequency of times the true parameter is within the 0.95 confidence intervals). With this framework, the expect value of a function  $f(\boldsymbol{\theta})$  can be approximated as

$$\mathbb{E}[f(\boldsymbol{\theta})|\mathbf{y}^{(j)}] \approx \mathbb{E}_{\text{IS}}[f(\boldsymbol{\theta})|\mathbf{y}^{(j)}] := \sum_{s=1}^S w(\boldsymbol{\theta}^{(s)}) f(\boldsymbol{\theta}^{(s)}).$$

Additionally, we will be interested in the Kullback-Leibler divergence between the true posterior and the Gaussian approximation to the posterior. Here,  $f(\boldsymbol{\theta}) = \log(r(\boldsymbol{\theta}|\mathbf{y}^{(j)}))$  is known up to a normalizing constant, but we can approximate it using the self-normalized importance ratios as follows

$$\begin{aligned} \text{KLD}(\pi(\cdot|\mathbf{y}^{(j)})||\pi_{\mathbf{Z}}) &= \int_{\mathbb{R}^5} \pi(\boldsymbol{\theta}|\mathbf{y}^{(j)}) \log(r(\boldsymbol{\theta})) \, d\boldsymbol{\theta} \sim \sum_{s=1}^S \bar{r}(\boldsymbol{\theta}^{(s)}) \log(S\bar{r}(\boldsymbol{\theta}^{(s)})) \\ &\sim \sum_{s=1}^S w(\boldsymbol{\theta}^{(s)}) \log(Sw(\boldsymbol{\theta}^{(s)})), \end{aligned}$$

where the first equality is the definition of the Kullback-Leibler divergence and the first and second approximations are the self-normalized importance sampling step ( $r \sim S\bar{r}$ ) and smoothing step, respectively. This can be seen to converge to the true Kullback-Leibler divergence as  $S \rightarrow \infty$  by using that  $\tilde{r} = \mathbb{E}_{\mathbf{Z}}[\tilde{r}]r$  and the central limit theorem.

- v. Using  $\pi_{\text{IS}}(\boldsymbol{\theta}|\mathbf{y}^{(j)})$  we approximate the mean, covariance, and KL divergence and build a 0.95 credible interval  $I$  for  $\boldsymbol{\theta}$ . We also check whether the true parameter  $\boldsymbol{\theta}^{(j)\text{true}}$  is in  $I$  and compare these results against the Gaussian approximation to the posterior in (58).
- vi. We calculate  $a_i = \mathbb{P}_{\text{est}}\left[\theta_i \leq \theta_i^{(j)\text{true}} | \mathbf{y}^{(j)}\right]$  for  $i = 1, \dots, 5$  both in the case where  $\boldsymbol{\theta}$  is sampled from  $\pi_{\text{IS}}(\boldsymbol{\theta}|\mathbf{y}^{(j)})$  and from the Gaussian approximation to the posterior using prior  $\pi_{\text{est}}$ . We then plot the empirical cumulative distribution function of  $a_i$  and compare it to the uniform distribution. If the implementation is well calibrated, then  $a_i \sim U(0, 1)$ . See [Talts et al. \(2018\)](#); [Modrák et al. \(2023\)](#).

The above was tried using the Gaussian distribution  $Z$  to replace the posterior and not using importance sampling. The method using no smoothing in the importance sampling was also tested. But both the methods gave worse results than Pareto smoothed importance sampling and we only display this approximation in the results. Using Item 1(b)v, we can check whether the posterior distribution for  $\boldsymbol{\theta}$  is accurate, and using Item 1(b)vi, we check whether the implementation is well-calibrated.

**Observation 4.** *Since the uniform priors give support to extreme values of  $\kappa, \mathbf{v}$ , sampling the true parameter  $\boldsymbol{\theta}^{\text{true}}$  from the uniform prior often leads to singularities in the calculation of the importance samples. These cases made up a high percentage of the simulations (in one case, 90%), for which reason the improper uniform priors were not used to sample from  $\boldsymbol{\theta}^{\text{true}}$  in the simulations below. Rather, the width of the beta priors was also reduced when simulating these parameters to avoid singularities.*

The results for the MAP estimate and the CI lengths were already presented for the anisotropy parameters  $\log(\kappa), \mathbf{v}$  in Section 5 Figure 5 and Figure 6. Here, we begin by

presenting these results for the remaining parameters  $\log(\sigma_u), \log(\sigma_\varepsilon)$  in Figure 14 and Figure 15.

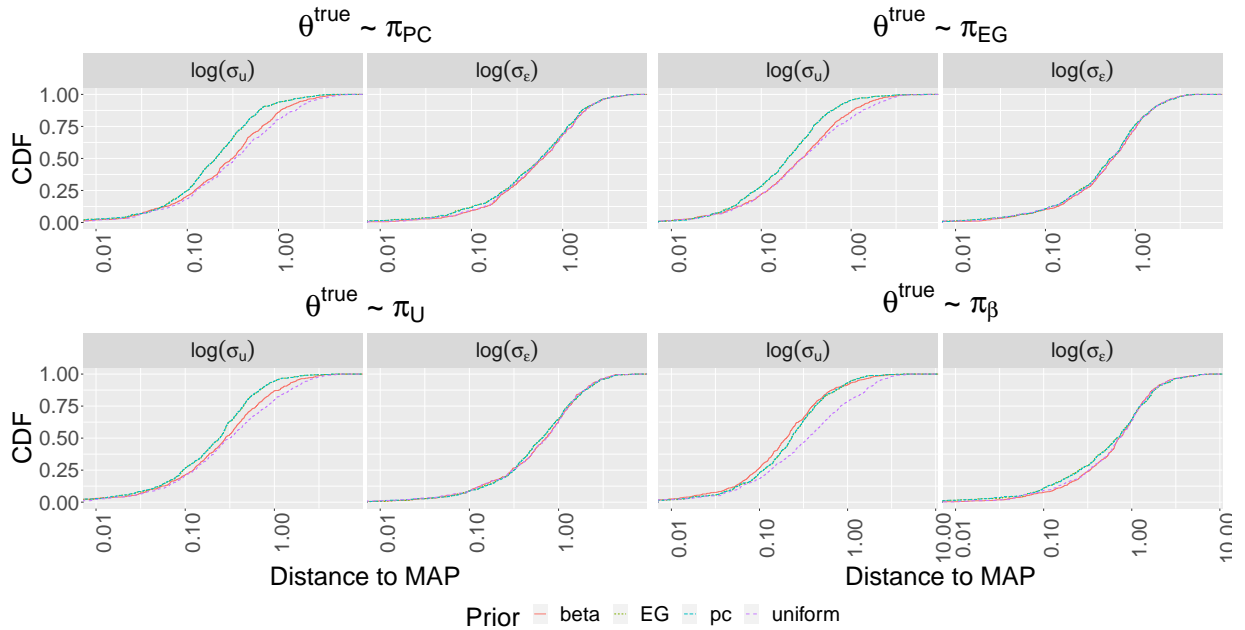


Figure 14: Empirical cumulative distribution function (eCDF) of the absolute distances between true parameter value ( $\theta_i^{\text{true}}$ ) and their estimated values ( $\hat{\theta}_i$ ) for each of  $\log(\sigma_u)$  and  $\log(\sigma_\varepsilon)$ . In the plots, arranged from left to right and top to bottom,  $\theta^{\text{true}}$  is simulated from the four distributions— $\pi_{\text{PC}}$ ,  $\pi_{\text{EG}}$ ,  $\pi_{\text{U}}$ , and  $\pi_{\beta}$ . Then,  $\mathbf{y} = \mathbf{A}\mathbf{u} + \varepsilon$  is observed with true parameter value  $\theta^{\text{true}}$ . Finally, for each prior (red, green, teal, purple), the MAP estimate  $\hat{\theta}$  is computed, and the eCDF over 600 simulations of the distances between  $\theta^{\text{true}}$  and  $\hat{\theta}$  is plotted.

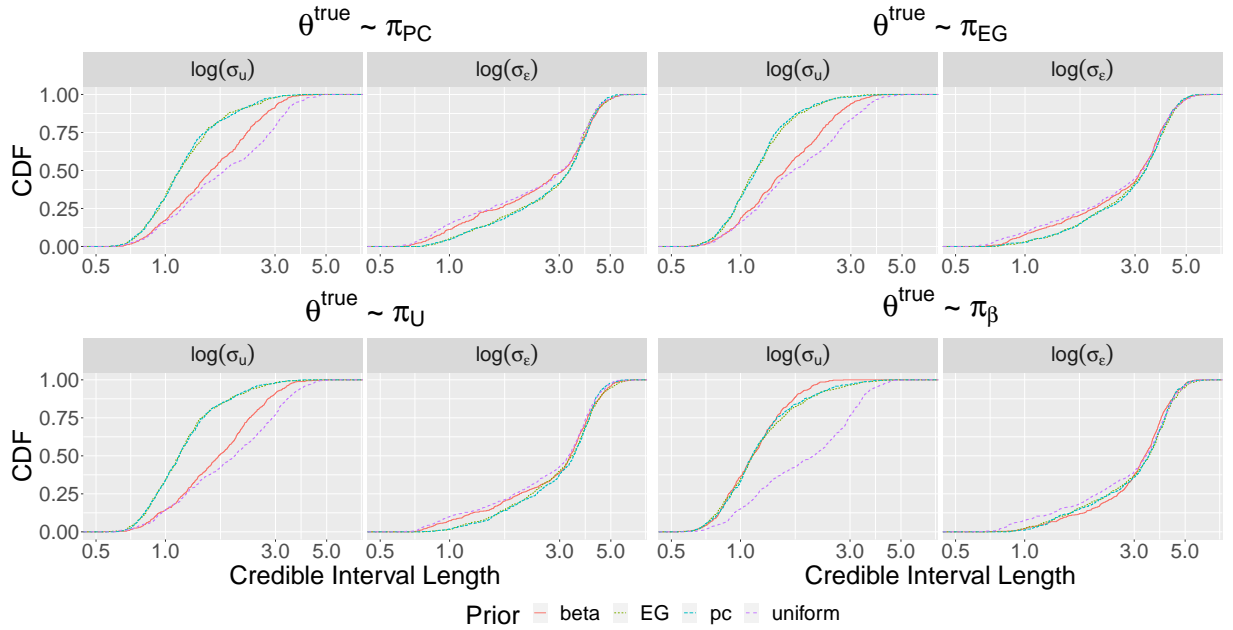


Figure 15: Empirical cumulative distribution function (eCDF) of the length of symmetric equal-tailed 0.95 credible intervals (CIs) for the posterior of the parameters  $\log(\sigma_u)$  and  $\log(\sigma_\epsilon)$ . In the plots, arranged from left to right and top to bottom,  $\theta^{\text{true}}$  is simulated from the four distributions— $\pi_{\text{PC}}$ ,  $\pi_{\text{EG}}$ ,  $\pi_{\text{U}}$ , and  $\pi_{\beta}$ . Then,  $\mathbf{y} = \mathbf{A}\mathbf{u} + \boldsymbol{\varepsilon}$  is observed with true parameter value  $\theta^{\text{true}}$ .

In Figure 16, we show the frequency of the true parameter being in the 0.95 credible interval. As can be seen in the graphs, the performance depends on the distribution from which  $\theta^{\text{true}}$  is sampled. If  $\theta^{\text{true}}$  is sampled from  $\pi_{\text{PC}}$  or  $\pi_{\text{EG}}$  then these two priors perform better, whereas otherwise  $\pi_{\text{U}}, \pi_{\beta}$  perform better. We also observe that the confidence intervals for  $\sigma_\epsilon$  are not wide enough. This may be due to the importance sampling. The results for the remaining parameters  $\log(\sigma_u), \log(\sigma_\epsilon)$  are more similar, which is explained by the fact that the same priors for these parameters are used in all cases. This is a common theme in the results, and we will not comment on it further.

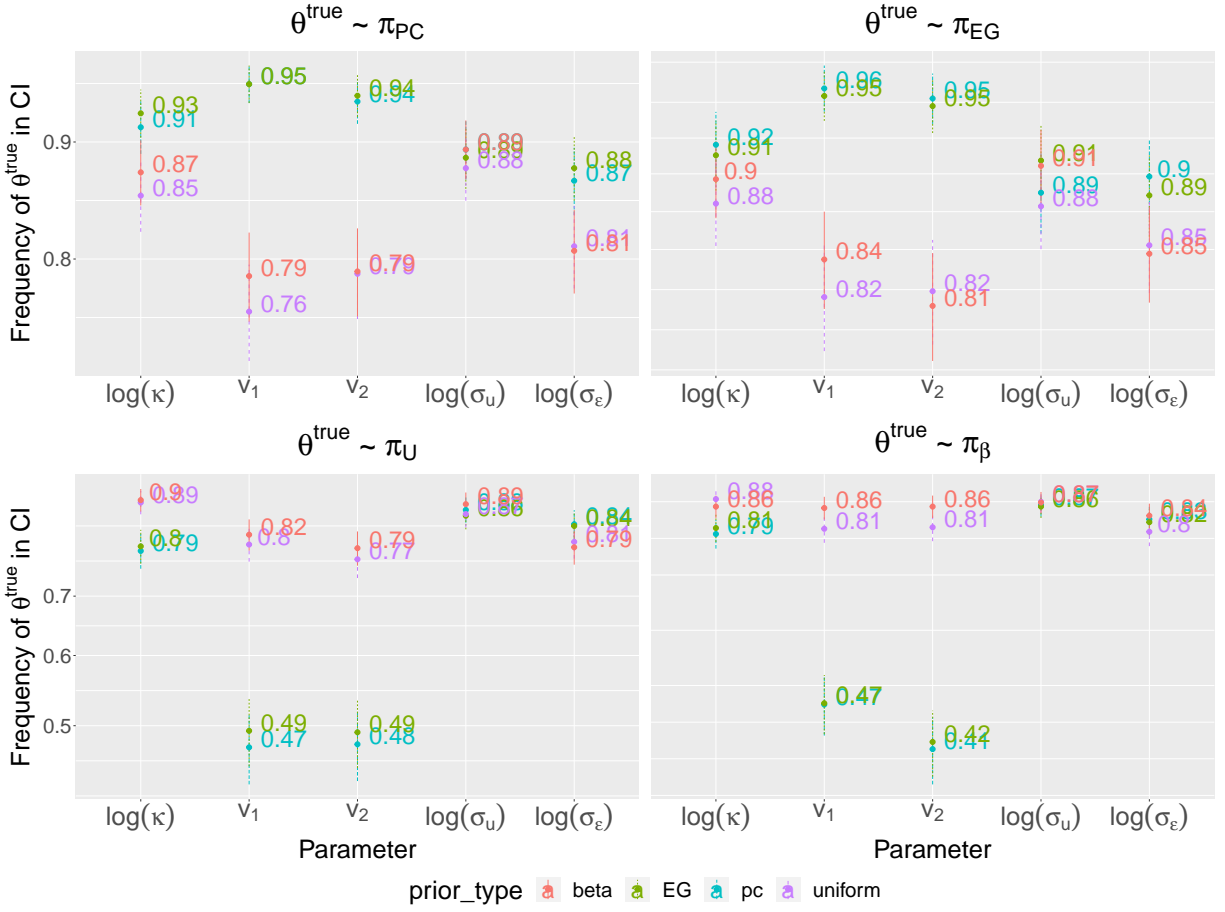


Figure 16: Frequency of true parameter being in the 0.95 credible interval

In Figure 17, we show the eCDF of probabilities  $a_i = \mathbb{P}[\theta_i \leq \theta_i^{\text{true}} | \mathbf{y}]$  for each of the five parameters. If the implementation is well calibrated, then  $a_i$  should be uniform when  $\pi_{\text{sim}} = \pi$ . Once more, the performance is divided into two cases. If  $\theta^{\text{true}}$  is sampled from  $\pi_{\text{PC}}$  or  $\pi_{\text{EG}}$  then these two priors perform better, whereas otherwise  $\pi_{\text{U}}, \pi_{\beta}$  perform better.

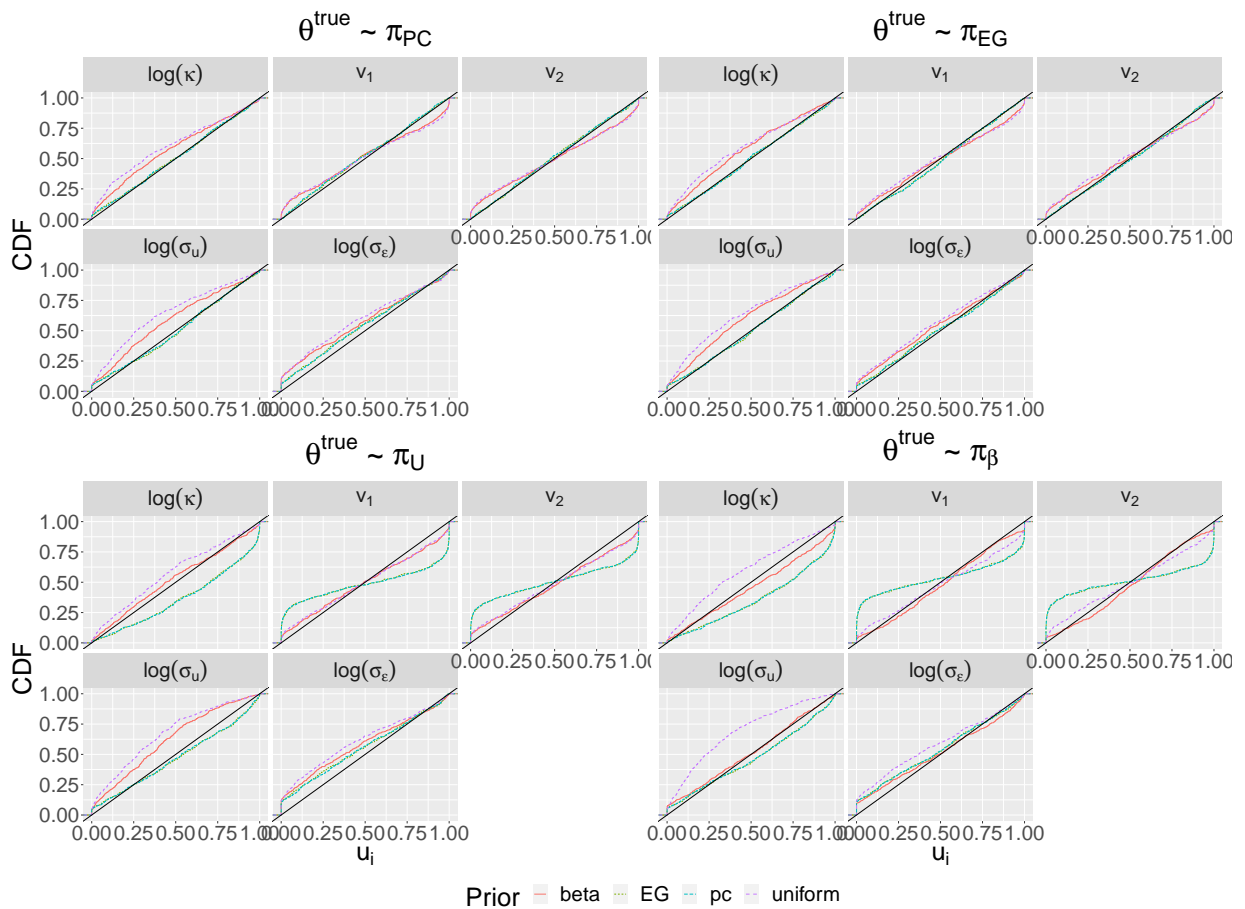


Figure 17: eCDF of probabilities  $a_i = \mathbb{P}_{\text{est}}[\theta_i \leq \theta_i^{\text{true}} | \mathbf{y}]$  where  $\theta^{\text{true}}$  and  $\mathbf{y}$  come from the true model.

In Table 6, we show the  $p$ -values for the KS test between  $a_i = \mathbb{P}_{\text{est}}[\theta_i \leq \theta_i^{\text{true}} | \mathbf{y}]$  and the CDF of the uniform distribution.

Prior	$\log(\kappa)$	$v_1$	$v_2$	$\log(\sigma_u)$	$\log(\sigma_\epsilon)$
$\pi_{\text{PC}}$	3.72e-01	2.34e-01	6.60e-01	1.17e-01	6.240e-03
$\pi_{\text{EG}}$	5.55e-01	2.55e-01	8.37e-01	1.05e-01	2.720e-03
$\pi_{\text{U}}$	0.00e+00	9.42e-08	3.07e-06	0.00e+00	1.020e-12
$\pi_{\beta}$	1.14e-08	1.44e-05	4.77e-05	1.71e-10	9.070e-10

Table 2:  $\theta^{\text{true}} \sim \pi_{\text{PC}}$

Prior	$\log(\kappa)$	$v_1$	$v_2$	$\log(\sigma_u)$	$\log(\sigma_\epsilon)$
$\pi_{\text{PC}}$	0.00e+00	0.00e+00	0.00e+00	2.55e-04	1.73e-06
$\pi_{\text{EG}}$	0.00e+00	0.00e+00	0.00e+00	5.69e-05	3.35e-07
$\pi_{\text{U}}$	2.70e-09	1.51e-03	6.95e-06	0.00e+00	0.00e+00
$\pi_{\beta}$	2.78e-02	1.25e-04	3.59e-05	0.00e+00	2.86e-12

Table 4:  $\theta^{\text{true}} \sim \pi_{\text{U}}$

Prior	$\log(\kappa)$	$v_1$	$v_2$	$\log(\sigma_u)$	$\log(\sigma_\epsilon)$
$\pi_{\text{PC}}$	7.46e-01	1.96e-01	5.57e-01	1.47e-01	2.060e-01
$\pi_{\text{EG}}$	8.42e-01	2.05e-01	6.62e-01	3.17e-01	1.380e-01
$\pi_{\text{U}}$	3.77e-15	1.63e-05	6.85e-04	0.00e+00	1.100e-06
$\pi_{\beta}$	2.25e-09	4.78e-04	1.60e-03	1.88e-12	8.440e-04

Table 3:  $\theta^{\text{true}} \sim \pi_{\text{EG}}$

Prior	$\log(\kappa)$	$v_1$	$v_2$	$\log(\sigma_u)$	$\log(\sigma_\epsilon)$
$\pi_{\text{PC}}$	0.00e+00	0.00e+00	0.00e+00	7.26e-04	3.15e-06
$\pi_{\text{EG}}$	0.00e+00	0.00e+00	0.00e+00	1.54e-03	6.40e-07
$\pi_{\text{U}}$	7.88e-15	8.50e-06	3.35e-04	0.00e+00	3.73e-13
$\pi_{\beta}$	1.06e-04	8.80e-03	2.57e-02	4.48e-03	5.06e-05

Table 5:  $\theta^{\text{true}} \sim \pi_{\beta}$

Table 6: KS statistic between  $a_i = \mathbb{P}_{\text{est}}[\theta_i \leq \theta_i^{\text{true}} | \mathbf{y}]$  and the CDF of the uniform distribution

In Figure 18, we show the empirical difference against  $F(a_i)$  together with a 95% confidence interval. As can be seen from the plots, the implementation is well-calibrated.

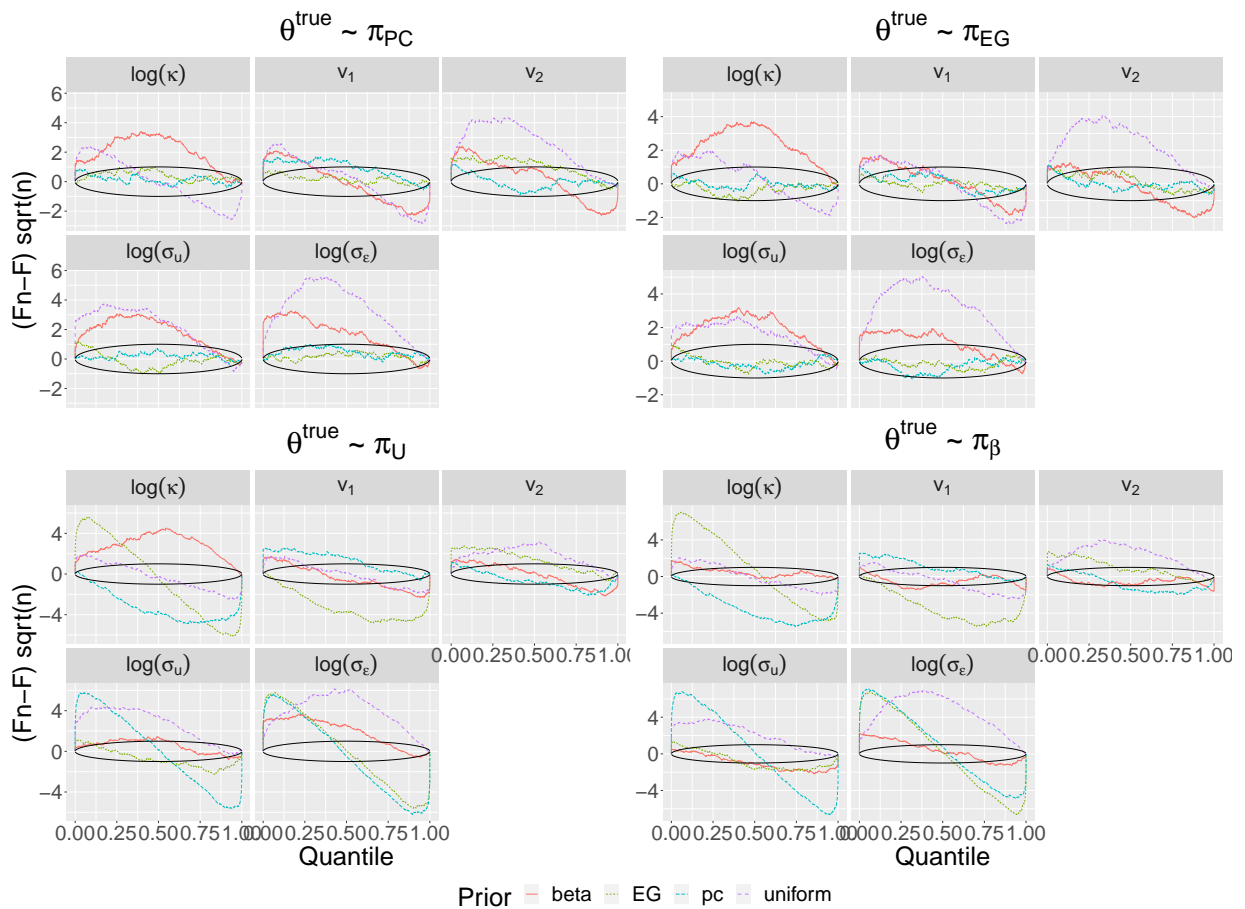


Figure 18: Plot of the empirical difference against  $F(a_i)$  together with a 95% confidence interval

In Figure 19, we show the eCDF of the Kullback-Leibler divergence between the posterior and the Gaussian approximation to the posterior around the median. As can be seen from the plots, in all cases  $\pi_{PC}(\cdot|\mathbf{y})$  and  $\pi_{EG}(\cdot|\mathbf{y})$  are closer to their respective Gaussian approximations than  $\pi_U(\cdot|\mathbf{y})$  and  $\pi_\beta(\cdot|\mathbf{y})$ . This is because the posteriors using  $\pi_U, \pi_\beta$  are very much not Gaussian.



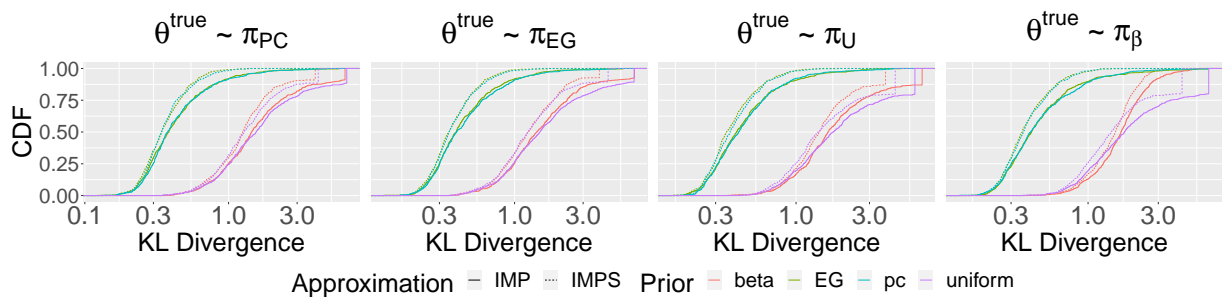


Figure 19: Kullback-Leibler divergence between the posterior and the Gaussian approximation to the posterior around the median.

To better compare PC and exponential-Gaussian priors, we also plot these separately. As can be seen, once more, they behave quite similarly, showing that both formulations lead to a practically identical penalization of complexity.

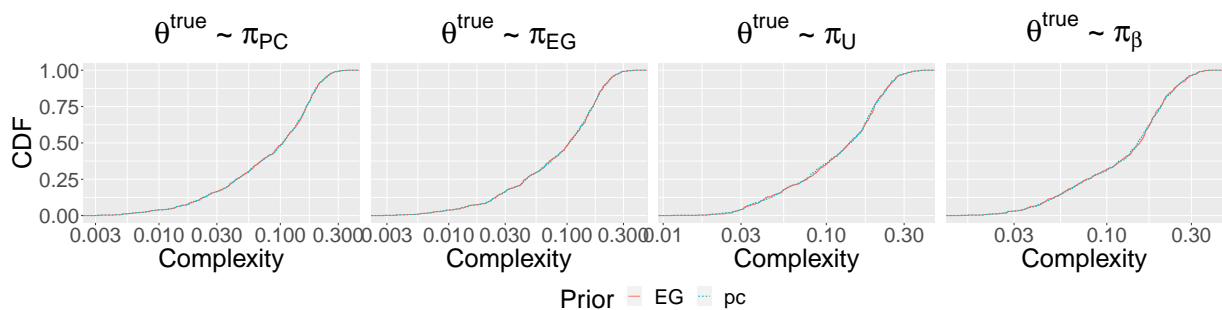


Figure 20: CDF of the posterior complexity  $d(\kappa, \mathbf{v})$  for PC and not exponential-Gaussian priors

## S6 Precipitation study details

### S6.1 Calculations

In this section, we show how to calculate scores of Section 6. For what follows, we first define the leave out one mean of  $y_i$  having observed all locations except  $y_i$

$$m_{y_i|\mathbf{y}_{-i}} := \int_{\mathbb{R}^5} \left( \int_{\mathbb{R}} y_i \pi(y_i|\mathbf{y}_{-i}, \boldsymbol{\theta}) dy_i \right) \pi(\boldsymbol{\theta}|\mathbf{y}) d\boldsymbol{\theta} = \int_{\mathbb{R}^5} m_{y_i|\mathbf{y}_{-i}, \boldsymbol{\theta}} \pi(\boldsymbol{\theta}|\mathbf{y}) d\boldsymbol{\theta}. \quad (59)$$

The expression of  $m_{y_i|\mathbf{y}_{-i}}$  is approximately that of  $\mathbb{E}[y_i|\mathbf{y}_{-i}]$ , with the exception that the integral in (59) is against  $\pi(\boldsymbol{\theta}|\mathbf{y})$  as opposed to  $\pi(\boldsymbol{\theta}|\mathbf{y}_{-i})$ . This is a common approach to calculating the LOO predictions as it avoids the need to approximate  $\pi(\boldsymbol{\theta}|\mathbf{y}_{-i})$  for each  $i$ . The expression is justified by the fact that the posterior distribution of  $\boldsymbol{\theta}$  does not depend much on any single observation. That is,  $\pi(\boldsymbol{\theta}|\mathbf{y}) \approx \pi(\boldsymbol{\theta}|\mathbf{y}_{-i})$ . Similarly, we will need the posterior leave out one variance

$$\sigma_{y_i|\mathbf{y}_{-i}}^2 := \int_{\mathbb{R}^5} \sigma_{y_i|\mathbf{y}_{-i}, \boldsymbol{\theta}}^2 \pi(\boldsymbol{\theta}|\mathbf{y}) d\boldsymbol{\theta}, \quad (60)$$

where  $\sigma_{y_i|\mathbf{y}_{-i}, \boldsymbol{\theta}}^2$  is the posterior variance of  $y_i$  having observed all locations except  $y_i$ . This will be used later in the computations.

Because of the independence of  $\mathbf{u}, \boldsymbol{\beta}$  from  $\boldsymbol{\theta}$  we have that

$$\mathbf{u}_\beta | \boldsymbol{\theta} \sim \mathcal{N}(\mathbf{0}, \mathbf{Q}_{\mathbf{u}_\beta}^{-1}), \quad \text{where} \quad \mathbf{Q}_{\mathbf{u}_\beta} := \begin{bmatrix} \mathbf{Q}_\beta & \mathbf{0}_{2 \times n} \\ \mathbf{0}_{n \times 2} & \mathbf{Q}_u \end{bmatrix}.$$

We can then calculate  $\hat{\boldsymbol{\theta}}$  to maximize the (unnormalized) log-posterior as in (54)

$$\tilde{\ell}(\boldsymbol{\theta}|\mathbf{y}) = \ell(\boldsymbol{\theta}) + \ell(\mathbf{u}_\beta|\boldsymbol{\theta}) + \ell(\mathbf{y}|\mathbf{u}_\beta, \boldsymbol{\theta}) - \ell(\mathbf{u}_\beta|\boldsymbol{\theta}, \mathbf{y}). \quad (61)$$

To calculate the RMSE, CRPS, and DSS, it is sufficient to calculate the posterior mean and variance of  $y_i$  given  $\mathbf{y}_{-i}$  and  $\boldsymbol{\theta}$ . We show how to do this efficiently.

Due to the independence of  $\mathbf{u}$  and  $\varepsilon$  and of  $\varepsilon_i$  and  $\varepsilon_{-i}$  knowing  $\boldsymbol{\theta}$ , we deduce that  $\mathbf{y}_{-i} = \mathbf{A}_{-i}\mathbf{u} + \varepsilon_{-i}$  and  $\varepsilon_i$  are independent knowing  $\boldsymbol{\theta}$ . As a result,

$$\begin{aligned} y_i|\mathbf{y}_{-i}, \boldsymbol{\theta} &= (\mathbf{A}_i\mathbf{u})|\mathbf{y}_{-i}, \boldsymbol{\theta} + \varepsilon_i|\boldsymbol{\theta} \sim \mathcal{N}(\mathbf{A}_i\mathbf{m}_{\mathbf{u}|\mathbf{y}_{-i},\boldsymbol{\theta}}, \mathbf{A}_i\boldsymbol{\Sigma}_{\mathbf{u}|\mathbf{y}_{-i},\boldsymbol{\theta}}\mathbf{A}_i^T + \sigma_\varepsilon^2) \\ &= \mathcal{N}(m_{y_i|\mathbf{y}_{-i},\boldsymbol{\theta}}, \sigma_{y_i|\mathbf{y}_{-i},\boldsymbol{\theta}}^2), \end{aligned} \quad (62)$$

where  $\mathbf{A}_i \in \mathbb{R}^{1 \times N}$  is the  $i$ -th row of  $\mathbf{A}$ . Furthermore, we have that, see (56)

$$\begin{aligned} \mathbf{Q}_{\mathbf{u}|\mathbf{y}_{-i},\boldsymbol{\theta}} &= \mathbf{Q}_{\mathbf{u}} + \sigma_\varepsilon^{-2}\mathbf{A}_{-i}^T\mathbf{A}_{-i} = \mathbf{Q}_{\mathbf{u}|\mathbf{y},\boldsymbol{\theta}} - \sigma_\varepsilon^{-2}\mathbf{A}_i^T\mathbf{A}_i \\ \mathbf{m}_{\mathbf{u}|\mathbf{y}_{-i},\boldsymbol{\theta}} &= \sigma_\varepsilon^{-2}\boldsymbol{\Sigma}_{\mathbf{u}|\mathbf{y}_{-i},\boldsymbol{\theta}}\mathbf{A}_{-i}^T\mathbf{y}_{-i}, \end{aligned} \quad (63)$$

where we wrote  $\mathbf{A}_{-i} \in \mathbb{R}^{(n-1) \times N}$  for the matrix  $\mathbf{A}$  with the  $i$ -th row removed. To avoid calculating an inverse for each  $i$ , we can calculate  $\boldsymbol{\Sigma}_{\mathbf{u}|\mathbf{y},\boldsymbol{\theta}}$  once and then use the rank 1 correction provided by the Sherman-Morrison formula to obtain

$$\boldsymbol{\Sigma}_{\mathbf{u}|\mathbf{y}_{-i},\boldsymbol{\theta}} = \boldsymbol{\Sigma}_{\mathbf{u}|\mathbf{y},\boldsymbol{\theta}} + \frac{\boldsymbol{\Sigma}_{\mathbf{u}|\mathbf{y},\boldsymbol{\theta}}\mathbf{A}_i^T\mathbf{A}_i\boldsymbol{\Sigma}_{\mathbf{u}|\mathbf{y},\boldsymbol{\theta}}}{\sigma_\varepsilon^2 - \mathbf{A}_i\boldsymbol{\Sigma}_{\mathbf{u}|\mathbf{y},\boldsymbol{\theta}}\mathbf{A}_i^T}. \quad (64)$$

Using (64) in (62) and writing  $V_i := \mathbf{A}_i\boldsymbol{\Sigma}_{\mathbf{u}|\mathbf{y},\boldsymbol{\theta}}\mathbf{A}_i^T$  and  $q_\varepsilon := \sigma_\varepsilon^{-2}$ , gives

$$\sigma_{y_i|\mathbf{y}_{-i},\boldsymbol{\theta}}^2 = V_i + \frac{V_i^2}{\sigma_\varepsilon^2 - V_i} + \sigma_\varepsilon^2 = \frac{V_i}{1 - q_\varepsilon V_i} + \sigma_\varepsilon^2 = \frac{\sigma_\varepsilon^2}{1 - q_\varepsilon V_i}. \quad (65)$$

Furthermore, for the mean, we have from (63) that

$$m_{y_i|\mathbf{y}_{-i},\boldsymbol{\theta}} = q_\varepsilon\mathbf{A}_i\boldsymbol{\Sigma}_{\mathbf{u}|\mathbf{y}_{-i},\boldsymbol{\theta}}\mathbf{A}_{-i}^T\mathbf{y}_{-i} = q_\varepsilon\mathbf{A}_i\boldsymbol{\Sigma}_{\mathbf{u}|\mathbf{y}_{-i},\boldsymbol{\theta}}\mathbf{A}^T\mathbf{y} - q_\varepsilon\mathbf{A}_i\boldsymbol{\Sigma}_{\mathbf{u}|\mathbf{y}_{-i},\boldsymbol{\theta}}\mathbf{A}_i^T y_i \quad (66)$$

Let us write

$$\eta_i := \mathbb{E}[\mathbf{A}_i\mathbf{u}|\mathbf{y}, \boldsymbol{\theta}] = \mathbf{A}_i\mathbf{m}_{\mathbf{u}|\mathbf{y},\boldsymbol{\theta}} = q_\varepsilon\mathbf{A}_i\boldsymbol{\Sigma}_{\mathbf{u}|\mathbf{y},\boldsymbol{\theta}}\mathbf{A}^T\mathbf{y},$$

Then, using the rank 1 correction in (64) we obtain for the first term in (66) that

$$\begin{aligned} q_\varepsilon\mathbf{A}_i\boldsymbol{\Sigma}_{\mathbf{u}|\mathbf{y}_{-i},\boldsymbol{\theta}}\mathbf{A}^T\mathbf{y} &= q_\varepsilon\mathbf{A}_i\boldsymbol{\Sigma}_{\mathbf{u}|\mathbf{y},\boldsymbol{\theta}}\mathbf{A}^T\mathbf{y} + q_\varepsilon\mathbf{A}_i\frac{\boldsymbol{\Sigma}_{\mathbf{u}|\mathbf{y},\boldsymbol{\theta}}\mathbf{A}_i^T\mathbf{A}_i\boldsymbol{\Sigma}_{\mathbf{u}|\mathbf{y},\boldsymbol{\theta}}}{\sigma_\varepsilon^2 - \mathbf{A}_i\boldsymbol{\Sigma}_{\mathbf{u}|\mathbf{y},\boldsymbol{\theta}}\mathbf{A}_i^T}\mathbf{A}^T\mathbf{y} \\ &= \eta_i + \frac{V_i}{\sigma_\varepsilon^2 - V_i}\eta_i = \frac{\eta_i}{1 - q_\varepsilon V_i}. \end{aligned} \quad (67)$$

Whereas, for the second term in (66), we have that

$$\begin{aligned} q_\varepsilon \mathbf{A}_i \boldsymbol{\Sigma}_{\mathbf{u}|\mathbf{y}_{-i}, \boldsymbol{\theta}} \mathbf{A}_i^T y_i &= q_\varepsilon \mathbf{A}_i \boldsymbol{\Sigma}_{\mathbf{u}|\mathbf{y}, \boldsymbol{\theta}} \mathbf{A}_i^T y_i + q_\varepsilon \mathbf{A}_i \frac{\boldsymbol{\Sigma}_{\mathbf{u}|\mathbf{y}, \boldsymbol{\theta}} \mathbf{A}_i^T \mathbf{A}_i \boldsymbol{\Sigma}_{\mathbf{u}|\mathbf{y}, \boldsymbol{\theta}}}{\sigma_\varepsilon^2 - \mathbf{A}_i \boldsymbol{\Sigma}_{\mathbf{u}|\mathbf{y}, \boldsymbol{\theta}} \mathbf{A}_i^T} \mathbf{A}_i^T y_i \\ &= q_\varepsilon V_i y_i + q_\varepsilon \frac{V_i^2}{\sigma_\varepsilon^2 - V_i} y_i = q_\varepsilon V_i y_i \left( 1 + q_\varepsilon \frac{V_i}{1 - q_\varepsilon V_i} \right) = \frac{q_\varepsilon V_i y_i}{1 - q_\varepsilon V_i} \end{aligned} \quad (68)$$

Using (67) and (68) in (66) we obtain

$$m_{y_i|\mathbf{y}_{-i}, \boldsymbol{\theta}} = \frac{\eta_i}{1 - q_\varepsilon V_i} - \frac{q_\varepsilon V_i y_i}{1 - q_\varepsilon V_i} = \frac{\eta_i - q_\varepsilon V_i y_i}{1 - q_\varepsilon V_i} = y_i + \frac{\eta_i - y_i}{1 - q_\varepsilon V_i}. \quad (69)$$

The term  $V_i$  can be calculated efficiently using a Takahashi recursion on the Cholesky factor of the posterior precision  $\mathbf{Q}_{\mathbf{u}|\mathbf{y}, \boldsymbol{\theta}}$  without the need to calculate a dense matrix inverse, as implemented by `inla.qinv`. To calculate  $\eta_i$ , we use a matrix-vector solve.

Next, since the expression of  $\pi(\boldsymbol{\theta}|\mathbf{y}_i)$  is known up to a normalizing constant, we can use importance sampling and Riemann integration together with (65), (69) to calculate (59).

To estimate the CRPS, we use importance sampling and the expression for the posterior predictive distribution (59). We have

$$F_i(t) := \int_{\mathbb{R}^5} \left( \int_{-\infty}^t \pi(y_i|\mathbf{y}_{-i}, \boldsymbol{\theta}) dy_i \right) p(\boldsymbol{\theta}|\mathbf{y}) d\boldsymbol{\theta} \approx \sum_{j=1}^J \Phi \left( \frac{t - m_{y_i|\mathbf{y}_{-i}, \boldsymbol{\theta}_j}}{\sigma_{y_i|\mathbf{y}_{-i}, \boldsymbol{\theta}_j}} \right) w_j,$$

where  $\Phi$  is the cumulative distribution function of a standard Gaussian variable, and  $\boldsymbol{\theta}_j, w_j$  are the importance samples and smoothed self-normalized weights. Using this expression and the fact that there is an exact expression for the CRPS of a Gaussian mixture [Grimit et al. \(2006\)](#), we obtain the CRPS.

## S6.2 Spatial analysis of the scores

We hypothesize that perhaps some of the models perform better than others in different spatial areas. To confirm this hypothesis, we begin by plotting the difference in the scores between the isotropic and anisotropic PC models. We plot the difference of the scores for the RMSE, CRPS, and DSS in Figure 21.

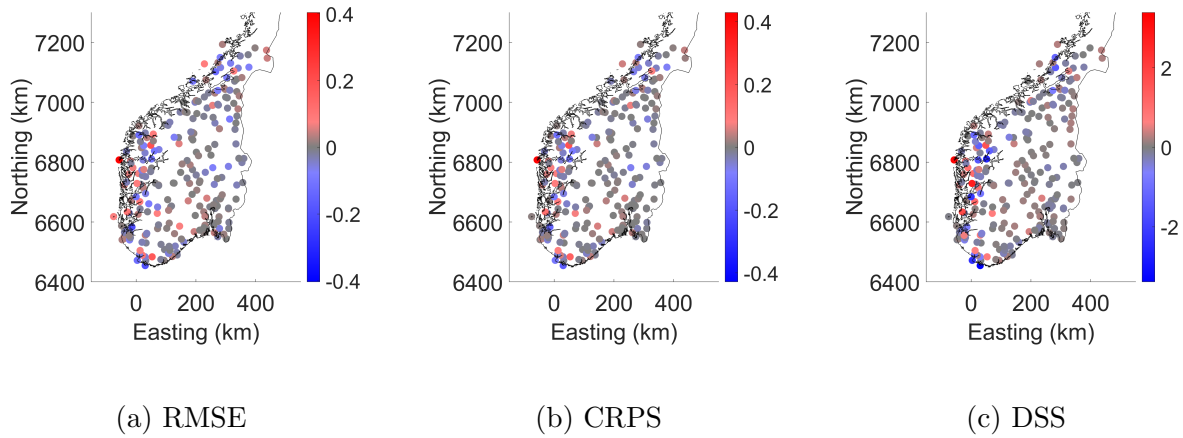


Figure 21: Difference of scores between the isotropic and anisotropic PC models

We also do the same for the difference in the scores between the isotropic and anisotropic EG models in Figure 22. The results are very similar. We observe that the anisotropic models perform better towards the western coast and worse in the remaining region. This is to be expected as the correlation structure is different in the region with high elevation than the lower elevation parts of the domain and indicates that a non-stationary model might be more appropriate as the anisotropy varies in space.

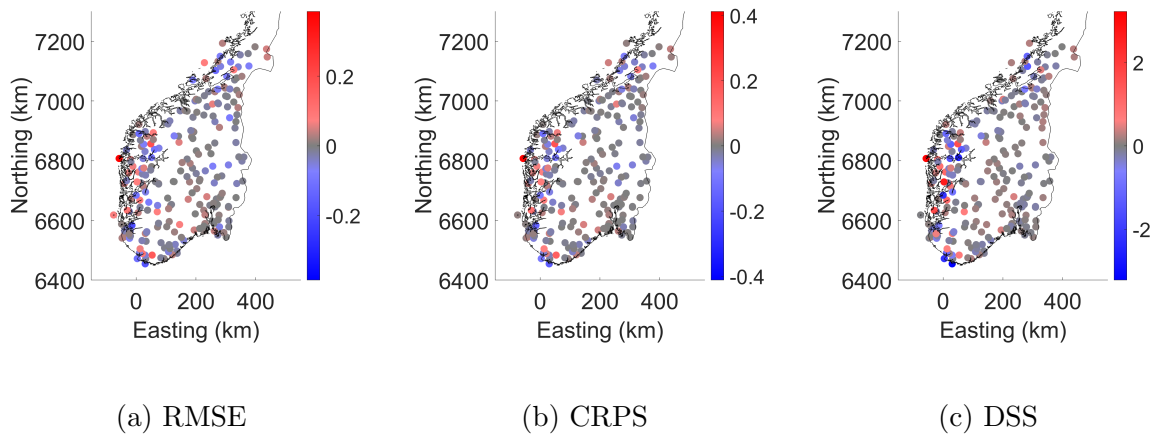


Figure 22: Difference of scores between the isotropic PC and anisotropic EG models

### S6.3 Precipitation simulation study

In this section, we repeat the structure of the simulations in Section 6, but now, to investigate how the quality of the prediction changes with increased data, we use synthetic data. To do so, we simulate precipitation data on 4000 uniformly distributed locations in Norway from the model in (25) with parameters

$$\begin{aligned} \hat{\rho} &= 201, & \hat{\mathbf{v}} &= (-0.45, 0.03), & \hat{\sigma}_u &= 0.63, & \hat{\sigma}_\varepsilon &= 0.14, & \beta_0 &= 0.96, & \beta_1 &= 0.67 \\ \hat{\rho} &= 132, & \hat{\mathbf{v}} &= (0.00, 0.00), & \hat{\sigma}_u &= 0.65, & \hat{\sigma}_\varepsilon &= 0.13, & \beta_0 &= 0.93, & \beta_1 &= 0.66. \end{aligned}$$

These correspond to data generated from anisotropic and isotropic models, respectively, using the MAP obtained for the precipitation data in Section 6.4 using anisotropic and isotropic PC priors, respectively. The data is shown in Figure 23.

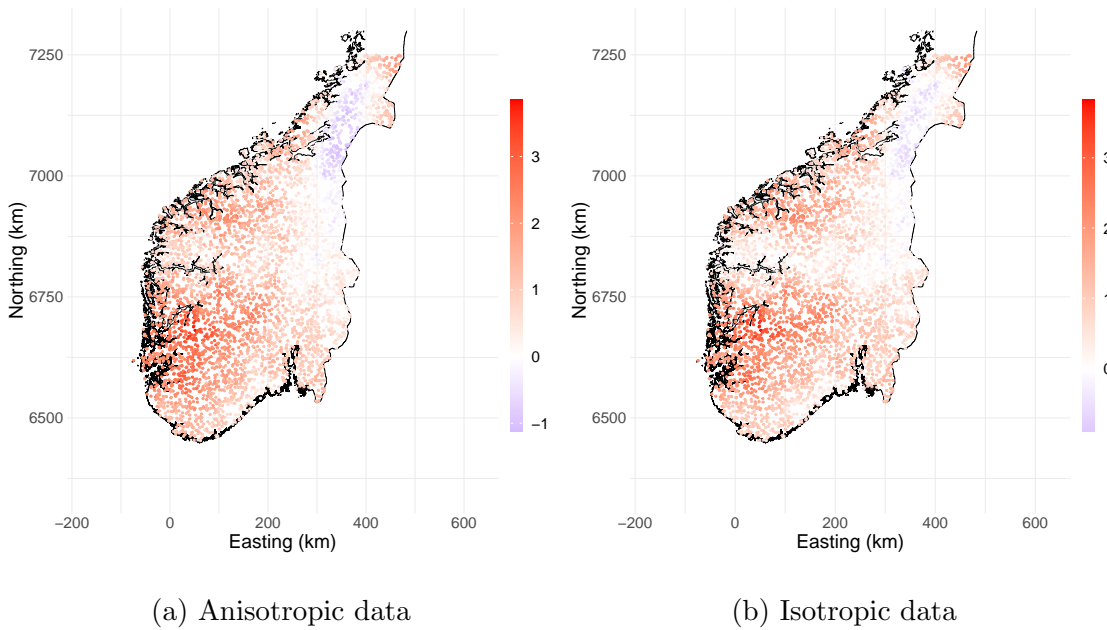


Figure 23: Precipitation data simulated using model (25) using an anisotropic and isotropic field  $u$  respectively

We then fit the model to the data and calculate the RMSE, CRPS, and DSS scores. We repeat this process for  $n_y = 25, 50, 100, 150, 200, 400, 600, 800, 1000$  observations sampled

uniformly from the simulated data. We repeat this process 100 times for each  $n_y$  and each prior. The results are shown in Figure 11. As can be seen from the plots, the anisotropic model performs better than the isotropic model for less data. However, as the number of observations increases, the scores become almost equal. The difference between the anisotropic PC and EG models is less pronounced than in the previous section.

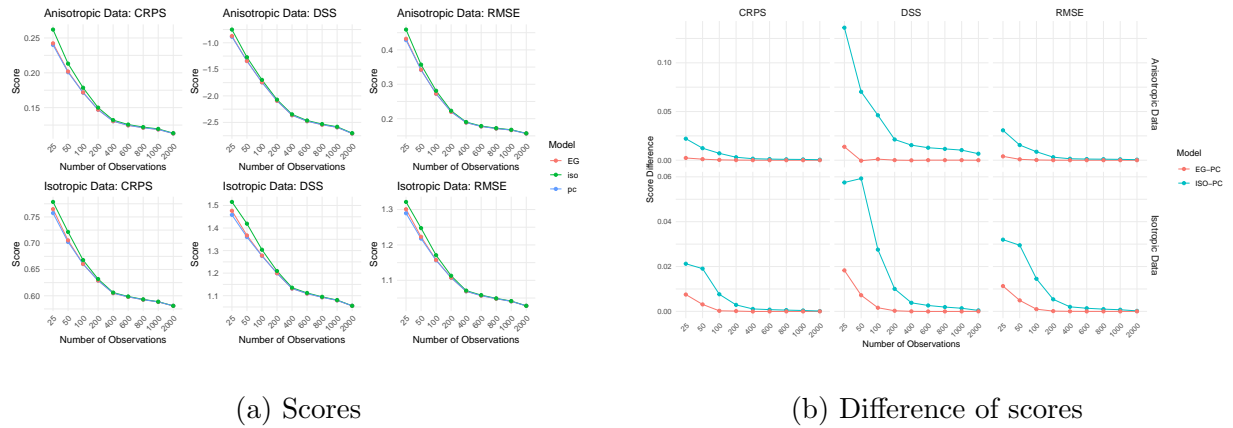


Figure 24: Comparison of the scores of the model for each prior for anisotropic and isotropic data, as the number of observations increases

Finally, we also plot the interval score for the parameters  $(\log(\kappa), v_1, v_2, \log(\sigma_u))$ . Given a credible interval  $(L_F, U_F)$  with confidence level  $\alpha$ , the interval score is defined by

$$S_{\text{INT}}(F, y) = U_F - L_F + \frac{2}{\alpha} (L_F - y) \mathbb{I}(y < L_F) + \frac{2}{\alpha} (y - U_F) \mathbb{I}(y > U_F).$$

The interval score is a proper scoring rule consistent for equal-tail error probability intervals:  $S(F, G)$  is minimized for the narrowest  $PI$  that has expected coverage  $1 - \alpha$ . The results are shown in Figure 25. As can be seen from the plots, the interval score for the parameters  $(\log(\kappa), \sigma_u)$  is generally better for the anisotropic model. This is especially pronounced for  $\log(\kappa)$  when there is less data. The interval score for  $v_1$  and  $v_2$  is not shown for the isotropic model as these parameters are not estimated in the isotropic model.

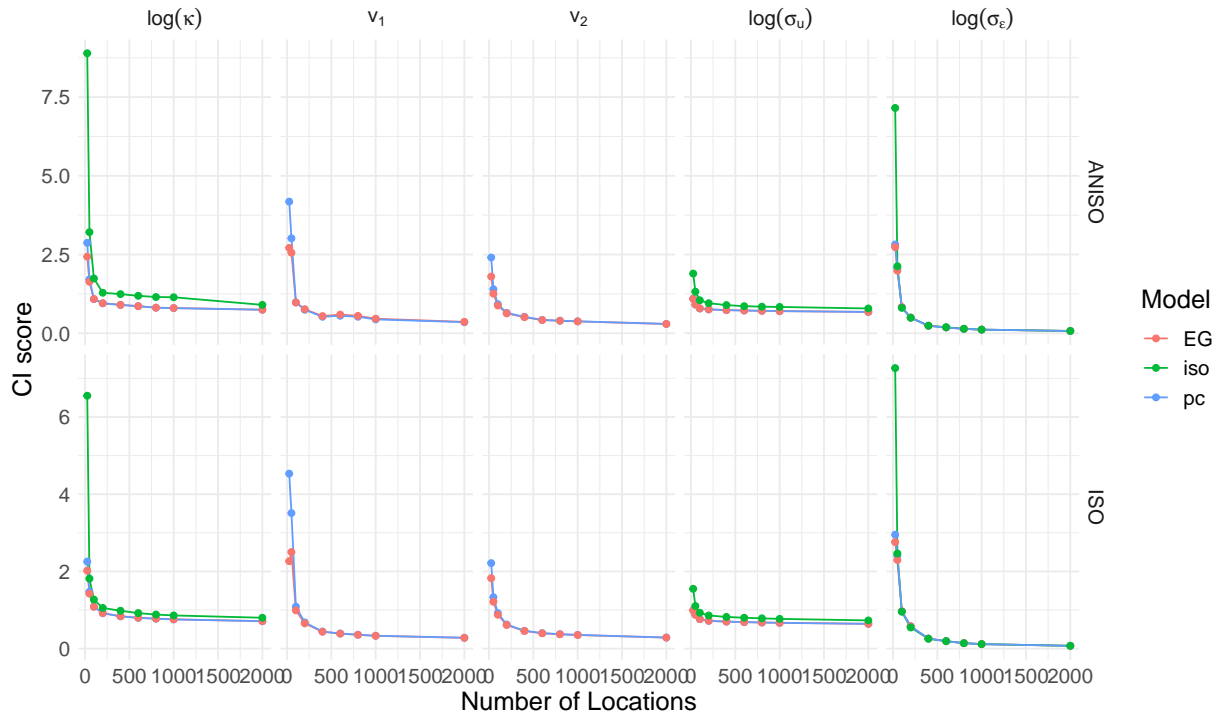


Figure 25: From top to bottom, anisotropic and isotropic data is observed. From left to right, the interval score for the parameters  $(\log(\kappa), v_1, v_2, \log(\sigma_u), \log(\sigma_\epsilon))$  with a varying number of observations is shown.

## References

- Adler, R. J., Taylor, J. E., et al. (2007). *Random fields and geometry*, volume 80. Springer.
- Banerjee, S., Carlin, B. P., and Gelfand, A. E. (2003). *Hierarchical modeling and analysis for spatial data*. Chapman and Hall/CRC.
- Bhatt, S., Weiss, D., Cameron, E., Bisanzio, D., Mappin, B., Dalrymple, U., Battle, K., Moyes, C., Henry, A., Eckhoff, P., et al. (2015). The effect of malaria control on *Plasmodium falciparum* in Africa between 2000 and 2015. *Nature*, 526(7572):207–211.



- Bolin, D., Simas, A. B., and Xiong, Z. (2023). Wasserstein complexity penalization priors: a new class of penalizing complexity priors. *arXiv preprint arXiv:2312.04481*.
- Cressie, N. and Wikle, C. K. (2015). *Statistics for spatio-temporal data*. John Wiley & Sons.
- Dawid, A. P. and Sebastiani, P. (1999). Coherent dispersion criteria for optimal experimental design. *Annals of Statistics*, pages 65–81.
- Dunlop, M. M., Girolami, M. A., Stuart, A. M., and Teckentrup, A. L. (2018). How deep are deep Gaussian processes? *Journal of Machine Learning Research*, 19(54):1–46.
- Dunlop, M. M., Iglesias, M. A., and Stuart, A. M. (2017). Hierarchical bayesian level set inversion. *Statistics and Computing*, 27:1555–1584.
- Evans, L. C. (2010). *Partial differential equations*, volume 19. American Mathematical Soc.
- Fuglstad, G.-A., Lindgren, F., Simpson, D., and Rue, H. (2015). Exploring a new class of non-stationary spatial Gaussian random fields with varying local anisotropy. *Statistica Sinica*, pages 115–133.
- Fuglstad, G.-A., Simpson, D., Lindgren, F., and Rue, H. (2019). Constructing priors that penalize the complexity of Gaussian random fields. *Journal of the American Statistical Association*, 114(525):445–452.
- Gelbrich, M. (1990). On a formula for the l<sub>2</sub> wasserstein metric between measures on euclidean and hilbert spaces. *Mathematische Nachrichten*, 147(1):185–203.
- Gel’fand, I. M. and Vilenkin, N. Y. (2014). *Generalized functions: Applications of harmonic analysis*, volume 4. Academic press.

- Gneiting, T. and Raftery, A. E. (2007). Strictly proper scoring rules, prediction, and estimation. *Journal of the American statistical Association*, 102(477):359–378.
- Grimit, E. P., Gneiting, T., Berrocal, V. J., and Johnson, N. A. (2006). The continuous ranked probability score for circular variables and its application to mesoscale forecast ensemble verification. *Quarterly Journal of the Royal Meteorological Society: A journal of the atmospheric sciences, applied meteorology and physical oceanography*, 132(621C):2925–2942.
- Ingebrigtsen, R., Lindgren, F., Steinsland, I., and Martino, S. (2015). Estimation of a non-stationary model for annual precipitation in southern Norway using replicates of the spatial field. *Spatial Statistics*, 14:338–364.
- Jaynes, E. T. (2003). *Probability theory: The logic of science*. Cambridge university press.
- Lindgren, F., Bakka, H., Bolin, D., Krainski, E., and Rue, H. (2020). A diffusion-based spatio-temporal extension of Gaussian Matérn fields. *arXiv preprint arXiv:2006.04917*.
- Lindgren, F., Bolin, D., and Rue, H. (2022). The SPDE approach for Gaussian and non-Gaussian fields: 10 years and still running. *Spatial Statistics*, page 100599.
- Lindgren, F., Rue, H., and Lindström, J. (2011). An explicit link between Gaussian fields and Gaussian Markov random fields: the stochastic partial differential equation approach. *Journal of the Royal Statistical Society: Series B (Statistical Methodology)*, 73.
- Lindgren, G. (2012). *Stationary stochastic processes: Theory and applications*. CRC Press.
- Modrák, M., Moon, A. H., Kim, S., Bürkner, P., Huurre, N., Faltejsková, K., Gelman, A., and Vehtari, A. (2023). Simulation-based calibration checking for bayesian computation: The choice of test quantities shapes sensitivity. *Bayesian Analysis*, 1(1):1–28.

- Rasmussen, C. E. (2003). Gaussian processes in machine learning. In *Summer school on machine learning*, pages 63–71. Springer.
- Roques, L., Allard, D., and Soubeyrand, S. (2022). Spatial statistics and stochastic partial differential equations: A mechanistic viewpoint. *Spatial Statistics*, 50:100591.
- Rue, H. and Held, L. (2005). *Gaussian Markov random fields: theory and applications*. Chapman and Hall/CRC.
- Sampson, P. D. and Guttorp, P. (1992). Nonparametric estimation of nonstationary spatial covariance structure. *Journal of the American Statistical Association*, 87(417):108–119.
- Simpson, D., Lindgren, F., and Rue, H. (2012). Think continuous: Markovian Gaussian models in spatial statistics. *Spatial Statistics*, 1:16–29.
- Simpson, D. P., Rue, H., Martins, T. G., Riebler, A., and Sørbye, S. H. (2014). Penalising model component complexity: A principled, practical approach to constructing priors. *Statistical Science*, 32:1–28.
- Stein, M. L. (2004). Equivalence of gaussian measures for some nonstationary random fields. *Journal of Statistical Planning and Inference*, 123(1):1–11.
- Talts, S., Betancourt, M., Simpson, D., Vehtari, A., and Gelman, A. (2018). Validating bayesian inference algorithms with simulation-based calibration. *arXiv preprint arXiv:1804.06788*.
- Uribe, F., Papaioannou, I., Latz, J., Betz, W., Ullmann, E., and Straub, D. (2021). Bayesian inference with subset simulation in varying dimensions applied to the karhunen–loève expansion. *International Journal for Numerical Methods in Engineering*, 122(18):5100–5127.

- Vehtari, A., Simpson, D., Gelman, A., Yao, Y., and Gabry, J. (2015). Pareto smoothed importance sampling. *arXiv preprint arXiv:1507.02646*.
- Wang, J. and Zuo, R. (2021). Spatial modelling of hydrothermal mineralization-related geochemical patterns using INLA+ SPDE and local singularity analysis. *Computers & Geosciences*, 154:104822.
- Zhang, H. (2004). Inconsistent estimation and asymptotically equal interpolations in model-based geostatistics. *Journal of the American Statistical Association*, 99(465):250–261.